Eur. Phys. J. C (2025) 85:1272
https://doi.org/10.1140/epjc/s10052-025-14682-0

THE EUROPEAN PHYSICAL JOURNAL C

Regular Article - Experimental Physics

A continuous calibration of the ATLAS flavour-tagging classifiers via optimal transportation maps

ATLAS Collaboration★

CERN, 1211 Geneva 23, Switzerland

Received: 20 May 2025 / Accepted: 26 September 2025

Abstract A calibration of the ATLAS flavour-tagging algorithms using a new calibration procedure based on optimal transportation maps is presented. Simultaneous, continuous corrections to the b-jet, c-jet, and light-flavour jet classification probabilities from jet-tagging algorithms in simulation are derived for b-jets using $t\bar{t} \rightarrow e\mu\nu\nu bb$ data. After application of the derived calibration maps, closure between simulation and observation is achieved for jet flavour observables used in ATLAS analyses of Large Hadron Collider (LHC) Run 2 proton-proton collision data. This continuous calibration opens up new possibilities for the future use of jet flavour information in LHC analyses and also serves as a guide for deriving high-dimensional corrections to simulation via transportation maps, an important development for a broad range of inference tasks.

Contents

N. D. Hehir, J. Khubua, B. Lund-Jensen, U. Mallik, I. P. J. Shipsey: Deceased

★ e-mail: atlas.publications@cern.ch

1 Introduction

The identification and classification of jets containing heavy-flavour hadrons (flavour tagging) is a crucial component of many analyses of the Large Hadron Collider [1] (LHC) data collected by the ATLAS detector [2]. For example, searches and measurements targeting processes producing top quarks (t) or Higgs bosons (H) are particularly dependent on flavour tagging because of the high branching fraction of these particles to heavy-flavour quarks [3–14].

Recent progress in flavour-tagging algorithms for classifying jets containing b-hadrons (b-jets) and c-hadrons (c-jets) has greatly increased the sensitivity of ATLAS analyses to possible new phenomena [15–17]. These algorithms are trained on samples produced by generators of proton-proton (pp) collision events that are subsequently passed through a sophisticated simulation of the ATLAS detector [18–20]. Contemporary algorithms take as input various observables related to a jet – primarily calorimeter and tracking information – and compute probabilities that each jet contains a b-hadron (p_b), a c-hadron (p_c), or neither of these (p_u). Traditionally, ATLAS analyses using flavour tagging define a summary observable based on these outputs and categorize jets by using this summary observable to separate signal from the background jets. The most common summary observable in use is the log-likelihood ratio of p_b, p_c, and p_u assuming some mixture of jet populations as a background hypothesis. For example, for b-jet identification ("b-tagging"), the ratio

$$D_b = \log \frac{p_b}{f_c p_c + (1 - f_c) p_u} \quad (1)$$

is an optimal discriminant between b-jets and non-b-jets when the c-jet fraction of non-b-jets is f_c.[1] Alternatively, if the goal is to identify c-jets and reject b-jets and light-flavour jets ("charm-tagging"), the discriminant used is

$$D_c = \log \frac{p_c}{f_b p_b + (1 - f_b) p_u}. \quad (2)$$

Typical values of f_c used in previous ATLAS analyses range between 0.018 and 0.08 for b-tagging, while for charm-tagging, choices of 0.3 or 0.4 for f_b are common.

From these discriminants, operating points are defined; e.g. the "70% b-tagging operating point" is the value of D_b for which 70% of b-jets with $p_{\mathrm{T}} > 20$ GeV in a Standard Model (SM) $t\bar{t}$ sample have a higher discriminant score.

The probability of jets to pass or fail selections based on these operating points is conventionally measured directly in data, and the flavour-tagging information about simulated jets is corrected such that on average it reflects the observed performance in data. These corrections are calculated in bins[2] of the jet's transverse momentum (p_{T}) because of the known dependence of tagger performance on this quantity [15]; however, the corrections are averaged over other jet properties. It is worth emphasizing that the calibration is derived purely based on the jet flavour-tagging information: other aspects of the simulation may only be altered through correlations with the flavour-tagging observables.

In ATLAS analyses of LHC Run 2 data, the calibration is obtained by measuring the tagging efficiencies (the probability that a signal jet passes some selection) or mis-tag rates (the probability that a background jet passes some selection) for b-jets, c-jets, and the remaining jet population (light jets) in regions enriched in each jet flavour. These tagging rates in data ($\varepsilon_{\mathrm{data}}$) are compared with the expected rates in simulation ($\varepsilon_{\mathrm{sim}}$), and correction scale factors ($\varepsilon_{\mathrm{data}}/\varepsilon_{\mathrm{sim}}$) are applied as weights to simulated jets [21–23]. For b-jets, these scale factors typically deviate from unity by less than 5%, but for c-jets and light-flavour jets, efficiency corrections may reach 20% or 50%, respectively. This enables extraction of physical parameters from ATLAS data that are unbiased by mismodelling of flavour-tagging performance in the simulation.

The resulting calibrations have a limited applicability: they only correct identification efficiencies for a particular choice of discriminant binning. For example, if an analysis requires a different combination of b- and c-jet tagging (e.g. a new b-tagging operating point or change in f_c or f_b), a completely new set of corrections must be derived for the relevant combination; this is especially pertinent in the search for $H \rightarrow cc$ decays [5,14]. Similarly, while calibrations have been performed with up to five bins of the tagging discriminant score ("pseudo-continuous calibrations"), they do not allow a truly continuous use of the tagging algorithms' output in physics analyses. Other analyses that would benefit from non-standard operating points are those that need very strong c-jet rejection, e.g. searches for rare top-quark production processes [24]; those that use a very loose b-jet veto, such as measurements of $H \rightarrow WW^*$ decays [25,26]; or those for which the optimal operating point is strongly dependent on event kinematics: for example searches for high-mass resonances decaying into b-jets [27].

This paper describes an alternative calibration based on changing (or *transporting*) the three flavour-tagging classifier outputs (p_u, p_c, p_b) such that the resulting probability density of these features in simulation matches data. The transportation map that calibrates the simulation is fully continuous (i.e. it is not binned); it does not involve reweighting simulated events but rather alters the output of the flavour-tagging algorithms for each jet. It is moreover designed such that it *minimally* alters the simulation in a well-defined sense that is made more formal in Sect. 3. The derivation of such minimal transport maps between probability distributions is the topic of optimal transportation theory [28,29].

ATLAS uses optimal-transportation-based corrections for the energy calibrations of muons [30], electrons [31], and hadronic jets [32], but these each rely on the shape of the detector energy responses being nearly Gaussian. In the Gaussian case, a transportation-based calibration amounts to correcting the first two moments of a distribution; as such, these calibrations are not usually formulated using the optimal-transportation nomenclature. However, in the case of jet flavour tagging, the probability density of discriminants is highly non-Gaussian and has no well-motivated simple parametric form. Nevertheless, recent advances in neural optimal-transport solvers allow the derivation of optimal transportation maps between distributions without known a priori densities as long as samples can be drawn from them [33–35]. Optimal transport has been proposed for several other purposes in particle physics, including for background estimates [36], measurements of multijet event shapes [37], and for anomaly detection [38]. In this paper, the focus is on the use of optimal transport for the calibration of the ATLAS flavour-tagging algorithms.

This calibration procedure has several advantages over more-traditional binned efficiency scale factors. Given a suitable choice of transport distance, there is a unique optimal transport map that yields a simulation that reflects the data while *minimally* altering the simulation. Transporting the observables of simulated jets is inherently unitary in the

[1] f_c should be interpreted as an effective parameter that controls the c-jet fraction at inference time; during the optimization of the classification algorithm, a different fraction might be chosen.

[2] In this work, a set of "bins", such as those used to define a histogram, is a collection of contiguous subsets that are used to build a piece-wise approximation of a function. For example, the ranges (0, 0.5], (0.5, 0.75], (0.75, 1.0) define a *binning* of the open unit interval (0, 1) made of three "bins".

sense that the number of jets in a sample is unaltered by applying the calibration; this is not in general the case when weighting by the data–simulation efficiency ratio, even after having applied corresponding scale factors for jets that fail the selection (“inefficiency scale factors”) [23]. Furthermore, instead of correcting the tagging probabilities of particular operating points or jet categories, their continuous density is calibrated; this allows much more flexibility in using said observables in data analysis. Finally, while flavour-tagging calibrations in ATLAS have so far been limited to a single one-dimensional discriminant with a fixed binning, in large part due to the “curse of dimensionality” that makes multi-dimensional binned distributions difficult to work with, calibrations based on neural optimal transport have the ability to handle high-dimensional calibration problems with relative ease and without any explicit binning choice.

The primary disadvantage of the transport-based calibration identified during the course of this study was that this approach does not yet allow for in situ constraints on nuisance parameters, such as the flavour fractions that are fitted in more-conventional flavour-tagging calibrations as in Ref. [23]. Reweighting-based calibrations may also reduce statistical fluctuations when considering systematic uncertainties of the calibration, since events cannot migrate across bin boundaries when applying weight variations. It is worth noting that the application of weights to correct the distribution of a particular observable will alter distributions over other observables through correlations, while in the transportation set-up only distributions that are explicitly corrected or have an explicit dependence on them are changed in the process; whether this is desirable depends on the particular use-case.

This paper presents the continuous calibration of the ATLAS DL1r flavour-tagging classification probabilities [15] (i.e. the discriminant outputs) for b-jets. A high-purity sample of b-jets is obtained by selecting events with an electron, a muon, and exactly two jets, which yields a population of jets dominated by $t\bar{t}$ production and decay into $e\mu\nu\nu bb$, following the optimized requirements of previous flavour-tagging calibrations [23]. Optimal calibration maps between the simulated and observed distributions of b-jet classification probabilities are derived.

The paper is laid out as follows. Section 2 introduces the ATLAS detector apparatus and coordinate system, and the calibration methodology is described in Sect. 3. Section 4 outlines the simulated and collected data samples used in this study. The data analysis and the estimation of uncertainties are described in Sects. 5 and 7, respectively, building largely on the work presented previously in Ref. [23]. Section 6 describes the calibration of the DL1r distribution for background jets, and Sect. 8 shows the extracted calibration maps and data-simulation comparisons for b-jets.

2 ATLAS detector

The ATLAS detector [2] at the LHC covers nearly the entire solid angle around the collision point.[3] It consists of an inner tracking detector surrounded by a thin superconducting solenoid, electromagnetic and hadronic calorimeters, and a muon spectrometer incorporating three large superconducting air-core toroidal magnets.

The inner-detector system (ID) is immersed in a 2T axial magnetic field and provides charged-particle tracking in the range $|\eta| < 2.5$. The high-granularity silicon pixel detector covers the vertex region and typically provides four measurements per track, the first hit generally being in the insertable B-layer installed before Run 2 [39,40]. It is followed by the silicon microstrip tracker, which usually provides eight measurements per track. These silicon detectors are complemented by the transition radiation tracker (TRT), which enables radially extended track reconstruction up to $|\eta| = 2.0$. The TRT also provides electron identification information based on the fraction of hits (typically 30 in total) above a higher energy-deposit threshold corresponding to transition radiation.

The calorimeter system covers the pseudorapidity range $|\eta| < 4.9$. Within the region $|\eta| < 3.2$, electromagnetic calorimetry is provided by barrel and endcap high-granularity lead/liquid-argon (LAr) calorimeters, with an additional thin LAr presampler covering $|\eta| < 1.8$ to correct for energy loss in material upstream of the calorimeters. Hadronic calorimetry is provided by the steel/scintillator-tile calorimeter, segmented into three barrel structures within $|\eta| < 1.7$, and two copper/LAr hadronic endcap calorimeters. The solid angle coverage is completed with forward copper/LAr and tungsten/LAr calorimeter modules optimized for electromagnetic and hadronic energy measurements respectively.

The muon spectrometer comprises separate trigger and high-precision tracking chambers measuring the deflection of muons in a magnetic field generated by the superconducting air-core toroidal magnets. The field integral of the toroids ranges between 2.0 and 6.0 T m across most of the spectrometer. Three layers of precision chambers, each consisting of layers of monitored drift tubes, cover the region $|\eta| < 2.7$, complemented by cathode-strip chambers in the forward region, where the background is highest. The muon

[3] ATLAS uses a right-handed coordinate system with its origin at the nominal interaction point (IP) in the centre of the detector and the z-axis along the beam pipe. The x-axis points from the IP to the centre of the LHC ring, and the y-axis points upwards. Polar coordinates (r, ϕ) are used in the transverse plane, ϕ being the azimuthal angle around the z-axis. The pseudorapidity is defined in terms of the polar angle θ as $\eta = -\ln\tan(\theta/2)$ and is equal to the rapidity $y = (1/2)\ln[(E + p_z)/(E - p_z)]$ in the relativistic limit. Angular distance is measured in units of $\Delta R \equiv \sqrt{(\Delta y)^2 + (\Delta\phi)^2}$.

trigger system covers the range $|\eta| < 2.4$ with resistive-plate chambers in the barrel, and thin-gap chambers in the endcap regions.

The luminosity is measured mainly by the LUCID-2 [41] detector, which records Cherenkov light produced in the quartz windows of photomultipliers located close to the beam pipe.

Events are selected by the first-level trigger system implemented in custom hardware, followed by selections made by algorithms implemented in software in the high-level trigger [42]. The first-level trigger accepts events from the 40 MHz bunch crossings at a rate below 100 kHz, which the high-level trigger reduces in order to record complete events to disk at about 1 kHz.

A software suite [43] is used in data simulation, in the reconstruction and analysis of real and simulated data, in detector operations, and in the trigger and data acquisition systems of the experiment.

3 Methodology

The aim of this study is to derive a p_{T}-dependent mapping $T_{p_{\mathrm{T}}}$ that moves the flavour-tagging outputs of simulated jets such that, after this movement, the probability density of the simulation matches that in data. The amount that a jet's flavour-tagging score moves can be used to define a distance metric between the original simulated distribution and the corrected distribution. In general, there are many mappings that will achieve closure between simulation and data, but an optimal mapping is one that moves the simulation as little as possible. In the following section, these concepts are introduced more formally, and the methods used to find the optimal solution are described.

Statement of the problem

The goal here is to derive $T_{p_{\mathrm{T}}} : \vec{Q} \to \vec{Q}$, where $\vec{Q}$ is a space of classifier outputs, p_u, p_c, and p_b, described in Refs. [15,16,23], such that after the application of $T_{p_{\mathrm{T}}}$ the probability density function ("density") in the corrected simulation is equivalent to that measured in data, $(T_{p_{\mathrm{T}}})_{\#}\, p_{\mathrm{sim}}(\vec{q}|p_{\mathrm{T}}) \approx p_{\mathrm{data}}(\vec{q}|p_{\mathrm{T}})$. Throughout this paper, $\vec{q}$ is an element of $\vec{Q}$, and the notation $M_{\#}\, p(X)$ denotes the pushforward [29] of a distribution p through a map M; i.e. M acts on elements $x \in X$ while $M_{\#}$ operates on probability distributions over X. If samples are taken from some density $x \sim p(X)$, then samples taken from the pushforward of p through M can be built by applying M to each sample, i.e. $Mx \sim M_{\#}\, p(X)$.

In general, there are many mappings that achieve the desired closure, but an *optimal* transport map is one that, given a distance metric c defined over $\vec{Q}$, minimizes the total distance that the simulation must move,

$$\hat{T}_{p_{\mathrm{T}}} = \arg \inf_{T_{p_{\mathrm{T}}}} \int_{\vec{q} \in \vec{Q}} c(\vec{q}, T_{p_{\mathrm{T}}}\, \vec{q})\, p_{\mathrm{sim}}(\vec{q}|p_{\mathrm{T}})\, d\vec{q};$$
$$\text{such that}$$
$$(T_{p_{\mathrm{T}}})_{\#}\, p_{\mathrm{sim}}(\vec{q}|p_{\mathrm{T}}) \approx p_{\mathrm{data}}(\vec{q}|p_{\mathrm{T}}).$$

For Euclidean distance metrics of the form $c^2(\vec{x}, \vec{y}) = (\vec{x} - \vec{y})^2$, the optimal transport map is known to be unique [29].

Optimality property of maps

The simulated samples used to analyse ATLAS data are based on a wealth of knowledge of physical processes from a wide variety of sources accumulated over many years. Carefully tuned aspects of the simulation particularly relevant to jet flavour tagging include high-fidelity approximations of soft and collinear emissions within jets of partons as well as the subsequent hadronization process [44–48], dedicated studies of the heavy-quark fragmentation process [49–54] and heavy-hadron decays [55,56], and a detailed understanding of particle interactions with detector components [19,20]. The calibration procedure is an exercise in fine-tuning the simulation to account for possible inconsistencies with observation at a detailed level; deriving a transport map that minimally alters the output of the simulation ensures that upstream predictions, which have been compared with (and tuned to agree with) previous measurements, are corrected as little as possible.

Choice of calibration space

This calibration is derived for the quantities $q_i = \mathrm{logit}\ p_i$, defined per component as

$$\mathrm{logit}\ p_i = \log \frac{p_i}{1 - p_i + \epsilon},$$

where $\epsilon = 10^{-10}$ is introduced to prevent divisions by zero, and the index i runs over the three flavours used in the ATLAS jet classifiers: u, c, and b. These $\vec{q}$ are closely related to the likelihood ratios used to discriminate between signal and background jets, as introduced in Eqs. (1) and (2), and their components can take any real-numbered values. Furthermore, up to a normalization constant the left inverse of logit p_i is the sigmoid activation function:[4] it is always possible to reconstruct the unique jet-flavour probabilities (p_b, p_c, p_u) from $\vec{q}$, meaning that a calibration of $\vec{q}$

[4] The sigmoid activation function is given by $p_i' = 1/(1 + \mathrm{e}^{-q_i})$. To ensure that the probabilities sum to unity, the sigmoid transformation is normalized using $p_i = p_i' / \sum_i p_i'$.

amounts to a calibration of (p_b, p_c, p_u). Unlike the space of (p_b, p_c, p_u), the $\vec{Q}$ space covers $\mathbb{R}^3$, and in this calibration, the $\vec{Q}$ space is treated as Euclidean with the usual quadratic distance between $\vec{q}$ and $\vec{q}\,'$, $\sqrt{(\vec{q}-\vec{q}\,')^2}$. Using this Euclidean distance means there is a unique optimal transport mapping.

For jet flavour tagging, ATLAS calibrations are parameterized by a jet's flavour (i.e. calibrations are derived separately for b-jets, c-jets, and light-flavour jets) and p_{T} [21–23] in order to ensure applicability across a wide range of analyses of LHC data. The method introduced here follows that prescription and provides corrections for b-jets as a function of p_{T}. This procedure could easily be extended to calibrations parameterized by additional jet properties that traditionally have been averaged over, which may lead to better generalization properties in future work; Ref. [57] is recommended for a broader discussion of calibration universality.

Deriving approximate calibration maps

For metric spaces with a quadratic distance metric, the optimal transport map between two continuous distributions is the gradient of a scalar convex function [29]. Partially input-convex neural networks (PICNNs) are flexible and generic approximators of functions that are convex in a subset of their arguments (i.e. "partially convex") [58], and it is possible to derive optimal transport maps for metric spaces that have a Euclidean transport cost by using PICNNs [33].

Following this prescription, the optimal transport map between p_{data} and p'_{sim} is derived via the loss function

$$\mathcal{L}(f, g) = \frac{1}{N_{\mathrm{data}}} \sum_{\vec{q}, p_{\mathrm{T}} \sim p_{\mathrm{data}}} f(\vec{q}, p_{\mathrm{T}}) + \frac{1}{N_{\mathrm{sim}}} \sum_{\vec{q}, p_{\mathrm{T}} \sim p'_{\mathrm{sim}}} \vec{q} \cdot \vec{\nabla}\, g(\vec{q}, p_{\mathrm{T}}) - f(\vec{\nabla}\, g(\vec{q}, p_{\mathrm{T}}), p_{\mathrm{T}}),$$

where f and g are convex functions of $\vec{q}$ but not necessarily of p_{T}, and N_{data} and N_{sim} are respectively the number of observed events and the number of simulated events, and $\vec{\nabla}$ indicates the gradient with respect to $\vec{q}$. After minimizing $\mathcal{L}$ with respect to f and maximizing it with respect to g, the optimal choices $\hat{f}$ and $\hat{g}$ have the property that

$$(\vec{\nabla}\, \hat{g})_{\#}\, p_{\mathrm{sim}}(\vec{q}\,|p_{\mathrm{T}}) \approx p_{\mathrm{data}}(\vec{q}\,|p_{\mathrm{T}})$$

and

$$(\vec{\nabla}\, \hat{f})_{\#}\, p_{\mathrm{data}}(\vec{q}\,|p_{\mathrm{T}}) \approx p_{\mathrm{sim}}(\vec{q}\,|p_{\mathrm{T}}),$$

i.e. the gradient of $\hat{g}$ pushes p_{sim} forward to p_{data}, and the gradient of $\hat{f}$ pushes p_{data} forward to p_{sim} [34]. The desired calibration transport maps are then given by $\hat{T}_{p_{\mathrm{T}}}(\vec{q}) = \vec{\nabla}\, \hat{g}(\vec{q}, p_{\mathrm{T}})$.

Background contamination and uncertainties

While a purposely selected population of jets may have a high fraction of b-jets, there is always some contamination from jets with other flavours. In this study, the salient information needed to correctly account for this background contamination is the fraction of b-jets at each point in $\vec{Q} \times p_{\mathrm{T}}$ space, $p(\mathrm{sig}|\vec{q},\ p_{\mathrm{T}})$.

A smooth signal jet fraction as a function of p_{T}, $f_{\mathrm{sig}}(p_{\mathrm{T}}) = p(\mathrm{sig}|p_{\mathrm{T}})$, is obtained via neural density ratio estimation techniques [59]: a classifier is trained to approximate the signal-to-background ratio as a function of p_{T}, $p(\mathrm{sig}|p_{\mathrm{T}})/p(\mathrm{bkg}|p_{\mathrm{T}})$, and then $p(\mathrm{sig}|p_{\mathrm{T}})$ is solved for by setting $p(\mathrm{bkg}|p_{\mathrm{T}}) = 1 - p(\mathrm{sig}|p_{\mathrm{T}})$.

In order for the PICNN minimization procedure to result in the correct mapping conditional on p_{T}, it is necessary for the p_{T} distributions in data and simulation to be approximately equal. To ensure that these are indeed identical, the conditional density $p_{\mathrm{sim}}(\vec{q}\,|p_{\mathrm{T}})$ is approximated using conditional normalizing flows [60], which are neural solvers that can approximate continuous multivariate distributions given samples from the target density. Separate normalizing flows are used to approximate $p_{\mathrm{sig}}(\vec{q}\,|p_{\mathrm{T}})$ and $p_{\mathrm{bkg}}(\vec{q}\,|p_{\mathrm{T}})$. Combined with $f_{\mathrm{sig}}(p_{\mathrm{T}})$, these yield the full prediction for $p'_{\mathrm{sim}}(\vec{q},\ p_{\mathrm{T}})$, which has the property $p'_{\mathrm{sim}}(p_{\mathrm{T}}) = p_{\mathrm{data}}(p_{\mathrm{T}})$, defined as

$$p'_{\mathrm{sim}}(\vec{q},\ p_{\mathrm{T}}) \equiv (f_{\mathrm{sig}}(p_{\mathrm{T}}) p_{\mathrm{sig}}(\vec{q}\,|p_{\mathrm{T}}) + (1 - f_{\mathrm{sig}}(p_{\mathrm{T}})) p_{\mathrm{bkg}}(\vec{q}\,|p_{\mathrm{T}}))\ p_{\mathrm{data}}(p_{\mathrm{T}}). \quad (3)$$

Training batches for simulation are built by sampling from p'_{sim}, which results in the desired, p_{T}-corrected distribution [61]. Given the data p_{T} distribution, p'_{sim} can be separated into a signal distribution p'_{sig} and a background distribution p'_{bkg}, defined as:

$$p'_{\mathrm{sig}}(\vec{q},\ p_{\mathrm{T}}) \propto p_{\mathrm{sig}}(\vec{q}\,|p_{\mathrm{T}})\ f_{\mathrm{sig}}(p_{\mathrm{T}})\ p_{\mathrm{data}}(p_{\mathrm{T}})$$
$$\text{and } p'_{\mathrm{bkg}}(\vec{q}, p_{\mathrm{T}}) \propto p_{\mathrm{bkg}}(\vec{q}\,|p_{\mathrm{T}})\ (1 - f_{\mathrm{sig}}(p_{\mathrm{T}}))\ p_{\mathrm{data}}(p_{\mathrm{T}}).$$

Non-b-jet samples are effectively subtracted during the determination of the calibration maps by leaving them in place for part of the training procedure, following

$$\hat{T}_{p_{\mathrm{T}}}\, \vec{q} = \begin{cases} \vec{\nabla}\, \hat{g}(\vec{q}) & \text{for } b\text{-jets} \\ \vec{q} & \text{for non-}b\text{-jets} \end{cases}.$$

A more thorough treatment of this mechanism can be found in Ref. [34].

Uncertainties in the predicted b-jet fractions, $f_{\mathrm{sig}}(p_{\mathrm{T}})$, and the non-$b$-jet shape, $p_{\mathrm{bkg}}(\vec{q}\,|p_{\mathrm{T}})$, are estimated by deriving a family of transport maps for a range of variations of each of them. For the purpose of illustrating the total uncertainty of the corrected simulation, each variation is assumed to correspond to a 1σ point of a normally distributed continuous parameter, and these parameters for different variations are treated as fully uncorrelated. Since the transport map for each variation is derived separately, a more careful uncertainty treatment is possible in analyses that depend on this calibration by using the full family of maps. Systematic uncertainties are assessed by altering the simulated prediction in various ways; these are described further in Sect. 7. In this study, the flavour fraction $f_{\text{sig}}(p_{\text{T}})$ is taken from simulation, while in previous work these were constrained using background-enriched sidebands. The uncertainty in the shape of the non-b-jet background, $p_{\text{bkg}}(\vec{q}\,|\,p_{\text{T}})$, is determined via a b-jet-depleted control region and laid out in Sect. 6. Statistical uncertainties coming from the limited size of the observed data set are estimated via bootstraps [62].

Figure 1 shows a schematic of the calibration process in the context of jet flavour tagging.

4 Samples of observed and simulated events

This analysis uses the LHC pp collision data recorded by the ATLAS detector during the years 2015–2018, with a collision centre-of-mass energy of $\sqrt{s} = 13$ TeV. The total integrated luminosity is 140.1 ± 1.2 fb^{-1} [63]. Only collision events recorded during normal running of the entire ATLAS detector are considered in this analysis [64]. As detailed in Sect. 5, these data events were collected by requiring at least one high-p_{T} electron or muon to be identified by the ATLAS trigger system [42,65,66].

A number of simulated event samples, corresponding to a Monte Carlo integration of the relevant Standard Model calculations [18], are used both to predict the processes that populate the analysis selection region and to assess uncertainties in the calibration of the simulation. The production of $t\bar{t}$ events was modelled using the POWHEG BOX V2 [67–70] generator at NLO with the NNPDF3.0$_{\text{NLO}}$ [71] set of parton distribution functions (PDFs) and the h_{damp} parameter[5] set to $1.5\,m_t$ [72]. The events were interfaced to PYTHIA 8.230 [73] to model the parton shower, hadronization, and underlying event, with parameter values set according to the A14 set of tuned parameters (tune) [48] and using the NNPDF2.3$_{\text{LO}}$ set of PDFs [74]. The decays of bottom and charm hadrons were performed by EVTGEN 1.6.0 [55].

Alternative samples were generated to assess the uncertainty in the $t\bar{t}$ prediction. The uncertainty due to initial-state radiation (ISR) is estimated by simultaneously varying the h_{damp} parameter and the renormalization and factorization scales (μ_{r} and μ_{f}), and choosing the Var3c up/down variants of the A14 tune. Final-state radiation (FSR) uncertainties are determined by scaling the parton-shower time-like shower scale μ_{r} in PYTHIA up and down by a factor of two. The impact of using a different parton shower and hadronization model is evaluated by comparing the nominal $t\bar{t}$ sample with another event sample also produced with the POWHEG BOX V2 generator using the NNPDF3.0$_{\text{NLO}}$ PDF set. Events in the latter sample were interfaced with HERWIG 7.04 [45,75], which used the H7UE set of tuned parameters [45] and the MMHT2014$_{\text{LO}}$ PDF set [76]. The decays of bottom and charm hadrons were again simulated using the EVTGEN 1.6.0 program.

The associated production of a top quark and W boson (tW) was modelled by the POWHEG BOX V2 generator at NLO in QCD using the five-flavour scheme and the NNPDF3.0$_{\text{NLO}}$ set of PDFs. The diagram removal scheme [77] was used to remove interference and overlap with $t\bar{t}$ production. The events were interfaced to PYTHIA 8.230, which used the A14 tune and the NNPDF2.3$_{\text{LO}}$ PDFs [74].

The production of W+jets and Z+jets was simulated with the SHERPA 2.2.1 [78] generator using next-to-leading-order (NLO) matrix elements (ME) for up to two partons, and leading-order (LO) matrix elements for up to four partons, calculated with the Comix [79] and OPENLOOPS [80–82] libraries. They were matched with the SHERPA parton shower [83] using the MEPS@NLO prescription [84–87] and the set of tuned parameters developed by the SHERPA Authors. The NNPDF3.0$_{\text{NNLO}}$ set of PDFs was used and the samples were normalized to a next-to-next-to-leading-order (NNLO) prediction [88].

The POWHEG BOX V2 generator was used to simulate the WW, WZ and ZZ [89] production processes at NLO accuracy in α_{s}. The effect of singly resonant amplitudes and interference effects due to Z/γ^* and same-flavour lepton combinations in the final state were included, where appropriate. Interference effects between WW and ZZ for same-flavour charged leptons and neutrinos were ignored. Events were interfaced to PYTHIA 8.210 [73] for the modelling of the parton shower, hadronization, and underlying event, with parameters set according to the AZNLO tune [90]. The CT10 PDF set [91] was used for the hard-scattering processes, whereas the CTEQ6L1 PDF set [92] was used for the parton shower. EVTGEN 1.2.0 [55] was used to decay bottom and charm hadrons.

The effect of multiple interactions in the same and neighbouring bunch crossings (pile-up) was modelled by overlaying the simulated hard-scattering event with inelastic proton–proton (pp) events generated with PYTHIA 8.186 [44] using the NNPDF2.3$_{\text{LO}}$ PDFs and the A3 tune [93].

[5] The h_{damp} parameter is a resummation damping factor and one of the parameters that controls the matching of POWHEG matrix elements to the parton shower and thus effectively regulates the high-p_{T} radiation against which the $t\bar{t}$ system recoils.

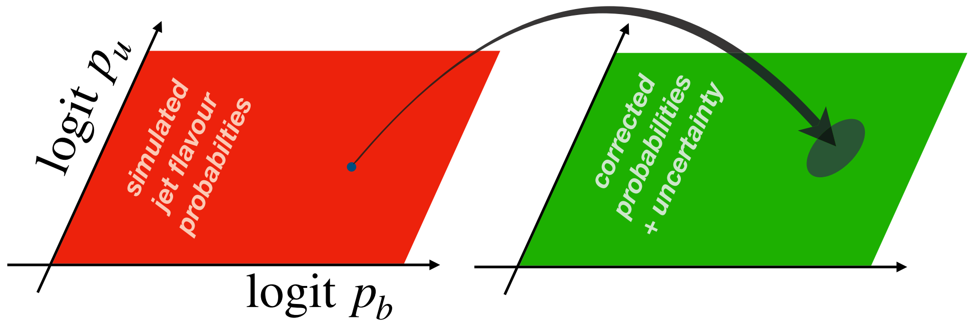

Fig. 1 Schematic of the optimal calibration maps derived in this study. Only two of the three calibrated log-probabilities are shown. The darkened region around the point of the arrow indicates that there is some uncertainty in the transport mapping. The transport maps are deterministic, so the uncertainty is calculated by deriving transport maps between alternative simulations and the data

5 Analysis

A precise calibration of the DL1r flavour probabilities for b-jets requires an event selection that yields a relatively pure b-jet sample and for which the backgrounds are well understood. In Sect. 5.1, the object and event selection used to achieve this are described; Sect. 5.2 shows the predicted event kinematics compared with observed data after this selection. Section 5.3 discusses the neural estimates of $f_{\text{sig}}(p_{\text{T}})$ and p_{sim} built from the MC predictions and the level of closure observed. Finally, the PICNN architecture used to perform the calibration is explained in Sect. 5.4.

5.1 Event selection

A population of jets enriched in b-jets is obtained by applying a selection targeting events from the dilepton $t\bar{t}(e\mu\nu\nu bb)$ process, which provides a high-cross-section source of b-jets with relatively low contamination from backgrounds. The event selection follows earlier ATLAS calibrations of flavour tagging for b-jets. The selection is described briefly below, but a more detailed description may be found in Ref. [23]. The major change in the event selection is a requirement applied in the new analysis on the invariant mass of lepton–jet pairs, $m_{\ell j} < 175$ GeV; previously the region $m_{\ell j} \geq 175$ GeV was used to define a background-enriched control region to constrain jet flavour fractions *in situ*, but such events are vetoed in this analysis.

5.1.1 Tracking and vertexing

The ID is used to reconstruct tracks corresponding to charged particles [94,95]. Primary vertices (PVs) are reconstructed by identifying points along the LHC beamline consistent with a high density of charged particles, based on reconstructed tracks [96]. At least one reconstructed PV is required in each event, and the PV with the highest sum of the squared constituent track transverse momenta is considered the "hard-scatter" vertex.

5.1.2 Charged leptons

Electrons and muons are used to preferentially select events with prompt leptons. Electron candidates are built from spatially compatible isolated electromagnetic energy clusters and ID tracks [97]; they are required to have $E_{\text{T}} > 28$ GeV and $|\eta| < 2.47$ after their energies are corrected using calorimeter shower shape information. Candidates in the calorimeter barrel-endcap transition region ($1.37 < |\eta| < 1.52$) are removed to avoid large uncertainties in the identification efficiency. TIGHT likelihood and isolation requirements are imposed to reduce the contamination from non-prompt and fake electron candidates further. Efficiency scale factors and energy calibration corrections derived in $Z \to ee$ events are applied to ensure the electron reconstruction and identification performance in data is reflected in simulation.

Muon candidates are ID tracks geometrically matched to tracks in the muon spectrometer [98]. They must have $p_{\text{T}} > 28$ GeV and $|\eta| < 2.5$, and a TIGHT identification requirement is applied. Furthermore, muons are required to be isolated from surrounding hadronic activity in order to remove contamination from hadronic jets and heavy-flavour decays, using the TIGHT isolation criterion. Muon identification efficiency and momentum response corrections are derived in $Z \to \mu\mu$ events, and the simulation is adjusted to ensure the predicted performance matches that observed in data [30].

5.1.3 Hadronic jets

Jets of hadronic particles are built from particle-flow candidates, which use tracking and calorimetry information to ensure a good jet constituent response for both the charged and neutral particles [99]. The anti-k_t combinatorial reconstruction algorithm is used with a radius parameter $R = 0.4$ [100], as implemented in FastJet [101]. The reconstructed jet transverse momenta are corrected to the particle-level jet p_{T} using simulation [32]. The jet response is measured in multijet, Z+jets, and γ+jets data, and the simulation is corrected to reflect the response in data events. Jets are required to have reconstructed transverse momenta $p_{\mathrm{T}} > 20$ GeV; they must also fall within the fiducial volume of the inner tracker, $|\eta| < 2.5$. A “jet vertex tagger” (JVT) is used to reduce the fraction of jets with large energy fractions from interaction other than the hard-scatter collision (“pile-up interactions”) [102]. The efficiency of the JVT selection in simulated jets from the hard-scatter collision is 92%, and for jets with $p_{\mathrm{T}} > 60$ GeV the fraction of jets from pile-up interactions is small enough that no JVT requirement is imposed.

5.1.4 Jet flavour tagging

For flavour tagging, reconstructed tracks with $p_{\mathrm{T}} > 500$ MeV are geometrically matched to hadronic jets using the ΔR_η measure.[6] The ΔR_η matching requirement varies with jet p_{T} since the opening angle of b-hadron decay products is wider for low-p_{T} b-hadrons than for those with high p_{T}. The matching criterion is $\Delta R_\eta(\text{track, jet}) < 0.45$ at jet $p_{\mathrm{T}} = 20$ GeV, and decreases asymptotically to $\Delta R_\eta < 0.25$ for very high p_{T} jets; tracks are assigned to the closest jet in the event that more than one valid match is found. A continuous calibration for the DL1r flavour-tagging algorithm [15], which uses a variety of low-level inputs built from charged-particle tracks, is derived in this study. The b- and c-jet identification discriminants, denoted by D_b^{DL1r} and D_c^{DL1r}, are the D_b and D_c log-likelihood ratios respectively introduced in Eqs. (1) and (2) for the DL1r tagging algorithm; f_c is set to 0.018 for D_b^{DL1r}, while $f_b = 0.3$ for D_c^{DL1r}.

In simulation, jets are designated as b-jets, c-jets, τ-jets, or light-flavour jets depending on the nearby final-state heavy-flavour hadrons and τ-leptons. Electroweakly decaying b- and c-hadrons and τ-leptons with $p_{\mathrm{T}} > 5$ GeV are matched to a reconstructed jet if they are within $\Delta R_\eta = 0.3$ of the jet axis; priority is given to the nearest jet if more than one match is found. If a b-hadron is matched to a jet, the jet is labelled a b-jet; if no b-hadron is matched, the jet is subsequently checked for charm hadrons and then τ-leptons, and given the c-jet or τ-jet designation. If no heavy hadron or τ-lepton is matched to a jet, it is considered a light-flavour jet. No special distinction is made for jets with more than one heavy hadron of the same flavour, e.g. bb or cc jets; similarly, no attempt is made to separate light-flavour jets based on their quark or gluon partonic origin. It should also be noted that the fraction of τ-jets after the following event selection is much smaller than the uncertainty in the light-flavour jet fraction. For the purposes of this calibration, τ-jets, c-jets, and light-flavour jets are treated coherently as a non-b-jet background population.

[6] $\Delta R_\eta \equiv \sqrt{(\Delta\eta)^2 + (\Delta\phi)^2}$.

5.1.5 Event requirements

To select a sample enriched in $t\bar{t} \to e\mu\nu\nu bb$ production, events are required to contain exactly one selected electron candidate and exactly one selected muon candidate. In order to avoid double counting the same object across multiple signatures, an object overlap-removal is applied among electrons, muons, and jets, following the prescription in Section 6.1 of Ref. [23]. After this, events with fewer than two prompt charged leptons make up a negligible fraction of the total rate, and the majority contribution of Drell–Yan $Z \to \ell\ell$ production is via the decays of two τ-leptons to one electron and one muon. At least one selected lepton candidate must match a corresponding object in the ATLAS trigger system [65,66], and efficiency scale factors are applied to correct the trigger efficiency in simulation to that in data.

In order to further improve the b-jet purity, additional selections are imposed to reduce the contribution from $t\bar{t}$+jets production, following the procedure in Ref. [23]. Events containing more than two selected jets are removed. Leptons and jets are then paired by minimizing the sum of the squared lepton-jet invariant masses over possible pairings: $\min_{\alpha\beta}\,(m^2_{j_1,\ell_\alpha} + m^2_{j_2,\ell_\beta})$, where α and β index the two reconstructed leptons, and j_1 and j_2 are the two reconstructed jets in the event. Only events where both resulting lepton-jet pair invariant masses are less than 175 GeV, i.e. consistent with two top-quark decays, are considered.

5.2 Comparisons of data and simulation

For relevant jet kinematics, agreement between data and simulation is observed within the assessed uncertainties, which are described in Sect. 7. Figure 2 shows this agreement for the jet p_{T}, jet η, D_b^{DL1r}, and D_c^{DL1r} after the full event selection described in Sect. 5.1, with the prediction separated by production process. Figure 3 shows comparisons broken down by jet flavour. It should be noted that the flavour-tagging observables are shown after correcting the non-b-jet distributions, as described in Sect. 6, but before applying any corrections to b-jets. The mismodelling of the jet p_{T} spectrum in $t\bar{t}$ events by these NLO predictions was also observed previously by ATLAS [7]; the modelling uncertainties assessed in this study cover this discrepancy at the 1σ level.

5.3 Approximations of $f_{\mathrm{sig}}(p_{\mathrm{T}})$ and $p_{\mathrm{sim}}(\vec{q}\,|p_{\mathrm{T}})$

As described in Sect. 3, key ingredients to the derivation of the $\vec{q}$ optimal calibration maps are continuous approxima-

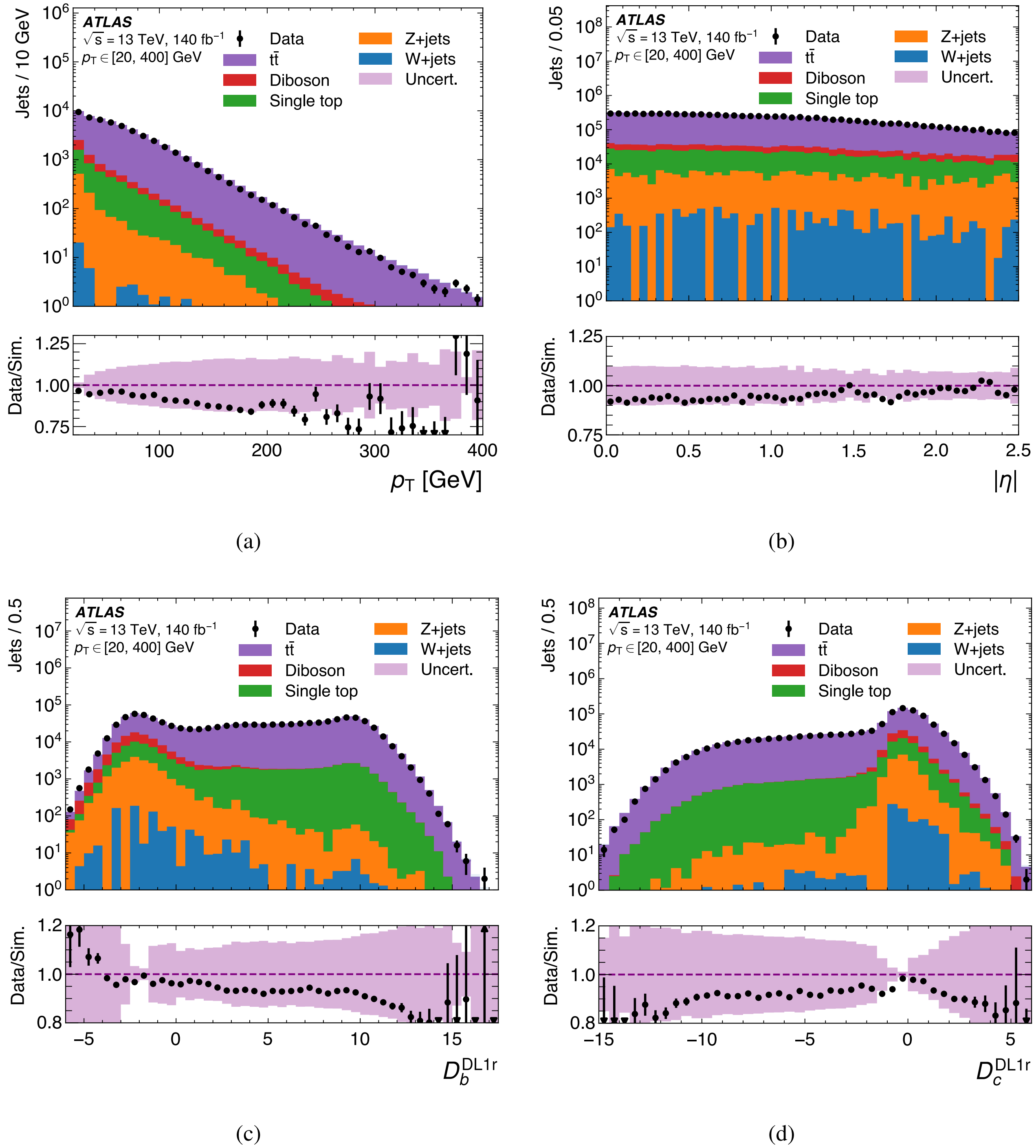

Fig. 2 Comparison of jet observables between the simulation's predictions and observed data, with the predictions separated by process: the selected jets' (**a**) p_{T}, (**b**) $|\eta|$, (**c**) D_b^{DL1r} and (**d**) D_c^{DL1r}. Non-b-jet distributions were estimated following the procedure in Sect. 6; no correction is applied to the simulation for b-jets. The uncertainty bands denote the impact of all uncertainties described in Sect. 7

tions of the b-jet fraction $f_{\mathrm{sig}}(p_{\mathrm{T}})$ and the jet-flavour probability distributions $p_{\mathrm{sim}}(\vec{q}\,|\,p_{\mathrm{T}})$ as a function of the jet p_{T}. The former is derived using a neural density ratio estimate trained on jets from the simulation, and the latter is estimated using conditional normalizing flows. Figure 4 shows the predicted b-jet purity for the neural density ratio estimate, compared for validation purposes with a binned estimate of the same ratio obtained directly from MC events.

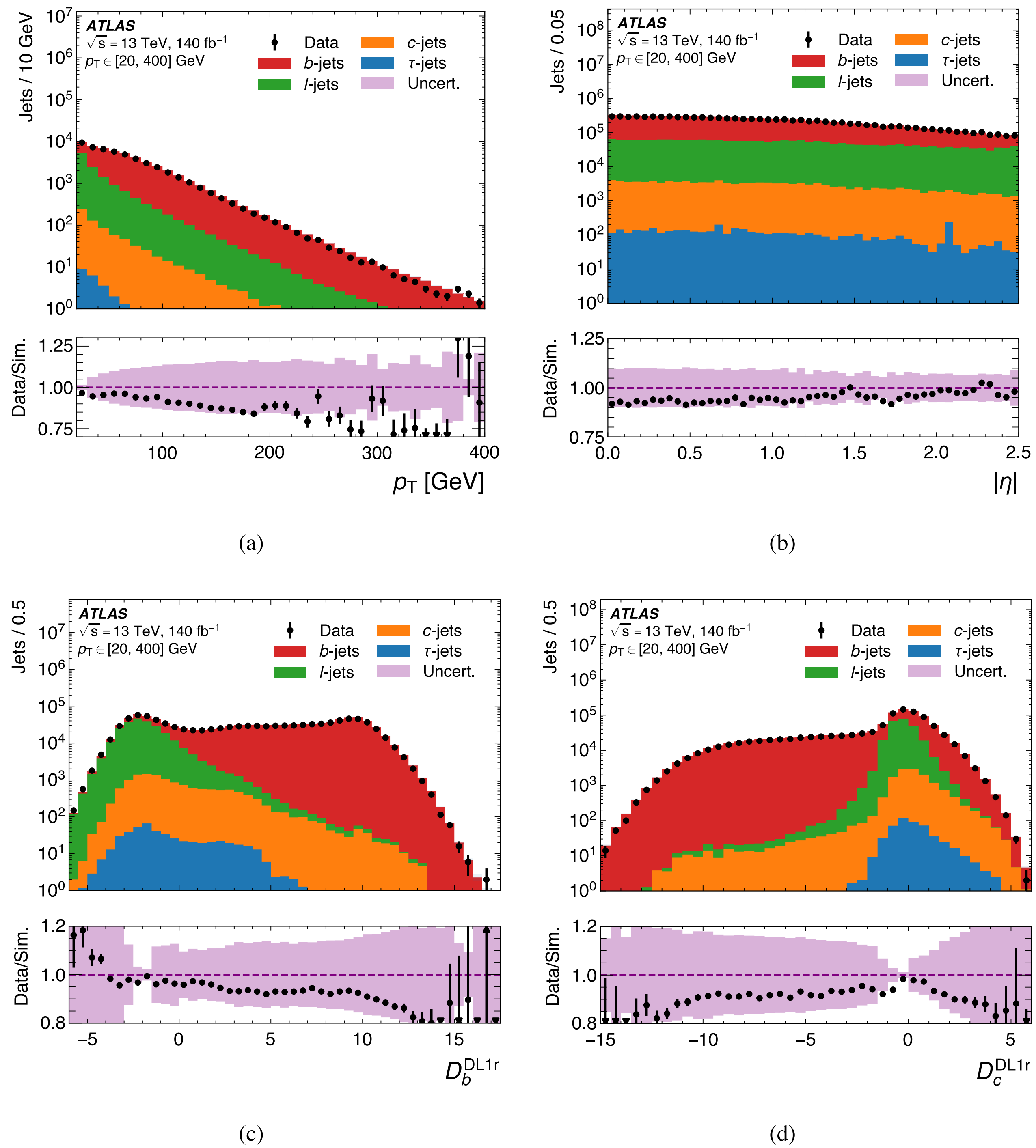

Fig. 3 Comparison of jet observables between the simulation's predictions and observed data, with the predictions separated by jet flavour: the selected jets' (**a**) p_{T}, (**b**) $|\eta|$, (**c**) D_b^{DL1r} and (**d**) D_c^{DL1r}. Non-b-jet distributions were estimated following the procedure in Sect. 6; no correction is applied to the simulation for b-jets. The uncertainty bands denote the impact of all uncertainties described in Sect. 7

Two conditional normalizing flows are used to parameterize $p_{\mathrm{sim}}(\vec{q}\,|p_{\mathrm{T}})$ for b-jets and non-b-jets, denoted by $p_{\mathrm{sig}}(\vec{q}\,|p_{\mathrm{T}})$ and $p_{\mathrm{bkg}}(\vec{q}\,|p_{\mathrm{T}})$ respectively. The c-jet and τ-jet fractions are predicted to be very small (1.9% and 0.2%, respectively), so they are treated together with the light-flavour jets in p_{bkg}. Comparisons between MC and neural estimates in the space of 1D marginal distributions of

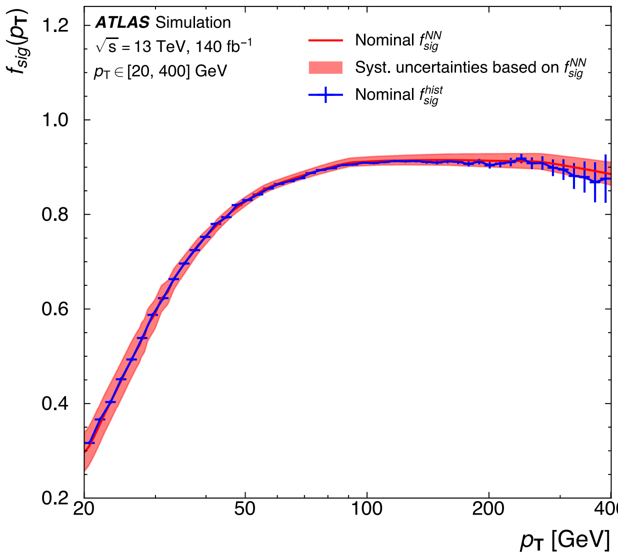

(a)

Fig. 4 The predicted b-jet purity, $f_{\text{sig}}(p_{\text{T}})$, after the event selection, is shown as a function of jet p_{T}. Both the binned MC ($f_{\text{sig}}^{\text{hist}}$) and neural purity ($f_{\text{sig}}^{\text{NN}}$) estimates are shown, with good agreement observed between the two. The uncertainty bands denote the impact of all uncertainties described in Sect. 7

$p_{\text{sim}}(\vec{q}, p_{\text{T}})$ are shown in Figures 5, 6, and 7. In all cases, good closure is observed.

5.4 NN training set-ups

The `PyTorch` library [103] is used to train the various neural networks (NN) in this analysis. Sample preparations, manipulations, and visualizations are performed with `NumPy` [104], `SciPy` [105], `Matplotlib` [106], `Pandas` [107], `Seaborn` [108], and `SciKit-HEP` [109].

Multi-layer perceptron for $f_{\text{sig}}(p_T)$

To approximate $f_{\text{sig}}(p_{\text{T}})$, a multi-layer perceptron composed of 6 hidden layers and 512 nodes per layer is used with the `LeakyReLU` activation function. Minimum-finding is performed with the `ADAMW` optimizer [110] with $\beta_0 = 0$, $\beta_1 = 0.9$ and a `Cosine Annealing` [111] learning rate schedule with an initial learning rate of 5×10^{-5} which decreases to 10^{-7}. The batch size is 1024.

Normalizing flows for $p_{\text{sig}}(\vec{q}|p_T)$ *and* $p_{\text{bkg}}(\vec{q}|p_T)$

Two conditional normalizing flows with identical hyperparameters are employed to approximate $p_{\text{sig}}(\vec{q}|p_{\text{T}})$ and $p_{\text{bkg}}(\vec{q}|p_{\text{T}})$. The base distribution is a uniform density over the unit cube. Neural spline flows [112] with 8 stacks of rational quadratic transforms, each with 12 bins, were found to provide good closure with the simulation. The training is performed over batches of 1024 samples with the `ADAMW` optimizer with the same settings as in the training of $f_{\text{sig}}(p_{\text{T}})$. The learning rate schedule used is the `Cosine Annealing` [111] scheduler with an initial learning rate of 10^{-4} that decreases to 10^{-7} over a total of 500 epochs.

PICNNs for f and g

The network architecture used for the calibration consists of two equally sized PICNNs [58,113,114], denoted by f and g, which are each formed of parallel convex and non-convex

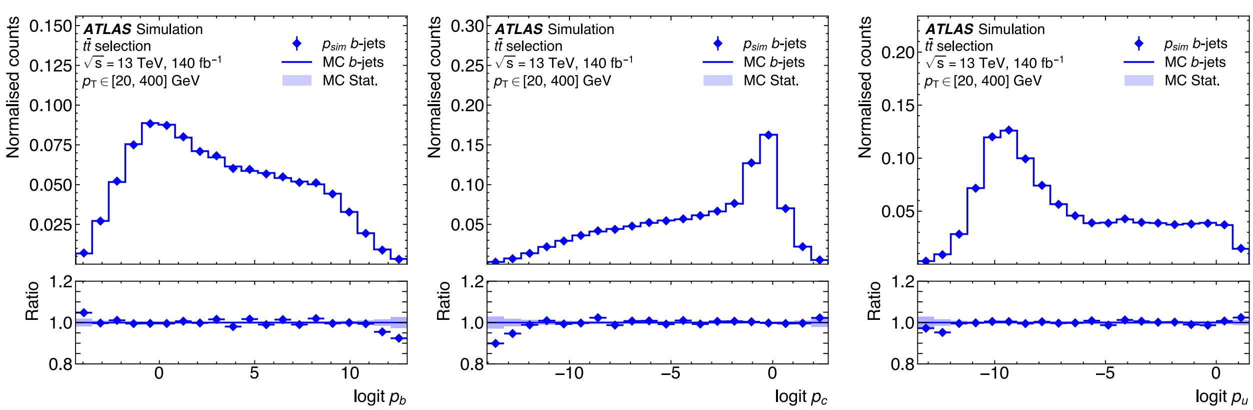

(a) (b) (c)

Fig. 5 Comparison of binned 1D marginals of p_{sig} between the simulation's predictions (MC) and the neural estimates (p_{sim}) integrated over jet p_{T} in the $t\bar{t}$ region: (**a**) logit p_b, (**b**) logit p_c, and (**c**) logit p_u. Only statistical uncertainties from the limited size of the sample used to fill the histograms are shown in the error bars

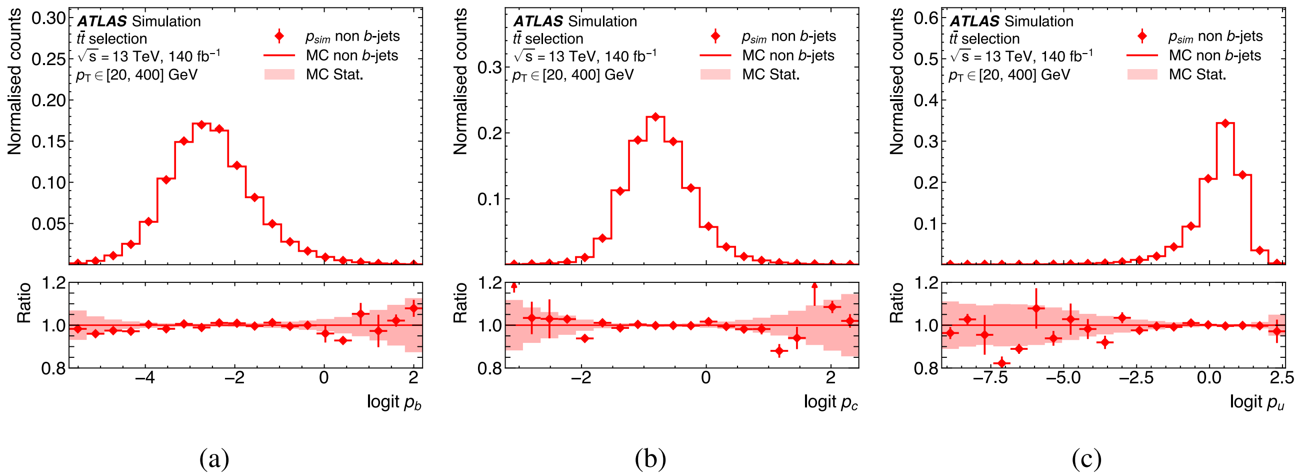

Fig. 6 Comparison of binned 1D marginals of p_{bkg} between the simulation's predictions (MC) and the neural estimates (p_{sim}) integrated over jet p_{T} in the $t\bar{t}$ region: (**a**) logit p_b, (**b**) logit p_c, and (**c**) logit p_u. Only statistical uncertainties from the limited size of the sample used to fill the histograms are shown in the error bars

Fig. 7 Comparison of binned 1D marginals between the simulation's predictions (MC) and the neural estimates (p_{sim}) integrated over jet p_{T} for (**a**) D_b^{DL1r} for p_{sig}, (**b**) D_c^{DL1r} for p_{sig}, (**c**) D_b^{DL1r} for p_{bkg}, and (**d**) D_c^{DL1r} for p_{bkg} in the $t\bar{t}$ region. Only statistical uncertainties from the limited size of the sample used to fill the histograms are shown in the error bars

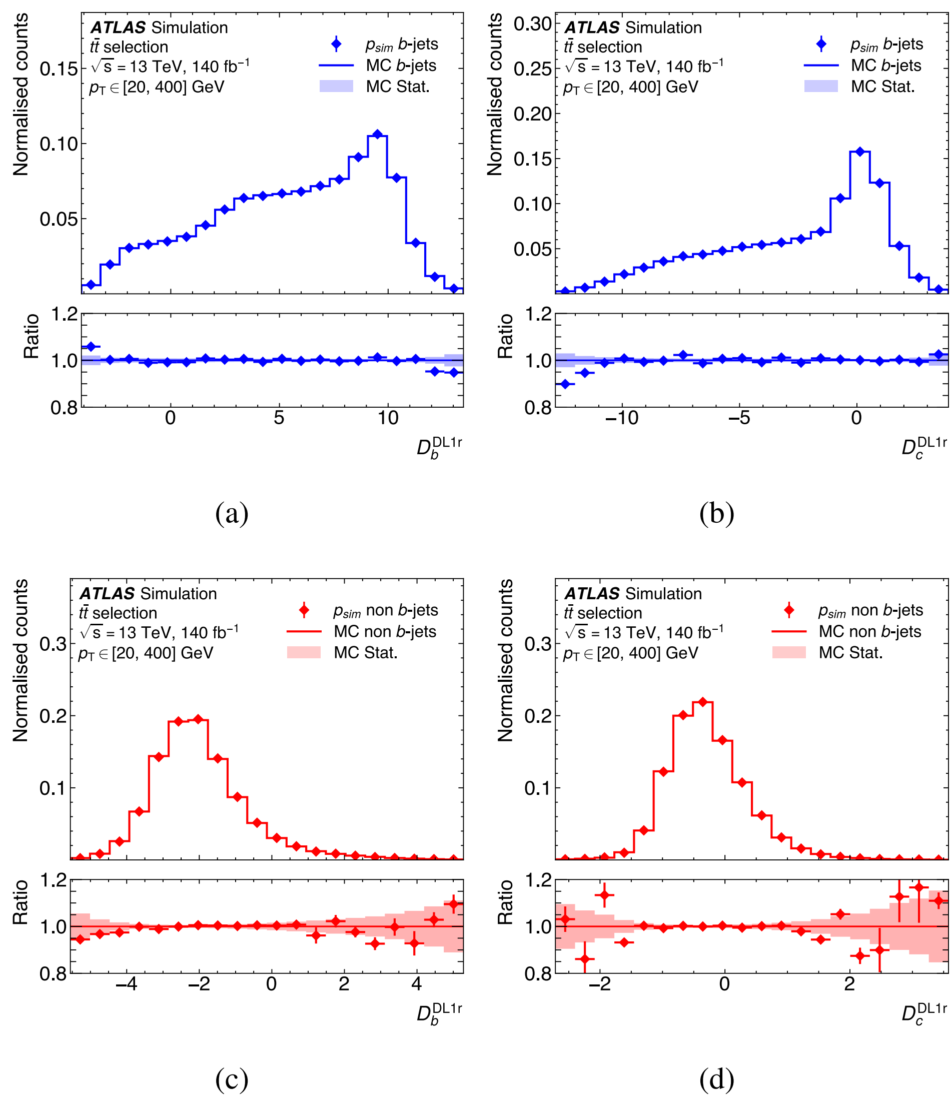

pathways [34]; after training, $\vec{\nabla} g$ yields the optimal transport map $\hat{T}_{p_\mathrm{T}}$. Both networks have a depth of 4 layers with 128 (8) neurons per layer in the convex (non-convex) pathway. After each convex layer except for the final layer, a zeroed softplus function[7] is used as the activation function, and for the non-convex layers, the CELU [115] activation function is used. The softplus function is also applied to enforce positive weights in the convex pathway. The ADAMW optimizer with $\beta_0 = 0$ and $\beta_1 = 0.9$ is used for minimum-finding, and a Cosine Annealing [111] learning rate schedule is chosen with an initial learning rate of 10^{-4} which decreases to 10^{-7}. The networks are trained for 500 epochs, each consisting of 512 training steps comprising 10 training batches for g and 4 iterations for f; training batches are built from 1024 jets.

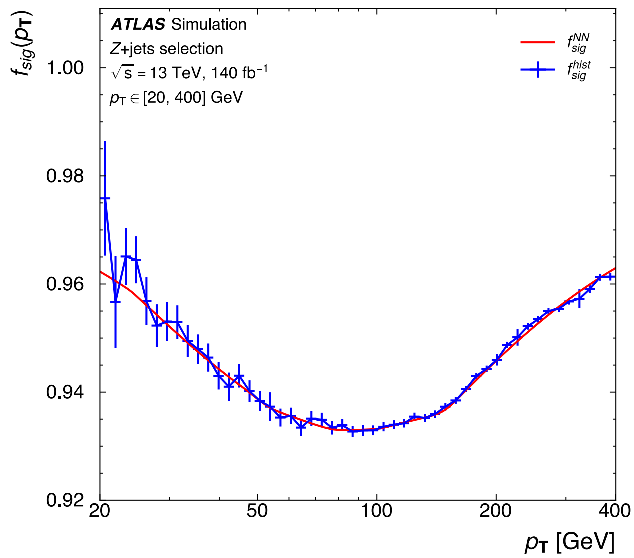

(a)

Fig. 8 The predicted non-b-jet purity, $f_\mathrm{sig}(p_\mathrm{T})$, after the Z+jets event selection, as a function of jet p_T. The predicted purity is shown from the binned ($f_\mathrm{sig}^\mathrm{hist}$) and neural ($f_\mathrm{sig}^\mathrm{NN}$) estimates. The uncertainty bars denote the statistical uncertainty on the binned estimate

6 Background shape estimate

The shape of the $\vec{q}$ distribution in background jets is dependent on a correct description of several aspects of the simulation that are difficult to model, such as the rates of light-hadron decays-in-flight and photon conversions; the detector resolution and efficiency of charged-particle tracking, which are also impacted by radiation damage over time; and the modelling of interactions between jet constituents and the detector material [116]. Indeed, in regions dominated by non-b-jets, a large discrepancy between data and simulation is observed, and this mismodelling of the non-b-jets would bias the b-jet calibration. To minimize this bias, a correction of the $\vec{q}$ shape versus p_T for non-b-jets is derived in such a region enriched in light-flavour jets and subsequently applied to non-b-jets in the $t\bar{t}$ phase space where the main b-jet calibration is performed.

A region primarily composed of Z+jets events is selected to yield a background-rich population of jets. The event selection largely follows that laid out in Ref. [21] but is summarized briefly here. Two same-flavour charged light leptons (ee or $\mu\mu$ pairs) are required, and the invariant mass $m_{\ell\ell}$ of this pair of leptons is required to lie near the Z-boson mass peak, $81 < m_{\ell\ell}/\mathrm{GeV} < 101$. The leading lepton must have $p_\mathrm{T} > 28$ GeV, and the single-lepton triggers must fire, as already described in Sect. 5.1. Due to poor modelling of events with low Z-boson transverse momentum, the p_T of the dilepton system must be greater than 50 GeV. At least one jet must be reconstructed with $p_\mathrm{T} > 20$ GeV and $|\eta| < 2.5$.

For this non-b-jet calibration, b-jets are treated as a background and are effectively subtracted to extract the transport maps for non-b-jets, following the description in Sect. 3. MC simulation predicts that the fraction of non-b-jets is above 93% across the full p_T range probed in the Z+jets phase space. The NN-based estimate used to describe the non-b-jet fraction vs jet p_T is shown in Fig. 8 and compared for validation purposes to its binned estimate. The ratio of charm jets to light-flavour jets in the Z+jets phase space is similar to that in the $t\bar{t}$ phase space, so these components are treated together in the background shape estimate: in Z+jets events approximately 8% of non-b-jets are charm jets, while this fraction is $\approx$ 6% in $t\bar{t}$ events. This difference in charm-jet fraction has a very small impact on the non-b-jet shape compared to the assessed uncertainties. The non-b-jet corrections are derived as optimal transportation maps between simulation and data for the leading jet (ordered by p_T) in each event.

In some regions, particularly at low jet p_T and high logit p_b, the predicted b-jet yield exceeds the data yield; this can occur if, for example, the $Z + b$ production cross-section is too large in simulation. Under these conditions, there is no transport map for non-b-jets that results in closure between corrected simulation and data. Since this portion of the $\vec{Q}$ space is ultimately dominated by uncertainties other than that on the shape of the non-b-jet background, a simple approach is used to enforce the existence of a solution: it is assumed that all jets in such regions are b-jets. A NN discriminator is trained to output a density ratio estimate of $r_b = f_b(p_\mathrm{T}) p^b_\mathrm{sim}(\vec{q}|p_\mathrm{T}) / p_\mathrm{data}(\vec{q}|p_\mathrm{T})$, where $f_b(p_\mathrm{T})$ is the predicted b-jet fraction and $p^b_\mathrm{sim}(\vec{q}|p_\mathrm{T})$ is the predicted b-jet distribution in the Z+jets phase space. If r_b is less than unity, jets in data are probabilistically down-sampled by $1 - r_b$ to subtract the b-jet background. Wherever this ratio is greater

[7] Softplus is defined as $\mathrm{softplus}(x) = \log(1+\mathrm{e}^x)$. For stability reasons, the zeroed softplus function, $\mathrm{softplus}^0(x) = \mathrm{softplus}(x) - \mathrm{softplus}(0)$, is used.

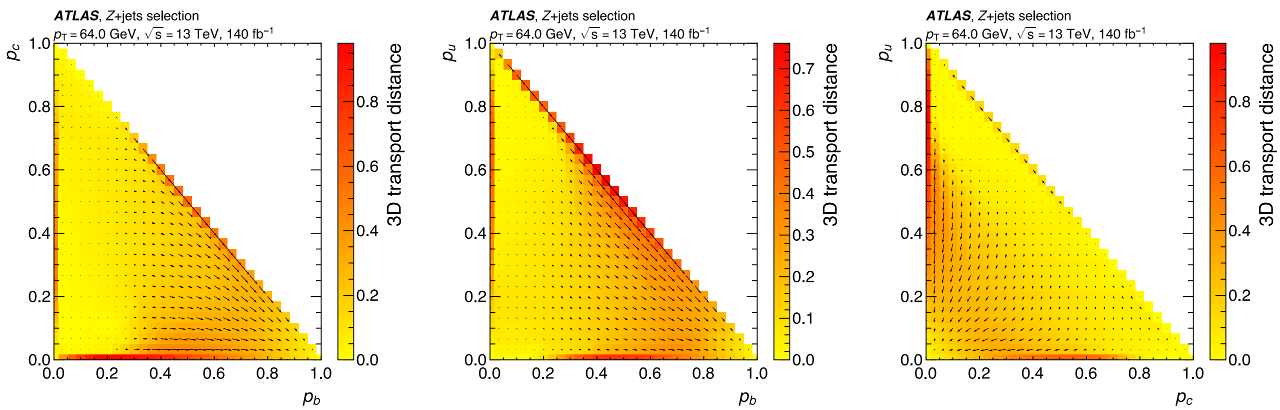

(a) (b) (c)

Fig. 9 2D slices of the calibration transport maps for non-b-jets with $p_{\mathrm{T}} = 64$ GeV: (**a**) p_b vs p_c, (**b**) p_b vs p_u, and (**c**) p_c vs p_u. Arrow directions and lengths correspond to the displacement of a non-b-jet at the arrow's origin, $\hat{T}$, needed to obtain closure between the data and simulation such that $\hat{T}_{\#}\ p_{\mathrm{sim}}(\vec{q}\,|p_{\mathrm{T}}) \approx p_{\mathrm{data}}(\vec{q}\,|p_{\mathrm{T}})$. The length of the arrows was normalized to avoid overlap and is indicated by the colour of the background. For each 2D map, the missing dimension is determined by requiring $\sum_i p_i = 1$.

than unity (i.e. the b-jet yield is predicted to be above the data yield), all data jets are removed. This amounts to enforcing $f_b(p_{\mathrm{T}})p^b_{\mathrm{sim}}(\vec{q}\,|p_{\mathrm{T}}) = p_{\mathrm{data}}(\vec{q}\,|p_{\mathrm{T}})$, i.e. assuming all jets in data in such cases are b-jets.

Figure 9 shows the 2D transport maps in $\vec{p}$ space for non-b-jets, evaluated at the mean observed jet p_{T} in the $t\bar{t}$ phase space, $\langle p_{\mathrm{T,data}}\rangle_{t\bar{t}} = 64$ GeV; to obtain these maps, the p_i are converted into q_i, the calibration is applied to obtain an updated set q'_i, and then these are translated back into altered p'_i to determine the displacement with respect to the original p_i. Figures 10 and 11 show comparisons between simulated and observed flavour observables in the Z+jets region after the non-b-jet corrections are applied. Good agreement is observed between the data and corrected simulation in the regions for which the non-b-jet background is important in the $t\bar{t}$ phase space, as can be seen in Fig. 3. As discussed in Sect. 7, the full difference between the distributions of $p_{\mathrm{bkg}}(\vec{q}\,|p_{\mathrm{T}})$ for uncalibrated and calibrated non-b-jets in the $t\bar{t}$ phase space is taken as a systematic uncertainty of the b-jet calibration maps.

7 Uncertainties

Several uncertainties in the optimal calibration maps are estimated by deriving alternative maps and comparing them with the nominal calibration. Statistical uncertainties are approximated by sampling the observed data with replacement ("bootstrapping") 33 times and rederiving the calibration maps – one for each bootstrap. Analyses utilizing this calibration can estimate the impact of its statistical uncertainty on their results by applying each alternative calibration, comparing these outcomes with the nominal, and considering the combined impact of these uncorrelated variations divided by $\sqrt{N_{\mathrm{bootstraps}}}$. The statistical uncertainties, as presented in Sect. 8, in most cases are small compared to the total uncertainty.

Systematic uncertainties are assessed by altering the simulation in a number of ways that impact $f_{\mathrm{sig}}(p_{\mathrm{T}})$ and $p_{\mathrm{bkg}}(\vec{q}\,|p_{\mathrm{T}})$ in Eq. (3). Each alternative simulation hypothesis results in a new calibration map, and, as with the statistical uncertainties, each set of corrections can be applied to estimate the corresponding uncertainty in the parameters of interest in a particular analysis. The systematic uncertainties assessed for $f_{\mathrm{sig}}(p_{\mathrm{T}})$ are those used in previous flavour-tagging calibration measurements using similar event selection criteria [23]. Notably, $p_{\mathrm{sig}}(\vec{q}\,|p_{\mathrm{T}})$ is *not* varied: a single normalizing-flow approximation of this density is used for all systematic variations.

Rather than training a new NN approximation of $f_{\mathrm{sig}}(p_{\mathrm{T}})$ for each variation, only a correction Δ to the nominal logit $f_{\mathrm{sig}}(p_{\mathrm{T}})$ is approximated with a secondary NN:

$$\mathrm{logit}\, f^{\mathrm{variation}}_{\mathrm{sig}}(p_{\mathrm{T}}) = \mathrm{logit}\, f^{\mathrm{nominal}}_{\mathrm{sig}}(p_{\mathrm{T}}) + \Delta^{\mathrm{variation}}(p_{\mathrm{T}})$$

This was found to converge more reliably than retraining an entirely new approximation of $f_{\mathrm{sig}}(p_{\mathrm{T}})$ for each variation.

The uncertainties with the most significant impact on $f_{\mathrm{sig}}(p_{\mathrm{T}})$ are evaluated in this measurement. Of the assessed uncertainties, those that had more than a 2% impact on the total $f_{\mathrm{sig}}(p_{\mathrm{T}})$ systematic uncertainty in any jet p_{T} region were retained. The retained systematic uncertainties are the ISR, FSR, and alternative parton-shower model uncertainties for $t\bar{t}$ production, as described in Sect. 5.2; the jet energy scale (JES) uncertainties from the η-intercalibration procedure, the jet flavour response for gluon- and b-jets, the jet flavour composition, and the jet-pile-up subtraction proce-

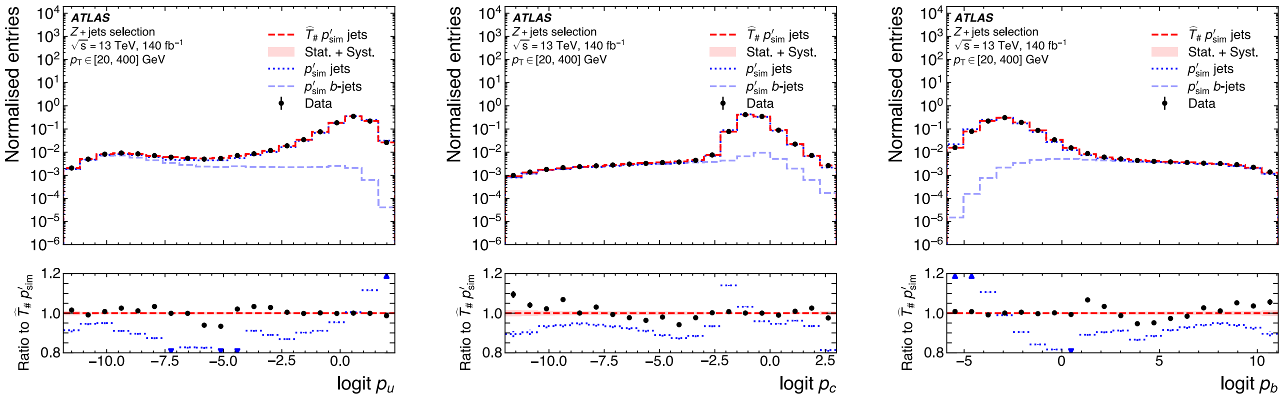

(a) (b) (c)

Fig. 10 Comparisons between the observed data, uncalibrated simulation, p'_{sim}, and corrected simulation, $\hat{T}_{\#}\,p'_{\mathrm{sim}}$, of the Z+jets selection in (**a**) logit p_u, (**b**) logit p_c, and (**c**) logit p_b. Both the non-b-jet and b-jet components of the simulation are included in the predicted yields. Only statistical uncertainties from the limited sample size of the data and simulation used to fill the histograms are shown in the error bars. In the b-jet calibration, the full difference between p'_{sim} and the corrected non-b-jets shape is taken as a systematic uncertainty. Blue triangles in the ratio panel indicate that the ratio is beyond the limits of the y-axis range

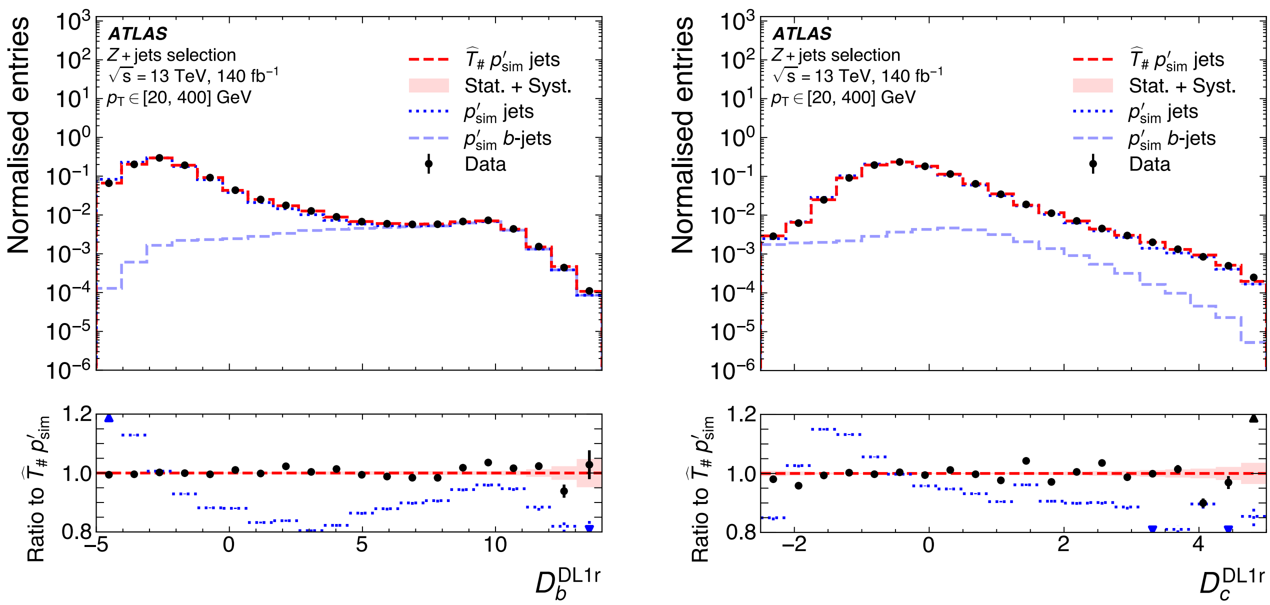

(a) (b)

Fig. 11 Comparisons between the observed data, uncalibrated simulation, p'_{sim}, and corrected simulation, $\hat{T}_{\#}\,p'_{\mathrm{sim}}$, of the Z+jets selection in (**a**) D_b^{DL1r} and (**b**) D_c^{DL1r}. Both the non-b-jet and b-jet components of the simulation are included in the predicted yields. Only statistical uncertainties from the limited sample size of the data and simulation used to fill the histograms are shown in the error bars. In the b-jet calibration, the full difference between p'_{sim} and the corrected non-b-jets shape is taken as a systematic uncertainty. Blue triangles in the ratio panel indicate that the ratio is beyond the limits of the y-axis range

dure; and uncertainties in the jet energy resolution (JER) eigenvector [32] for the leading jet. Uncertainties that were determined to have a negligible impact include all other JES and JER uncertainties; uncertainties due to parton distribution functions; uncertainties from charged-lepton triggering, reconstruction, identification, and isolation efficiencies; and uncertainties related to charged-lepton momentum resolutions. The uncertainty due to limited-size simulated samples was also determined to be negligible. It was found that the neglected uncertainties did not meaningfully change the

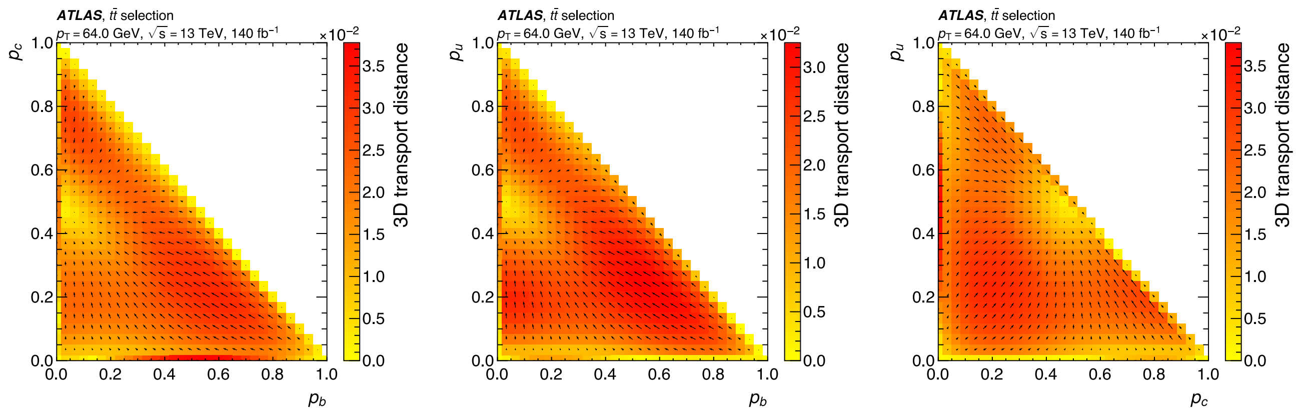

(a) (b) (c)

Fig. 12 2D slices of the calibration transport maps for b-jets with the mean jet p_T in the $t\bar{t}$ phase space, $\langle p_{T,\text{data}} \rangle_{t\bar{t}} = 64$ GeV: (**a**) p_b vs p_c, (**b**) p_b vs p_u, and (**c**) p_c vs p_u. Arrow directions and lengths correspond to the displacement of a b-jet at the arrow's origin, $\hat{T}$, needed to obtain closure between the data and simulation such that $\hat{T}_{\#}\ p_{\text{sim}}(\vec{q}\,|p_T) \approx p_{\text{data}}(\vec{q}\,|p_T)$. The length of the arrows was normalized to avoid overlap and is indicated by the colour of the background. For each 2D map, the missing dimension is determined by requiring $\sum_i p_i = 1$

$f_{\text{sig}}(p_T)$ uncertainty covariance when it was calculated for ten p_T bins.

In most cases, systematic uncertainties comprise two variations, "up" and "down", which are symmetrized around the nominal prediction: the magnitude of the uncertainty v is set to $|v| = |v_{\text{up}} - v_{\text{down}}|/2$. This symmetrized variation is generally assumed to correspond to the standard deviation of a nuisance parameter prior or constraint.

An additional uncertainty in the estimate of the non-b-jet background is derived by correcting $p_{\text{bkg}}(\vec{q}\,|p_T)$ in the Z+jets phase space, as described in Sect. 6. The difference between the b-jet calibration maps before and after applying these corrections to non-b-jets in the $e\mu\nu\nu bb$ measurement region is taken as a systematic uncertainty. For each other systematic variation, the expected impact on the non-b-jet background shape was found to be negligible compared to this difference.

In order to illustrate the total uncertainty of the calibrated simulation in this study, each uncertainty's impact on the prediction is assessed, and the total uncertainty is calculated in the Gaussian approximation as the quadrature sum of all uncertainties.

8 Calibration results for *b*-jets

With continuous estimates of the b-jet purity as a function of jet p_T, $f_{\text{sig}}(p_T)$, and with the b-jet and background jet $\vec{q}$ densities conditional on p_T, $p_{\text{sig}}(\vec{q}\,|p_T)$ and $p_{\text{bkg}}(\vec{q}\,|p_T)$, the optimal calibration maps of the jet flavour probabilities are derived from the simulated and observed jets. In the following figures, $p'_{\text{sim}}(\vec{q}, p_T)$ is obtained from a simulated sample 30 times larger than the data sample.

8.1 Extracted optimal calibration maps and comparisons with data

Figure 12 shows the 2D transport maps for b-jets evaluated at the mean p_T in data in the $t\bar{t}$ region, $\langle p_{T,\text{data}} \rangle_{t\bar{t}} = 64$ GeV. As in Sect. 6, the p_i are converted into q_i, the calibration applied, and the resulting q'_i translated back into p'_i to calculate the calibration displacement with respect to the original p_i.

Similarly, the mean 1D displacements for the nominal calibration, $\delta\vec{q}_i \equiv (\hat{T}_{p_T}\,\vec{q} - \vec{q})_i$, $i \in (b, c, u)$, for each of the three components is shown in Fig. 13 as a function of p_T. In the range $30 < p_T/\text{GeV} < 100$ the average correction is modest ($|\delta q_i| \lesssim 0.1$) but grows to be as large as $|\delta q_i| \sim 0.5$–0.75 at low and high p_T. In particular, the mean logit p_b correction is negative for all p_T in the calibration range, while for logit p_u and logit p_c the mean correction is always positive: the tagging algorithm slightly overstates its separating power between b- and non-b-jets in data, especially at low- and high-p_T.

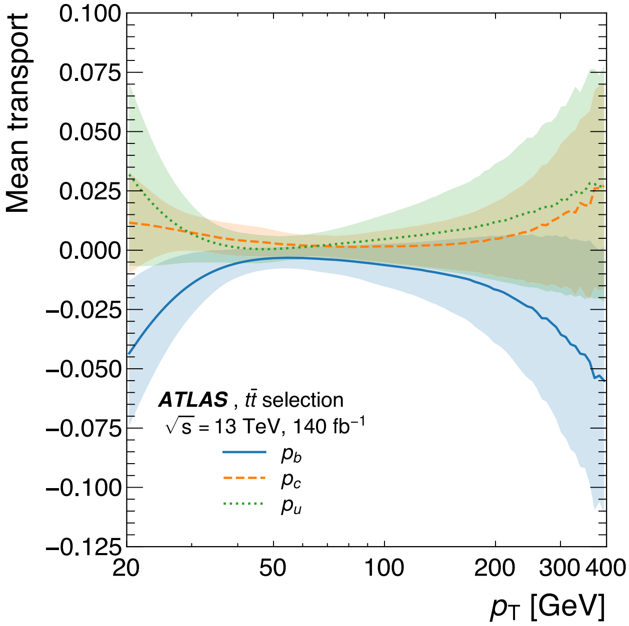

Fig. 13 The mean and standard deviation of the 1D transport displacements δq_i as a function of p_T for b-jets in the $t\bar{t}$ phase space. The solid lines and shaded areas respectively indicate the mean and standard deviation of the 1D displacements as a function of p_T. Only the nominal transport map is shown, and dimensions in $\vec{q}$ space that are not shown are marginalized over p'_{sim}

Figures 14, 15, and 16 compare distributions from jets in data and simulation, before and after calibrations are applied, for $\vec{q}$, the flavour-tagging probabilities, and DL1r b- and c-tagging variants, respectively. In all cases, the calibrated distributions are in agreement with the data.

8.2 Closure tests for common D_b^{DL1r} operating points

Given the optimal transport maps, efficiencies can be obtained for a given selection built from the jet flavour probabilities and compared with the uncalibrated simulation and LHC data: if the simulation has been calibrated adequately, efficiencies in simulation should match those in data. In this section the four common D_b^{DL1r} selections used by the ATLAS Collaboration during LHC Run 2 (defined as the 85%, 77%, 70%, and 60% efficiency operating points derived in SM $t\bar{t}$ events with at least one prompt final-state lepton) are considered [15]. These operating points amount to requiring that the jet D_b^{DL1r} score is above 0.67, 2.20, 3.25, or 4.57, respectively. The b-jet efficiencies in the uncalibrated and calibrated simulations are compared in Fig. 17 as a function of the jet transverse momentum for the same operating points, highlighting the impact of the calibration in correcting the simulation for these selections. The absolute and relative uncertainties on the b-tagging efficiency vs the jet p_T for these operating points are shown in Fig. 18.

After applying the calibration, the probability that simulated jets satisfy some selection criterion should match the probability observed in data. The b-tagging selection probabilities in simulation and data are compared as a function of the jet p_T in Fig. 19; the corrected simulation matches the observed data well within the calibration uncertainties.

Similarly, the measured b-jet efficiency, $\varepsilon_{\text{sig,data}}$, of a selection can be defined as the fraction of jets passing the selection after accounting for the background prediction:

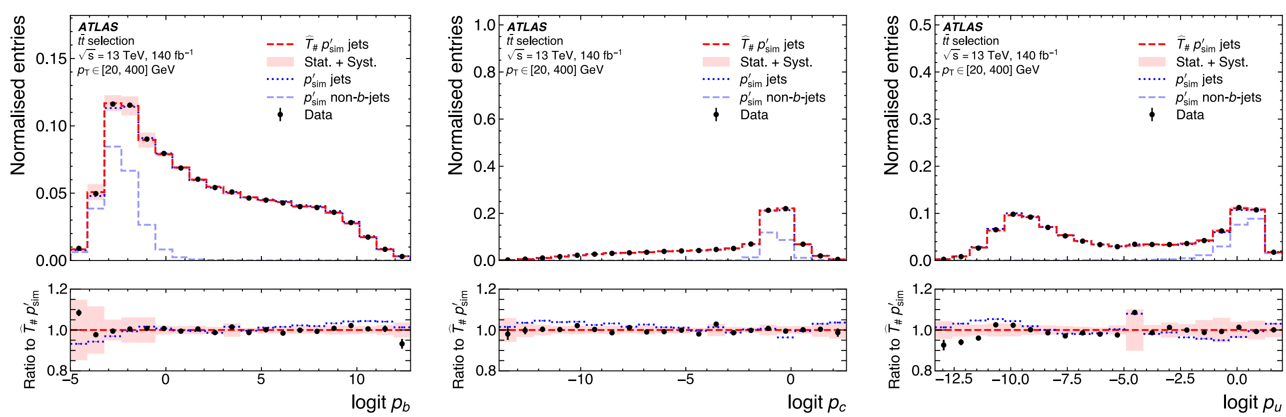

(a) (b) (c)

Fig. 14 Comparisons between the observed data, uncalibrated simulation, p'_{sim}, and corrected simulation, $\hat{T}_\# p'_{\text{sim}}$, for (**a**) logit p_b, (**b**) logit p_c, and (**c**) logit p_u. Both the non-b-jet and total (non-b-jet + b-jet) normalized yields are shown for simulation. The uncertainty band of the corrected simulation denotes the impact of all uncertainties described in Sect. 7 on the calibration maps. All marginals are shown for the p_T-corrected density $p'_{\text{sim}}(\vec{q}, p_T) = p_{\text{sim}}(\vec{q}|p_T)p_{\text{data}}(p_T)$. Non-$b$-jets in simulation were corrected using transport maps derived in Sect. 6

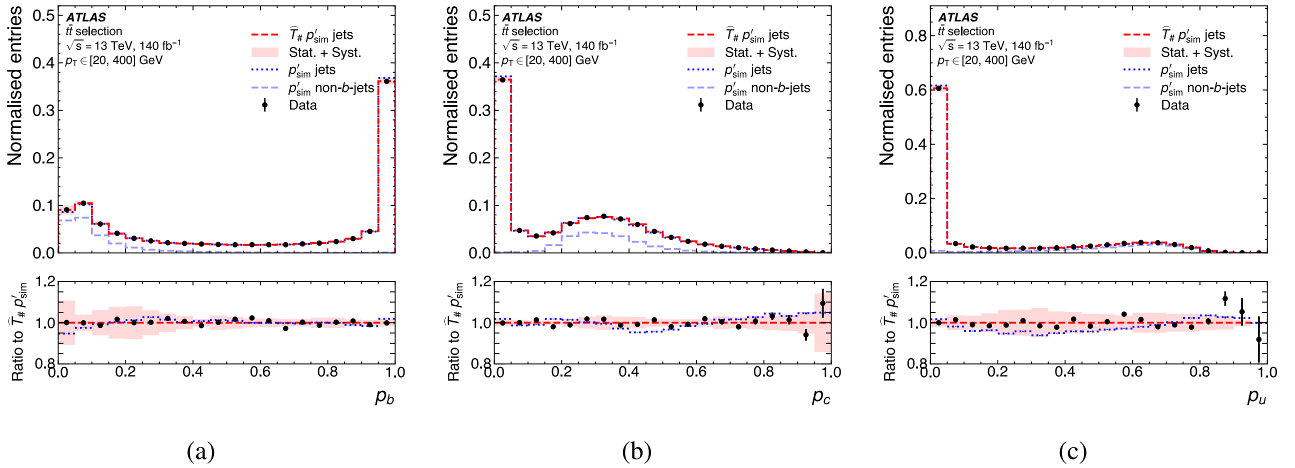

Fig. 15 Comparisons between the observed data, uncalibrated simulation, p'_{sim}, and corrected simulation, $\hat{T}_{\#} p'_{\mathrm{sim}}$, for (**a**) p_b, (**b**) p_c, and (**c**) p_u. Both the non-b-jet and total (non-b-jet + b-jet) normalized yields are shown for simulation. The uncertainty band of the corrected simulation denotes the impact of all uncertainties described in Sect. 7 on the calibration maps. All marginals are shown for the p_{T}-corrected density $p'_{\mathrm{sim}}(\vec{q}, p_{\mathrm{T}}) = p_{\mathrm{sim}}(\vec{q}|p_{\mathrm{T}})p_{\mathrm{data}}(p_{\mathrm{T}})$. Non-$b$-jets in simulation were corrected using transport maps derived in Section 6

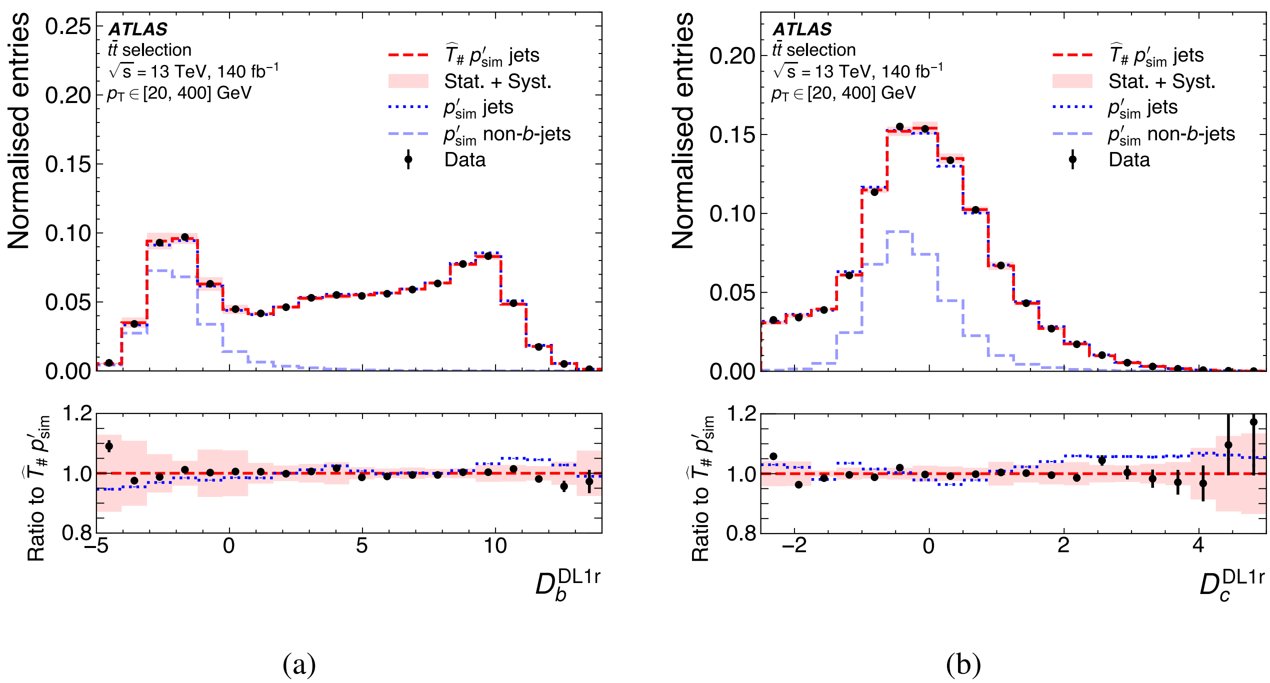

Fig. 16 Comparisons between the observed data, uncalibrated simulation, p'_{sim}, and corrected simulation, $\hat{T}_{\#} p'_{\mathrm{sim}}$, for (**a**) D_b^{DL1r} and (**b**) D_c^{DL1r}. Both the non-b-jet and total (non-b-jet + b-jet) normalized yields are shown for simulation. The uncertainty band of the corrected simulation denotes the impact of all uncertainties described in Sect. 7 on the calibration maps. All marginals are shown for the p_{T}-corrected density $p'_{\mathrm{sim}}(\vec{q}, p_{\mathrm{T}}) = p_{\mathrm{sim}}(\vec{q}|p_{\mathrm{T}})p_{\mathrm{data}}(p_{\mathrm{T}})$. Non-$b$-jets in simulation were corrected using transport maps derived in Sect. 6

$$\varepsilon_{\mathrm{sig,data}} = \frac{N^{\mathrm{pass}}_{\mathrm{sig,data}}}{N_{\mathrm{sig,data}}},$$

where $N_{\mathrm{sig,data}}$ is the number of b-jets in data, and $N^{\mathrm{pass}}_{\mathrm{sig,data}}$ is the number of those that pass some operating point selection. By dividing the numerator and denominator by the total number of jets in data, this efficiency can be approximated by taking $f_{\mathrm{sig}}(p_{\mathrm{T}})$ and the probability of a background jet to satisfy the operating point, $\varepsilon_{\mathrm{bkg,sim}}$, from simulation after the correction described in Sect. 6,

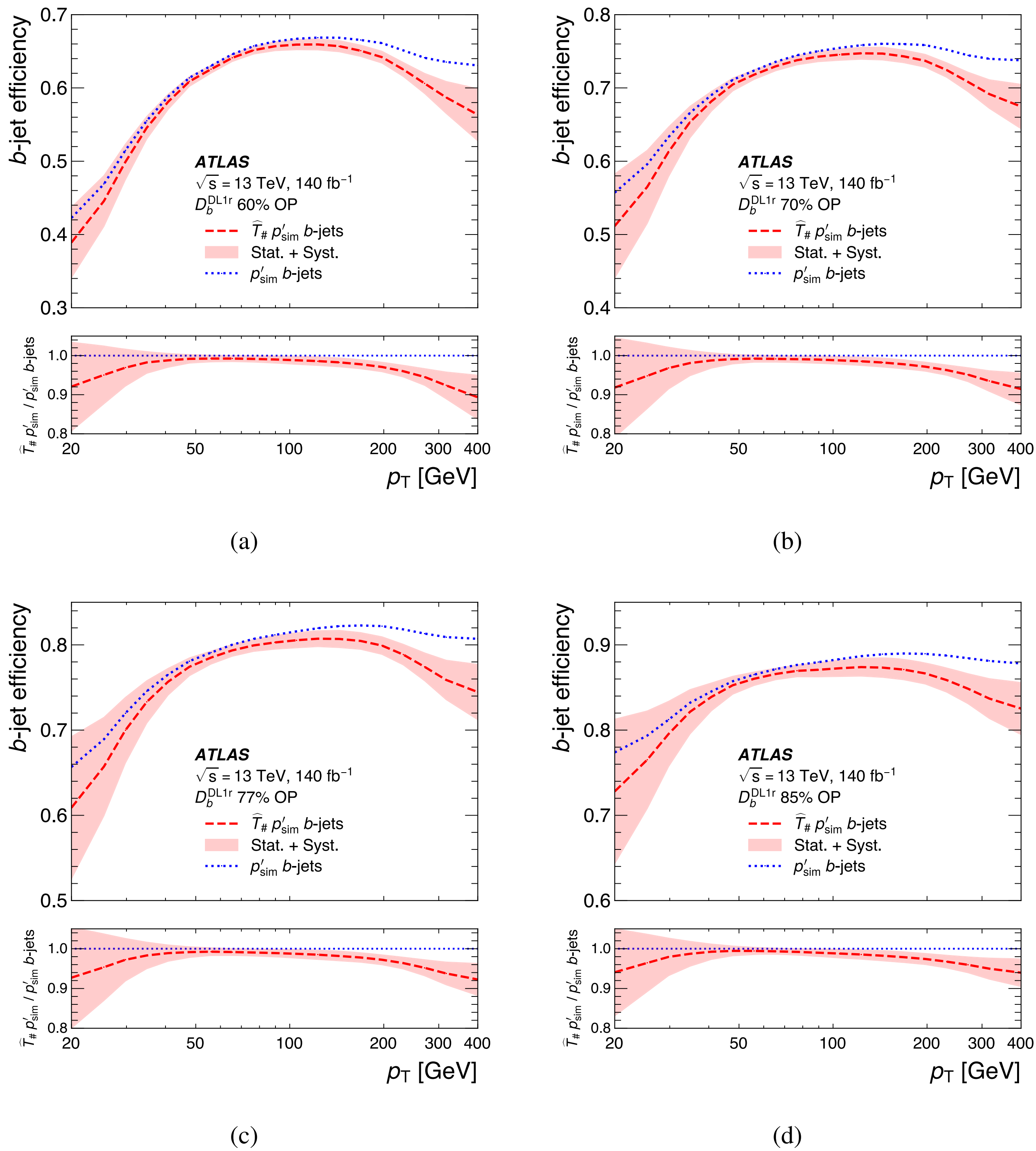

Fig. 17 Comparison between D_b^{DL1r} b-jet efficiencies predicted by the nominal simulation, p'_{sim}, and the calibrated simulation, $\hat{T}_{\#}\,p'_{\text{sim}}$. The D_b^{DL1r} (**a**) 60%, (**b**) 70%, (**c**) 77%, and (**d**) 85% efficiency operating points are shown. The uncertainty band of the calibrated simulation denotes the impact of all uncertainties described in Sect. 7 on the calibration maps.

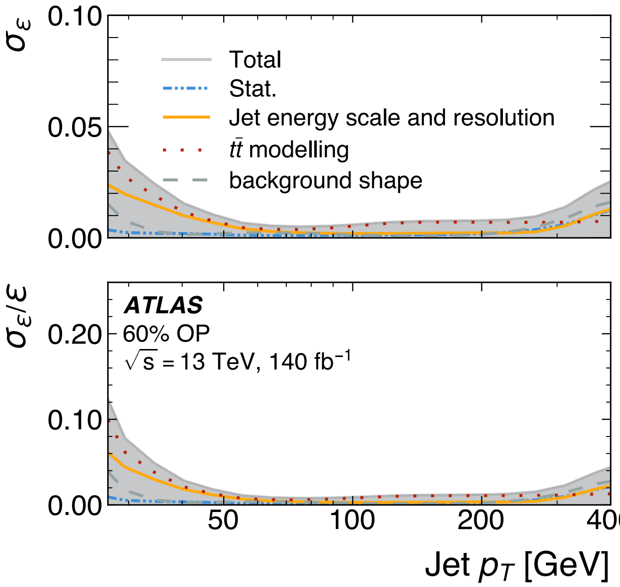

(a)

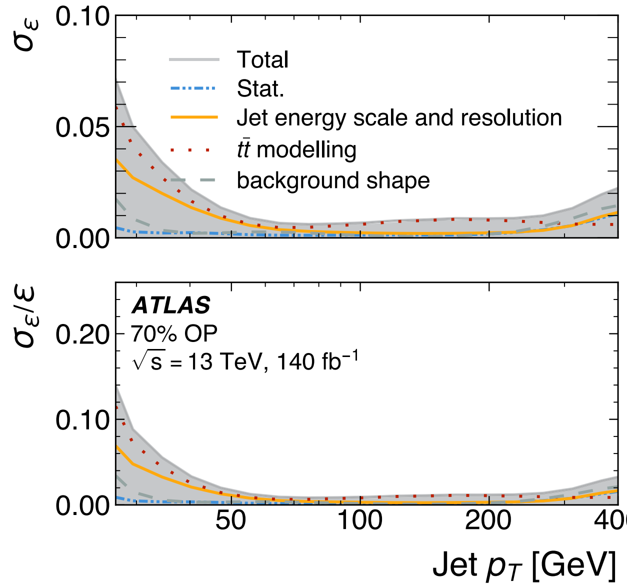

(b)

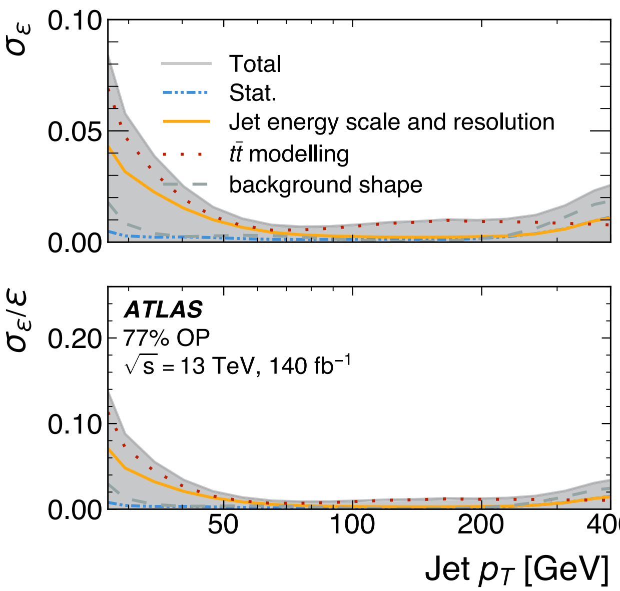

(c)

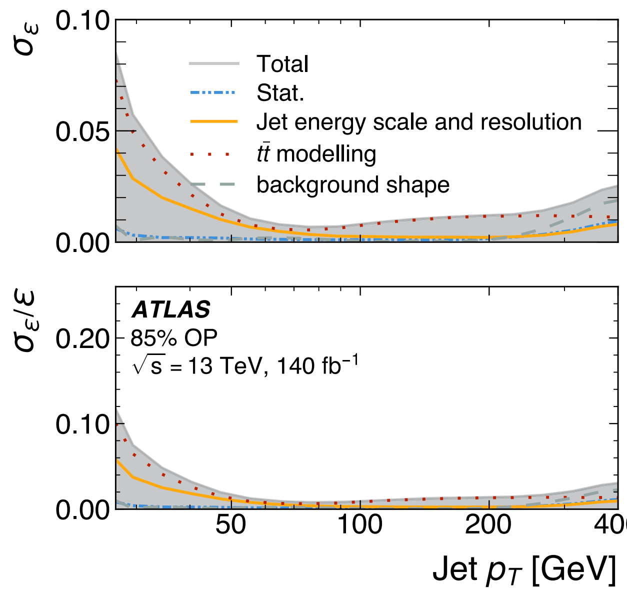

(d)

Fig. 18 Uncertainty breakdown of the calibrated simulation, $\hat{T}_{\#} p'_{\text{sim}}$, for D_b^{DL1r} b-jet efficiency versus jet p_{T} for various b-tagging operating points. The top panel shows the absolute uncertainties, while the bottom panel shows the relative uncertainties. The (**a**) 60%, (**b**) 70%, (**c**) 77%, and (**d**) 85% efficiency operating points are shown. The grey uncertainty band of the calibrated simulation denotes the impact of all uncertainties described in Sect. 7 on the calibration maps

$$\varepsilon_{\text{sig}} = \frac{f_{\text{data}}^{\text{pass}} - (1 - f_{\text{sig}}(p_{\text{T}}))\varepsilon_{\text{bkg}}}{f_{\text{sig}}(p_{\text{T}})},$$

where $f_{\text{data}}^{\text{pass}}$ is the fraction of jets in data that pass the operating point selection. In order to validate the methodology used to derive the calibration maps, Fig. 20 compares the measured efficiency in the $t\bar{t}$ phase space with the predicted efficiencies before and after calibrations are applied. Good

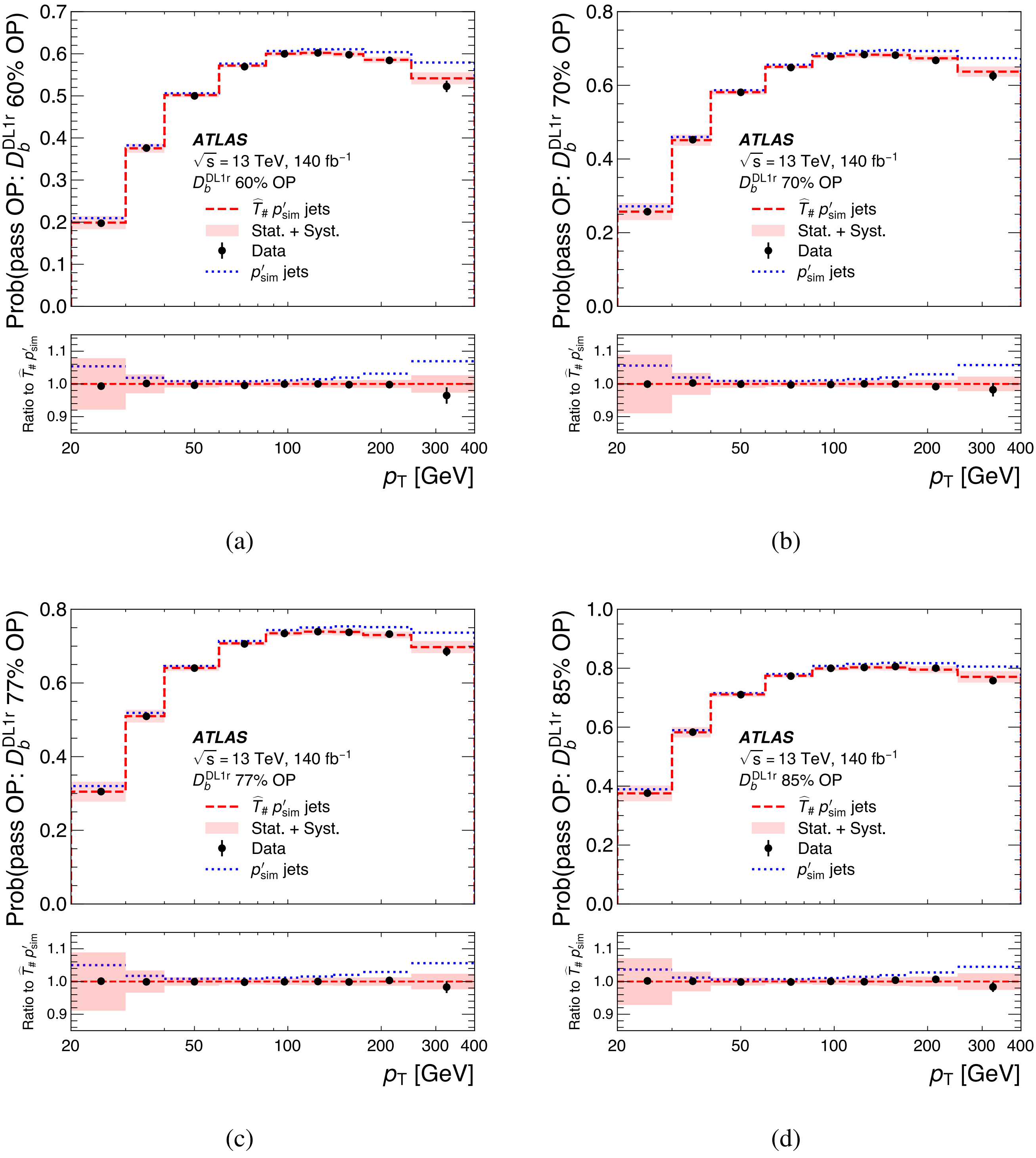

Fig. 19 Comparison of the probability of a selected jet to pass various D_b^{DL1r} operating points, between data, the nominal simulated prediction, p'_{sim}, and the calibrated simulation, $\hat{T}_{\#}p'_{\mathrm{sim}}$, as a function of the jet p_{T}. The D_b^{DL1r} (**a**) 60%, (**b**) 70%, (**c**) 77%, and (**d**) 85% efficiency operating points are shown. The uncertainty band of the calibrated simulation shows the impact of all uncertainties described in Sect. 7 on the calibration maps. Non-*b*-jets in simulation were corrected using transport maps derived in Sect. 6 and are included in curves for the nominal and calibrated simulation

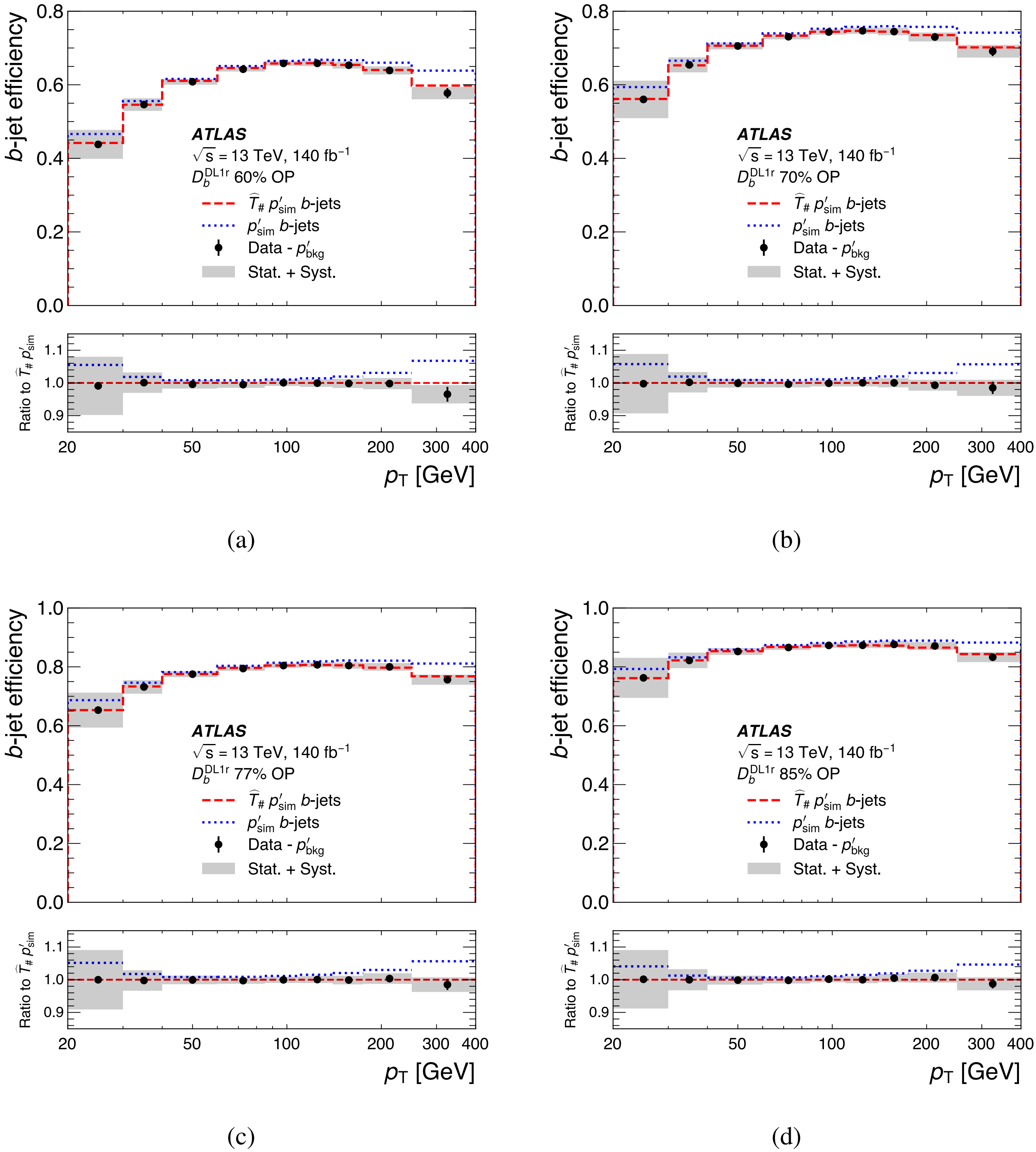

Fig. 20 Comparison of b-jet efficiencies at different D_b^{DL1r} operating points, between the nominal simulation, p'_{sim}, the calibrated simulation, $\hat{T}_\# p'_{\text{sim}}$, and background-subtracted data (Data $- p'_{\text{bkg}}$), versus jet p_T. The D_b^{DL1r} efficiency operating points shown are (**a**) 60%, (**b**) 70%, (**c**) 77%, and (**d**) 85%. The uncertainty band of Data $- p'_{\text{bkg}}$ is calculated by applying each variation of $(1 - f_{\text{sig,variation}}) \cdot p'_{\text{bkg,variation}}$, where the variations used are described in Sect. 7. Non-b-jets in simulation were corrected using the transport maps derived in Sect. 6

agreement between the measured efficiencies and the calibrated efficiencies is observed across the full p_T range.

Finally, Fig. 21 shows a comparison of binned and neural estimates of the b-tagging efficiency scale factors versus p_T, where the binned scale factors were derived by applying the

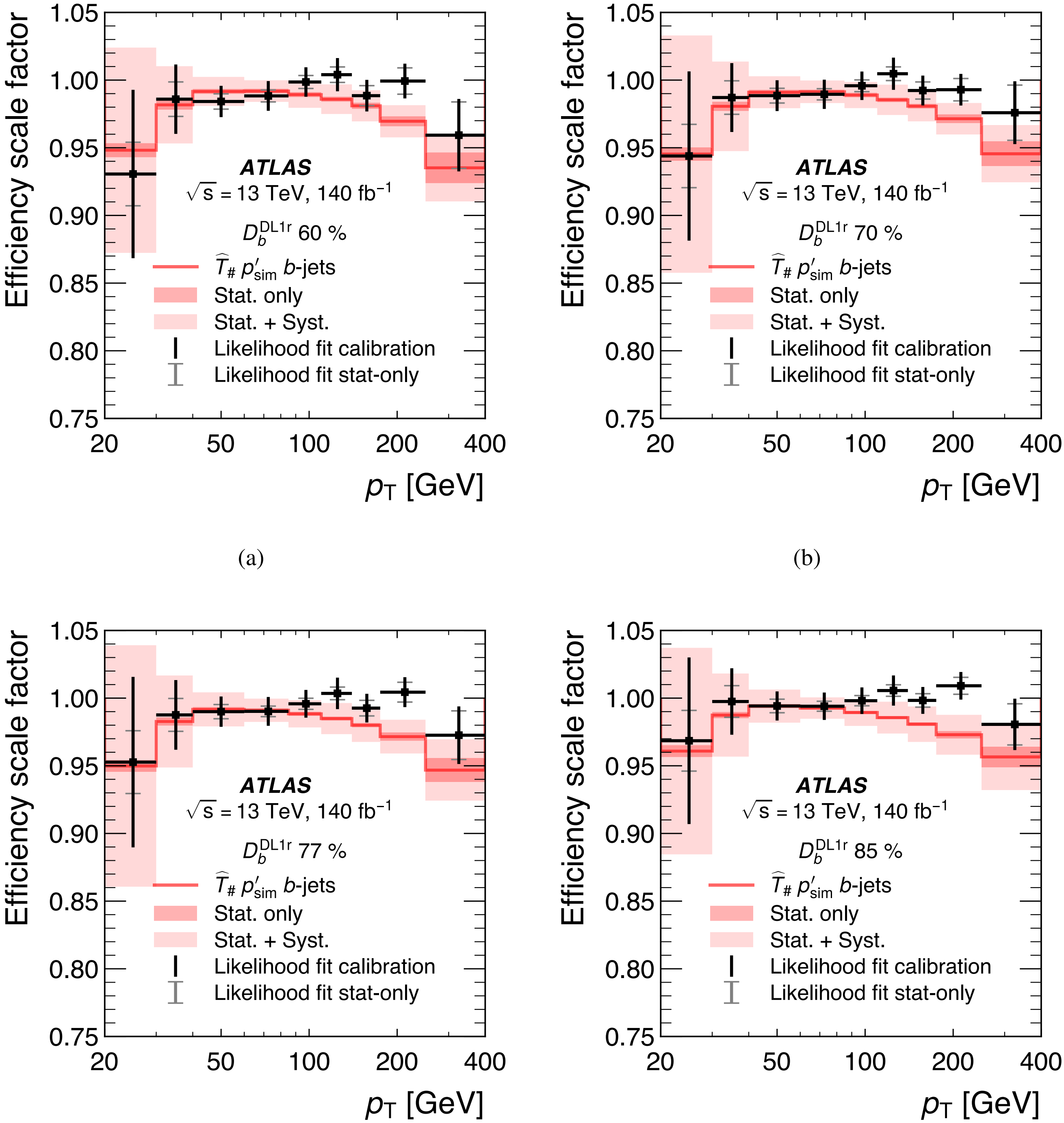

(a) (b) (c) (d)

Fig. 21 Comparison between D_b^{DL1r} efficiency scale factors derived using the calibration transport maps and a likelihood-fit-based binned scale-factor approach for the (**a**) 60%, (**b**) 70%, (**c**) 77%, and (**d**) 85% efficiency operating points. The pale red uncertainty band denotes the total impact of all uncertainties described in Sect. 7 on the transport-based scale factors. It should be noted that the optimal transport calibration comprises a single, general correction that is universal in the sense that all operating points ought to be calibrated after its application; the likelihood-fit-based calibrations were derived individually for particular operating points. The "likelihood fit calibration" curve follows the method for measuring the *b*-tagging efficiency described in Ref. [23], in which the jet flavour fractions are extracted jointly with the *b*-tagging efficiency. The grey serifs attached to the error bars of the likelihood-based calibration scale factors show their statistical uncertainties

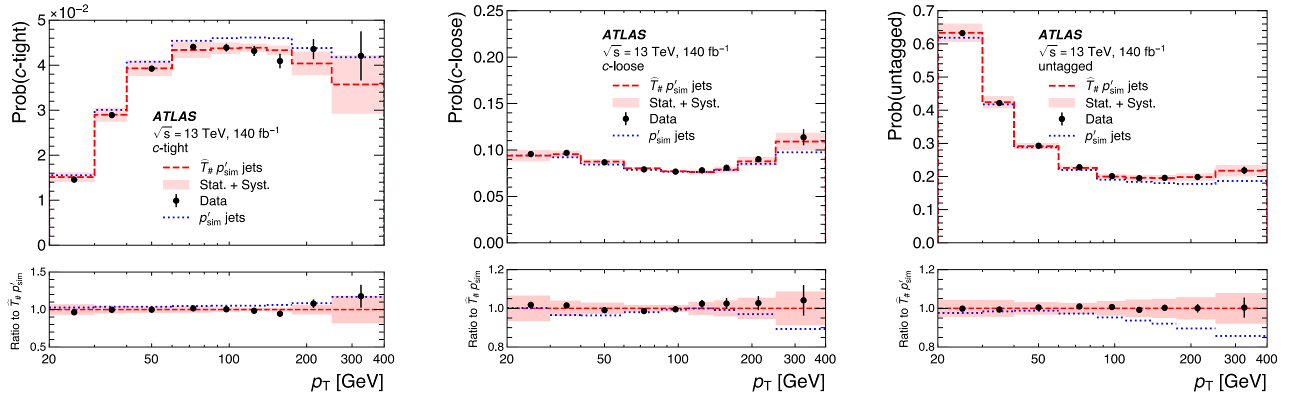

(a) (b) (c)

Fig. 22 Comparison of the probability that a selected jet passes various $VH, H \to cc$ c-tagging selections, between data ("Data"), the nominal simulated prediction, p'_{sim}, and the calibrated simulation, $\hat{T}_{\#}p'_{\text{sim}}$, as a function of the jet p_{T} in the $t\bar{t}$ phase space. The (**a**) *c-tight*, (**b**) *c-loose*, and (**c**) *untagged* c-tagging categories are shown. The uncertainty band of the corrected simulation denotes the impact of all uncertainties described in Sect. 7 on the calibration maps. Error bars denote statistical uncertainties. All efficiencies are shown for the p_{T}-corrected density $p'_{\text{sim}}(\vec{q}, p_{\text{T}}) = p_{\text{sim}}(\vec{q}|p_{\text{T}})p_{\text{data}}(p_{\text{T}})$. Non-$b$-jets in simulation were corrected using transport maps derived in Sect. 6 and are included in curves for the nominal and calibrated simulation

likelihood-fit approach in Ref. [23] to each operating point individually. The two calibrations have similar precision, but two important differences should be noted. First, the optimal transport calibrations are inherently continuous both versus the flavour-tagging discriminant and versus p_{T} since they are approximated as neural networks. This requirement reduces the statistical uncertainty compared to the binned calibration, which has no continuity imposed. Second, the likelihood-fit approach for measuring efficiencies in p_{T} bins includes in situ constraints on the jet flavour fractions and therefore has smaller uncertainties for backgrounds in the $t\bar{t}$ phase space. In particular, this mitigates the dominant uncertainties from the modelling of $t\bar{t}$ production; the transport-based calibration does not currently benefit from this in situ constraint.

8.3 Closure tests for charm-tagging selections

With continuous calibration maps derived for the full tagging probability space, the efficiency of more sophisticated selections based on a jet's flavour probability scores should also be properly calibrated. To illustrate this, the b-jet efficiencies of selections used in the recent ATLAS search for $H \to c\bar{c}$ decays via VH production [14] are compared between simulation, simulation corrected by the transport calibration, and observed data. Only jets that do not satisfy the DL1r 70% b-tagging efficiency operating point are considered as potential charm-jet candidates in the $VH, H \to cc$ analysis. The remaining jets are categorized by their D_c^{DL1r} score: those with $D_c^{\text{DL1r}} > 1.76$ are labelled *c-tight*; the remaining jets are labelled *c-loose* if they satisfy $D_c^{\text{DL1r}} > 0.6735$ and *untagged* otherwise. In a $t\bar{t}$ sample with at least one leptonic W-boson decay, about 25% (20%) of c-jets pass the *c-tight* (*c-loose*) requirement, and about 50% are *untagged*; for b-jets these fraction are 10% for *c-tight*, 5% for *c-loose*, and 15% for untagged.

The measured probability that a jet in the $t\bar{t}$ phase space satisfies the various $VH, H \to cc$ charm-tagging categories as a function of jet p_{T} is shown in Fig. 22.

Good agreement with the data is observed after calibration. Using the background-subtraction procedure introduced in Sect. 8.2, the b-jet efficiencies in data are similarly measured for the charm-tagging working points and shown as a function of jet p_{T} in Fig. 23.

Figure 24 shows a comparison between the efficiencies obtained from the uncalibrated and calibrated simulations as a function of the jet p_{T} in the three c-tagging categories.

Finally, Fig. 25 shows the absolute and relative uncertainties as a function of jet p_{T} in the three c-tagging categories.

9 Conclusion

Flavour tagging is a key component of a broad range of analyses of LHC data collected by the ATLAS detector. Recent advances in flavour-tagging performance, driven in part by the uptake of state-of-the-art machine-learning techniques, have improved the sensitivity to possible new phenomena across a variety of final states.

In this study, a new strategy for deriving unbinned calibrations for high-dimensional simulations is developed. Neural solvers are used to find optimal transport maps to calibrate the multi-class flavour-tagging discriminators used to anal-

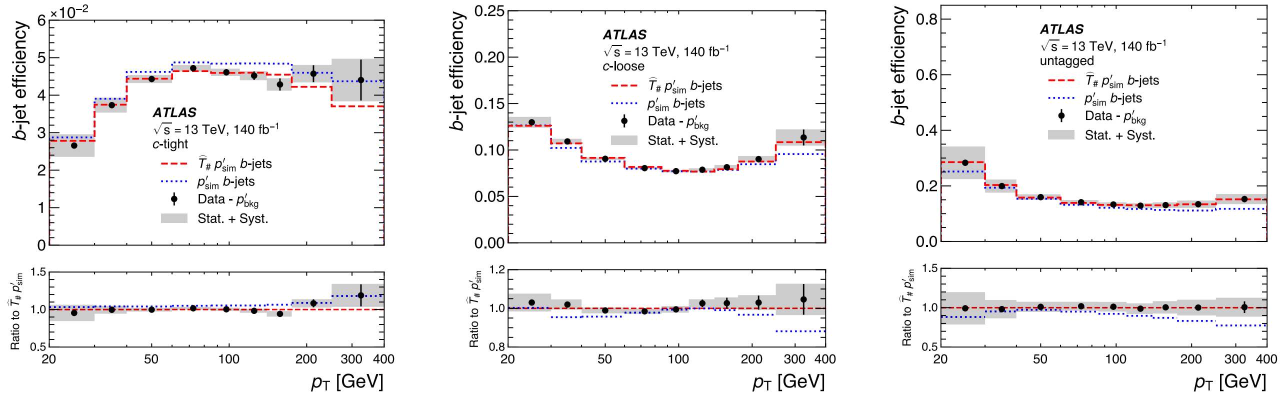

(a) (b) (c)

Fig. 23 Comparison of b-jet efficiencies for the $VH, H \rightarrow cc$ c-tagging categories, between the p_T-corrected simulation, p'_{sim}, calibrated simulation, $\hat{T}_{\#}\, p'_{sim}$, and background-subtracted data (data$-p'_{bkg}$), versus jet p_T in the $t\bar{t}$ phase space. The b-jets efficiency in data is calculated by subtracting the simulated non-b-jet contribution from data (Data $- (1 - f_{sig}) \cdot p'_{bkg}$). The (**a**) *c-tight*, (**b**) *c-loose*, and (**c**) *untagged* c-tagging categories are shown. The uncertainty band of Data $- \, p'_{bkg}$ is calculated by subtracting each $(1 - f_{sig,\,variation}) \cdot p'_{bkg,\,variation}$ from the data. The variations used are described in Sect. 7. Non-b-jets in simulation were corrected using transport maps derived in Sect. 6

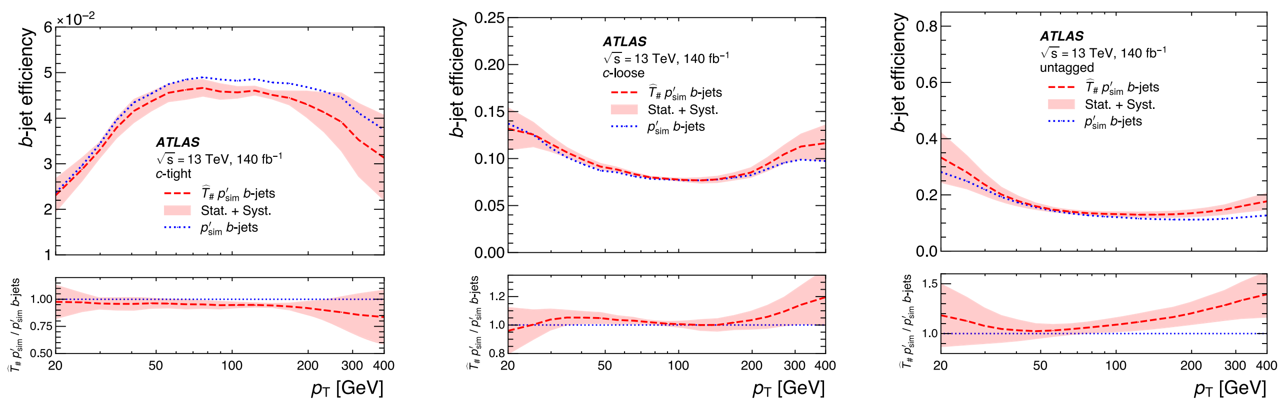

(a) (b) (c)

Fig. 24 Comparison of b-jet efficiencies for the $VH, H \rightarrow cc$ c-tagging categories, between the nominal simulation, p'_{sim}, and calibrated simulation, $\hat{T}_{\#}\, p'_{sim}$, in the $t\bar{t}$ phase space. The (**a**) *c-tight*, (**b**) *c-loose*, and (**c**) *untagged* c-tagging categories are shown. The uncertainty band of the corrected simulation denotes the impact of all uncertainties described in Sect. 7 on the calibration maps. Error bars show statistical uncertainties. All efficiencies are shown for the p_T-corrected density $p'_{sim}(\vec{q}, p_T) = p_{sim}(\vec{q}|p_T)\, p_{data}(p_T)$

yse ATLAS data. As opposed to traditional strategies, which involve deriving per-jet weights from data-to-simulation efficiency ratios, the optimal-transportation-based calibration presented here alters the flavour probabilities for individual jets such that the performance in simulation matches that in data. Moreover, the derived transportation maps are constructed such that the simulation is minimally altered while achieving closure with the performance in data.

This calibration strategy is applied in a sample of b-jets obtained from $t\bar{t}$ events in Run 2 LHC pp collision data with $\sqrt{s} = 13$ TeV collected by the ATLAS detector. The outcome is a set of continuous corrections that yield a calibrated simulation in the three-dimensional space of jet flavour probabilities conditional on the jet p_T. After applying the calibration transport map to the simulation, the performance observed in data is reproduced for a wide range of b-tagging operating points, with efficiencies ranging from 60 to 85%. The corrected simulation also accurately reflects the performance achieved in data with more sophisticated selections built from the jet classification scores, such as those recently developed in the ATLAS search for $H \rightarrow c\bar{c}$ decays.

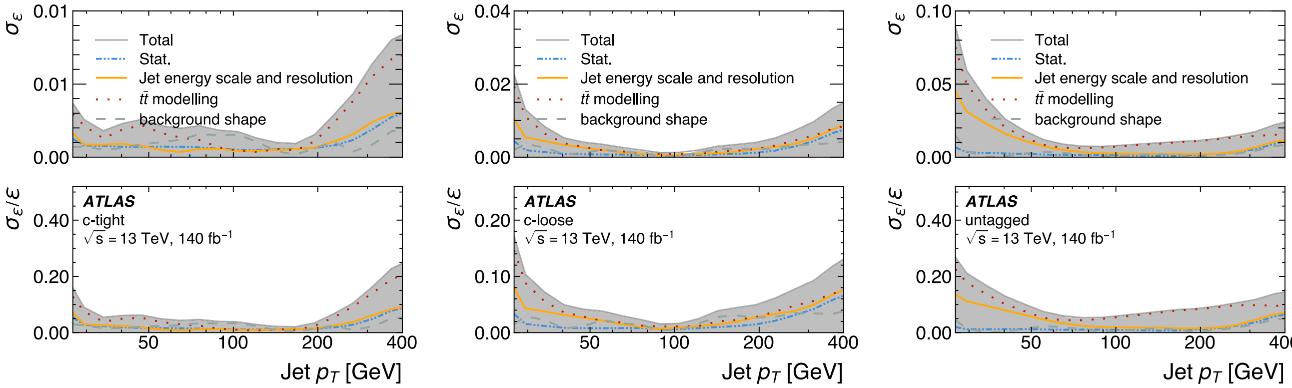

(a) (b) (c)

Fig. 25 Uncertainty breakdown of the calibrated simulation, $\hat{T}_\# p'_{\text{sim}}$, for corrected b-jet efficiencies versus jet p_{T} for various c-tagging operating points. The top panel shows the absolute uncertainties, while the bottom panel shows the relative uncertainties. The (**a**) *c-tight*, (**b**) *c-loose*, and (**c**) *untagged* operating points are shown. The grey uncertainty band of the calibrated simulation denotes the impact of all uncertainties described in Sect. 7 on the calibration maps

The presented calibration provides a robust set of three-dimensional corrections to the ATLAS simulation for the jet flavour-tagging algorithms used to analyse LHC collision data. This enables a more effective exploitation of jet flavour information in ATLAS analyses, including those which benefit from simultaneous bottom- and charm-jet identification such as joint measurements of $H \to bb$ and $H \to cc$ [14]; that require very strong c-jet rejection, such as searches for rare top-quark processes [24]; or which would gain from tagging operating points that smoothing vary with event kinematics, such as searches for high-mass resonances [27]. This development also opens several promising avenues for future research, including calibrations derived for finer-grained features, conditioned on more relevant kinematic information, or integrated into the training of inference networks [117]. These developments lay the groundwork for a more general and flexible framework for reliable inference based on imperfect simulation.

Acknowledgements We thank CERN for the very successful operation of the LHC and its injectors, as well as the support staff at CERN and at our institutions worldwide without whom ATLAS could not be operated efficiently. The crucial computing support from all WLCG partners is acknowledged gratefully, in particular from CERN, the ATLAS Tier-1 facilities at TRIUMF/SFU (Canada), NDGF (Denmark, Norway, Sweden), CC-IN2P3 (France), KIT/GridKA (Germany), INFN-CNAF (Italy), NL-T1 (Netherlands), PIC (Spain), RAL (UK) and BNL (USA), the Tier-2 facilities worldwide and large non-WLCG resource providers. Major contributors of computing resources are listed in Ref. [118]. We gratefully acknowledge the support of ANPCyT, Argentina; YerPhI, Armenia; ARC, Australia; BMWFW and FWF, Austria; ANAS, Azerbaijan; CNPq and FAPESP, Brazil; NSERC, NRC and CFI, Canada; CERN; ANID, Chile; CAS, MOST and NSFC, China; Minciencias, Colombia; MEYS CR, Czech Republic; DNRF and DNSRC, Denmark; IN2P3-CNRS and CEA-DRF/IRFU, France; SRNSFG, Georgia; BMFTR, HGF and MPG, Germany; GSRI, Greece; RGC and Hong Kong SAR, China; ISF and Benoziyo Center, Israel; INFN, Italy; MEXT and JSPS, Japan; CNRST, Morocco; NWO, Netherlands; RCN, Norway; MNiSW, Poland; FCT, Portugal; MNE/IFA, Romania; MSTDI, Serbia; MSSR, Slovakia; ARIS and MVZI, Slovenia; DSI/NRF, South Africa; MICIU/AEI, Spain; SRC and Wallenberg Foundation, Sweden; SERI, SNSF and Cantons of Bern and Geneva, Switzerland; NSTC, Taipei; TENMAK, Türkiye; STFC/UKRI, United Kingdom; DOE and NSF, United States of America. Individual groups and members have received support from BCKDF, CANARIE, CRC and DRAC, Canada; CERN-CZ, FORTE and PRIMUS, Czech Republic; COST, ERC, ERDF, Horizon 2020, ICSC-NextGenerationEU and Marie Skłodowska-Curie Actions, European Union; Investissements d'Avenir Labex, Investissements d'Avenir Idex and ANR, France; DFG and AvH Foundation, Germany; Herakleitos, Thales and Aristeia programmes co-financed by EU-ESF and the Greek NSRF, Greece; BSF-NSF and MINERVA, Israel; NCN and NAWA, Poland; La Caixa Banking Foundation, CERCA Programme Generalitat de Catalunya and PROMETEO and GenT Programmes Generalitat Valenciana, Spain; Göran Gustafssons Stiftelse, Sweden; The Royal Society and Leverhulme Trust, United Kingdom. In addition, individual members wish to acknowledge support from Armenia: Yerevan Physics Institute (FAPERJ); CERN: European Organization for Nuclear Research (CERN PJAS); Chile: Agencia Nacional de Investigación y Desarrollo (FONDECYT 1230812, FONDECYT 1240864); China: Chinese Ministry of Science and Technology (MOST-2023YFA1605700, MOST-2023YFA1609300), National Natural Science Foundation of China (NSFC - 12175119, NSFC 12275265, NSFC-12075060); Czech Republic: Czech Science Foundation (GACR - 24-11373S), Ministry of Education Youth and Sports (ERC-CZ-LL2327, FORTE CZ.02.01.01/00/22_008/0004632), PRIMUS Research Programme (PRIMUS/21/SCI/017); EU: H2020 European Research Council (ERC - 101002463); European Union: European Research Council (ERC - 948254, ERC 101089007), Horizon 2020 Framework Programme (MUCCA - CHIST-ERA-19-XAI-00), European Union, Future Artificial Intelligence Research (FAIR-NextGenerationEU PE00000013), Italian Center for High Performance Computing, Big Data and Quantum Computing (ICSC, NextGenerationEU); France: Agence Nationale de la Recherche (ANR-20-CE31-0013, ANR-21-CE31-0013, ANR-21-CE31-0022, ANR-22-EDIR-0002); Germany: Baden-Württemberg Stiftung (BW Stiftung-Postdoc Eliteprogramme), Deutsche Forschungsgemeinschaft (DFG - 469666862, DFG - CR 312/5-2); Italy: Istituto Nazionale di Fisica Nucleare (ICSC, NextGenerationEU), Ministero dell'Università e della Ricerca (NextGenEU 153D23001490006 M4C2.1.1, NextGenEU I53D23000820006 M4C2.1.1, NextGenEU I53D23001490006 M4C2.1.1); Japan: Japan Society for the Promotion of Science (JSPS KAKENHI JP22H01227, JSPS KAKENHI JP22H04944, JSPS KAKENHI JP22KK0227, JSPS KAKENHI JP23KK0245); Netherlands: Netherlands Organisation for Scientific Research (NWO Veni 2020 - VI.Veni.202.179); Norway: Research Council of Norway (RCN-314472); Poland: Ministry of Science and Higher Education (IDUB AGH, POB8, D4 no 9722), Polish National Agency for Academic Exchange (PPN/PPO/2020/1/00002/U/00001), Polish National Science Centre (NCN 2021/42/E/ST2/00350, NCN OPUS 2023/51/B/ST2/02507, NCN OPUS nr 2022/47/B/ST2/03059, NCN UMO-2019/34/E/ST2/00393, NCN & H2020 MSCA 945339, UMO-2020/37/B/ST2/01043, UMO-2021/40/C/ST2/00187, UMO-2022/47/O/ST2/00148, UMO-2023/49/B/ST2/04085, UMO-2023/51/B/ST2/00920); Portugal: Foundation for Science and Technology (FCT); Slovenia: Slovenian Research Agency (ARIS grant J1-3010); Spain: Generalitat Valenciana (Artemisa, FEDER, IDIFEDER/2018/048), Ministry of Science and Innovation (MCIN & NextGenEU PCI2022-135018-2, MICIN & FEDER PID2021-125273NB, RYC2019-028510-I, RYC2020-030254-I, RYC2021-031273-I, RYC2022-038164-I); Sweden: Carl Trygger Foundation (Carl Trygger Foundation CTS 22:2312), Swedish Research Council (Swedish Research Council 2023-04654, VR 2018-00482, VR 2021-03651, VR 2022-03845, VR 2022-04683, VR 2023-03403), Knut and Alice Wallenberg Foundation (KAW 2018.0458, KAW 2019.0447, KAW 2022.0358); Switzerland: Swiss National Science Foundation (SNSF - PCEFP2_194658); United Kingdom: Leverhulme Trust (Leverhulme Trust RPG-2020-004), Royal Society (NIF-R1-231091); United States of America: U.S. Department of Energy (ECA DE-AC02-76SF00515), Neubauer Family Foundation.

Data Availability Statement This manuscript has no associated data. [Authors' comment: All ATLAS scientific output is published in journals, and preliminary results are made available in Conference Notes. All are openly available, without restriction on use by external parties beyond copyright law and the standard conditions agreed by CERN. Data associated with journal publications are also made available: tables and data from plots (e.g. cross section values, likelihood profiles, selection efficiencies, cross section limits, ...) are stored in appropriate repositories such as HEPDATA (http://hepdata.cedar.ac.uk/). ATLAS also strives to make additional material related to the paper available that allows a reinterpretation of the data in the context of new theoretical models. For example, an extended encapsulation of the analysis is often provided for measurements in the framework of RIVET (http://rivet.hepforge.org/)." This information is taken from the ATLAS Data Access Policy, which is a public document that can be downloaded from http://opendata.cern.ch/record/413 [opendata.cern.ch.].

Code Availability Statement This manuscript has no associated code/software. [Authors' comment: ATLAS collaboration software is open source, and all code necessary to recreate an analysis is publicly available. The Athena (http://gitlab.cern.ch/atlas/athena) software repository provides all code needed for calibration and uncertainty application, with configuration files that are also publicly available via Docker containers and cvmfs. The specific code and configurations written in support of this analysis are not public; however, these are internally preserved.].

Funded by SCOAP[3].

References

1. L. Evans, P. Bryant, L.H.C. Machine, JINST **3**, S08001 (2008). https://doi.org/10.1088/1748-0221/3/08/S08001
2. ATLAS Collaboration, The ATLAS experiment at the CERN Large Hadron Collider, JINST 3 (2008) S08003 https://doi.org/10.1088/1748-0221/3/08/S08003
3. ATLAS Collaboration, A detailed map of Higgs boson interactions by the ATLAS experiment ten years after the discovery, Nature 607 (2022) 52, https://doi.org/10.1038/s41586-022-04893-w arXiv:2207.00092 [hep-ex], Erratum: Nature 612 (2022) E24 https://doi.org/10.1038/s41586-022-05581-5
4. ATLAS Collaboration, Probing the CP nature of the top-Higgs Yukawa coupling in $t\bar{t}H$ and tH events with $H \to b\bar{b}$ decays using the ATLAS detector at the LHC, Phys. Lett. B 849 (2024) 138469, https://doi.org/10.1016/j.physletb.2024.138469 arXiv:2303.05974 [hep-ex]
5. ATLAS Collaboration, Direct constraint on the Higgs-charm coupling from a search for Higgs boson decays into charm quarks with the ATLAS detector, Eur. Phys. J. C 82 (2022) 717, https://doi.org/10.1140/epjc/s10052-022-10588-3 arXiv:2201.11428 [hep-ex]
6. ATLAS Collaboration, Measurements of WH and ZH production in the $H \to b\bar{b}$ decay channel in pp collisions at 13 TeV with the ATLAS detector, Eur. Phys. J. C 81 (2021) 178, https://doi.org/10.1140/epjc/s10052-020-08677-2 arXiv:2007.02873 [hep-ex]
7. ATLAS Collaboration, Inclusive and differential cross-sections for dilepton $t\bar{t}$ production measured in $\sqrt{s} = 13$ TeV pp collisions with the ATLAS detector, JHEP 07 (2023) 141, arXiv:2303.15340 [hep-ex] https://doi.org/10.1007/JHEP07(2023)141
8. ATLAS Collaboration, Measurement of the top quark mass in the $t\bar{t} \to$ lepton+jets channel from $\sqrt{s} = 8$ TeV ATLAS data and combination with previous results, Eur. Phys. J. C 79 (2019) 290, https://doi.org/10.1140/epjc/s10052-019-6757-9 arXiv:1810.01772 [hep-ex]
9. ATLAS Collaboration, Search for $t\bar{t}$ resonances in fully hadronic final states in pp collisions at $\sqrt{s} = 13$ TeV with the ATLAS detector, JHEP 10 (2020) 061, https://doi.org/10.1007/JHEP10(2020)061 arXiv:2005.05138 [hep-ex]
10. ATLAS Collaboration, Search for nonresonant pair production of Higgs bosons in the $b\bar{b}b\bar{b}$ final state in pp collisions at $\sqrt{s} = 13$ TeV with the ATLAS detector, Phys. Rev. D 108 (2023) 052003, https://doi.org/10.1103/PhysRevD.108.052003 arXiv:2301.03212 [hep-ex]
11. ATLAS Collaboration, Constraints on the Higgs boson self-coupling from single- and double-Higgs production with the ATLAS detector using pp collisions at $\sqrt{s} = 13$ TeV, Phys. Lett. B 843 (2023) 137745, https://doi.org/10.1016/j.physletb.2023.137745 arXiv:2211.01216 [hep-ex]
12. ATLAS Collaboration, Search for resonant and non-resonant Higgs boson pair production in the $b\bar{b}\tau^+\tau^-$ decay channel using 13 TeV pp collision data from the ATLAS detector, JHEP 07 (2023) 040, https://doi.org/10.1007/JHEP07(2023)040 arXiv:2209.10916 [hep-ex]

13. ATLAS Collaboration, Search for Higgs boson pair production in the two bottom quarks plus two photons final state in pp collisions at $\sqrt{s} = 13$ TeV with the ATLAS detector, Phys. Rev. D 106 (2022) 052001, https://doi.org/10.1103/PhysRevD.106.052001 arXiv:2112.11876 [hep-ex]
14. ATLAS Collaboration, Measurements of WH and ZH production with Higgs boson decays into bottom quarks and direct constraints on the charm Yukawa coupling in 13 TeV pp collisions with the ATLAS detector, (2024), arXiv:2410.19611 [hep-ex]
15. ATLAS Collaboration, ATLAS flavour-tagging algorithms for the LHC Run 2 pp collision dataset, Eur. Phys. J. C 83 (2023) 681, https://doi.org/10.1140/epjc/s10052-023-11699-1 arXiv:2211.16345 [physics.data-an]
16. ATLAS Collaboration, Graph Neural Network Jet Flavour Tagging with the ATLAS Detector, ATL-PHYS-PUB-2022-027, 2022, URL: https://cds.cern.ch/record/2811135
17. ATLAS Collaboration, Deep Sets based Neural Networks for Impact Parameter Flavour Tagging in ATLAS, ATL-PHYS-PUB-2020-014, 2020, URL: https://cds.cern.ch/record/2718948
18. A. Buckley et al., General-purpose event generators for LHC physics. Phys. Rept. **504**, 145 (2011). https://doi.org/10.1016/j.physrep.2011.03.005. arXiv:1101.2599 [hep-ph]
19. S. Agostinelli et al., Geant4 - a simulation toolkit. Nucl. Instrum. Meth. A **506**, 250 (2003). https://doi.org/10.1016/S0168-9002(03)01368-8
20. ATLAS Collaboration, The ATLAS Simulation Infrastructure, Eur. Phys. J. C 70 (2010) 823, https://doi.org/10.1140/epjc/s10052-010-1429-9 arXiv:1005.4568 [physics.ins-det]
21. ATLAS Collaboration, Calibration of the light-flavour jet mistagging efficiency of the b-tagging algorithms with Z+jets events using 139 fb^{-1} of ATLAS proton-proton collision data at $\sqrt{s} = 13$ TeV, Eur. Phys. J. C 83 (2023) 728, https://doi.org/10.1140/epjc/s10052-023-11736-z arXiv:2301.06319 [hep-ex]
22. ATLAS Collaboration, Measurement of the c-jet mistagging efficiency in $t\bar{t}$ events using pp collision data at $\sqrt{s} = 13$ TeV collected with the ATLAS detector, Eur. Phys. J. C 82 (2022) 95, https://doi.org/10.1140/epjc/s10052-021-09843-w arXiv:2109.10627 [hep-ex]
23. ATLAS Collaboration, ATLAS b-jet identification performance and efficiency measurement with $t\bar{t}$ events in pp collisions at $\sqrt{s} = 13$ TeV, Eur. Phys. J. C 79 (2019) 970, https://doi.org/10.1140/epjc/s10052-019-7450-8 arXiv:1907.05120 [hep-ex]
24. ATLAS Collaboration, Search for flavour-changing neutral-current interactions of a top quark and a gluon in pp collisions at $\sqrt{s} = 13$ TeV with the ATLAS detector, Eur. Phys. J. C 82 (2022) 334, https://doi.org/10.1140/epjc/s10052-022-10182-7 arXiv:2112.01302 [hep-ex]
25. ATLAS Collaboration, Integrated and differential fiducial cross-section measurements for the vector boson fusion production of the Higgs boson in the $H \to WW^* \to e\nu\mu\nu$ decay channel at 13 TeV with the ATLAS detector, Phys. Rev. D 108 (2023) 072003, https://doi.org/10.1103/PhysRevD.108.072003 arXiv:2304.03053 [hep-ex]
26. ATLAS Collaboration, Measurements of differential cross sections of Higgs boson production through gluon fusion in the $H \to WW^* \to e\nu\mu\nu$ final state at $\sqrt{s} = 13$ TeV with the ATLAS detector, Eur. Phys. J. C 83 (2023) 774, https://doi.org/10.1140/epjc/s10052-023-11873-5 arXiv:2301.06822 [hep-ex]
27. ATLAS Collaboration, Search for resonances in the mass distribution of jet pairs with one or two jets identified as b-jets in proton-proton collisions at $\sqrt{s} = 13$ TeV with the ATLAS detector, Phys. Rev. D 98 (2018) 032016, https://doi.org/10.1103/PhysRevD.98.032016 arXiv:1805.09299 [hep-ex]
28. G. Monge, *Mémoire sur la théorie des déblais et des remblais*, Imprimerie royale, (1781)
29. C. Villani, *Optimal Transport: Old and New* (Grundlagen der Mathematischen Wissenschaften, Springer, Berlin Heidelberg, 2008). 9783540710509, https://doi.org/10.1007/978-3-540-71050-9
30. ATLAS Collaboration, Studies of the muon momentum calibration and performance of the ATLAS detector with pp collisions at $\sqrt{s} = 13$ TeV, Eur. Phys. J. C 83 (2023) 686, https://doi.org/10.1140/epjc/s10052-023-11584-x arXiv:2212.07338 [hep-ex]
31. ATLAS Collaboration, Electron and photon performance measurements with the ATLAS detector using the 2015–2017 LHC proton-proton collision data, JINST 14 (2019) P12006, https://doi.org/10.1088/1748-0221/14/12/P12006 arXiv:1908.00005 [hep-ex]
32. ATLAS Collaboration, Jet energy scale and resolution measured in proton-proton collisions at $\sqrt{s} = 13$ TeV with the ATLAS detector, Eur. Phys. J. C 81 (2021) 689, https://doi.org/10.1140/epjc/s10052-021-09402-3 arXiv:2007.02645 [hep-ex]
33. A. Makkuva, A. Taghvae, S. Oh, J. Lee, 'Optimal transport mapping via input convex neural networks', Proceedings of the 37th International Conference on Machine Learning, ed. by H. D. III and A. Singh, vol. 119, Proceedings of Machine Learning Research, PMLR, 2020 6672, arXiv:1908.10962 [cs.LG]
34. C. Pollard, P. Windischhofer, Transport away your problems: Calibrating stochastic simulations with optimal transport. Nucl. Instrum. Meth. A **1027**, 166119 (2022). https://doi.org/10.1016/j.nima.2021.166119. arXiv:2107.08648 [physics.data-an]
35. C. Bunne, A. Krause, M. Cuturi, Supervised training of conditional monge maps, NeurIPS 35 (2023) 6859, https://doi.org/10.48550/arXiv.2206.14262 arXiv:2206.14262
36. T. Manole, P. Bryant, J. Alison, M. Kuusela, L. Wasserman, Background Modeling for Double Higgs Boson Production: Density Ratios and Optimal Transport, (2024), arXiv:2208.02807 [stat.AP]
37. ATLAS Collaboration, Measurements of multijet event isotropies using optimal transport with the ATLAS detector, JHEP 10 (2023) 060, https://doi.org/10.1007/JHEP10(2023)060 arXiv:2305.16930 [hep-ex]
38. N. Craig, J. N. Howard, H. Li, Exploring Optimal Transport for Event-Level Anomaly Detection at the Large Hadron Collider, (2024), https://doi.org/10.48550/arXiv.2401.15542 arXiv:2401.15542 [hep-ph]
39. ATLAS Collaboration, ATLAS Insertable B-Layer: Technical Design Report, ATLAS-TDR-19, CERN-LHCC-2010-013, 2010, https://cds.cern.ch/record/1291633, Addendum: ATLAS-TDR-19-ADD-1, CERN- LHCC-2012-009, 2012, https://cds.cern.ch/record/1451888
40. B. Abbott et al., Production and integration of the ATLAS Insertable B-Layer. JINST **13**, T05008 (2018). https://doi.org/10.1088/1748-0221/13/05/T05008. arXiv:1803.00844 [physics.ins-det]
41. G. Avoni et al., The new LUCID-2 detector for luminosity measurement and monitoring in ATLAS. JINST **13**, P07017 (2018). https://doi.org/10.1088/1748-0221/13/07/P07017
42. ATLAS Collaboration, Performance of the ATLAS trigger system in, Eur. Phys. J. C **77**(2017), 317 (2015). https://doi.org/10.1140/epjc/s10052-017-4852-3. arXiv:1611.09661 [hep-ex]
43. ATLAS Collaboration, Software and computing for Run 3 of the ATLAS experiment at the LHC, Eur. Phys. J. C 85 (2025) 234, https://doi.org/10.1140/epjc/s10052-024-13701-w arXiv:2404.06335 [hep-ex]
44. T. Sjostrand, S. Mrenna, P. Skands, A brief introduction to PYTHIA 8.1, Comput. Phys. Commun. 178 (2008) 852, https://doi.org/10.1016/j.cpc.2008.01.036 arXiv:0710.3820 [hep-ph]
45. J. Bellm et al., Herwig++7.0/Herwig++ 3.0 release note, Eur. Phys. J. C 76 (2016) 196, https://doi.org/10.1140/epjc/s10052-016-4018-8 arXiv:1512.01178 [hep-ph]

46. T. Gleisberg et al., Event generation with SHERPA 1.1, JHEP 02 (2009) 007, https://doi.org/10.1088/1126-6708/2009/02/007 arXiv:0811.4622 [hep-ph]
47. P. Skands, S. Carrazza, J. Rojo, Tuning PYTHIA 8.1: the Monash 2013 Tune, Eur. Phys. J. C 74 (2014) 3024, https://doi.org/10.1140/epjc/s10052-014-3024-y arXiv:1404.5630 [hep-ph]
48. ATLAS Collaboration, ATLAS Pythia 8 tunes to 7 TeV data, ATL-PHYS-PUB-2014-021, 2014, URL: https://cds.cern.ch/record/1966419
49. DELPHI Collaboration, A study of the b-quark fragmentation function with the DELPHI detector at LEP I and an averaged distribution obtained at the Z pole, Eur. Phys. J. C 71 (2011) 1557, https://doi.org/10.1140/epjc/s10052-011-1557-x arXiv:1102.4748 [hep-ex]
50. O.P.A.L. Collaboration, Inclusive analysis of the b-quark fragmentation function in Z decays at LEP. Eur. Phys. J. C **29**, 463 (2003). https://doi.org/10.1140/epjc/s2003-01229-x. arXiv:hep-ex/0210031
51. ALEPH Collaboration, Study of the fragmentation of b quarks into B mesons at the Z peak, Phys. Lett. B 512 (2001) 30, https://doi.org/10.1016/S0370-2693(01)00690-6 arXiv:hep-ex/0106051
52. S.L.D. Collaboration, Measurement of the b-quark fragmentation function in Z^0 decays. Phys. Rev. D **65**, 092006 (2002). https://doi.org/10.1103/PhysRevD.65.092006. arXiv:hep-ex/0202031, Erratum: Phys. Rev. D 66 (2002) 79905 10.1103/PhysRevD.66.079905
53. ATLAS Collaboration, Measurements of jet observables sensitive to b-quark fragmentation in $t\bar{t}$ events at the LHC with the ATLAS detector, Phys. Rev. D 106 (2022) 032008, https://doi.org/10.1103/PhysRevD.106.032008, arXiv:2202.13901 [hep-ex]
54. ATLAS Collaboration, Measurement of b-quark fragmentation properties in jets using the decay $B^{\pm} \rightarrow J/\psi K^{\pm}$ in pp collisions at $\sqrt{s} = 13$ TeV with the ATLAS detector, JHEP 12 (2021) 131, https://doi.org/10.1007/JHEP12(2021)131 arXiv:2108.11650 [hep-ex]
55. D.J. Lange, The EvtGen particle decay simulation package. Nucl. Instrum. Meth. A **462**, 152 (2001). https://doi.org/10.1016/S0168-9002(01)00089-4
56. ATLAS Collaboration, Reweighing heavy-flavor production fractions to reduce flavor modelling uncertainties for ATLAS, ATL-PHYS-PUB-2022-035, 2022, URL: https://cds.cern.ch/record/2816367
57. R. Gambhir, B. Nachman, J. Thaler, Bias and priors in machine learning calibrations for high energy physics. Phys. Rev. D **106**, 036011 (2022). https://doi.org/10.1103/PhysRevD.106.036011. arXiv:2205.05084 [hep-ph]
58. B. Amos, L. Xu, J. Z. Kolter, 'Input convex neural networks', International Conference on Machine Learning, PMLR, 2017 146, arXiv:1609.07152 [cs.LG]
59. K. Cranmer, J. Pavez, G. Louppe, Approximating Likelihood Ratios with Calibrated Discriminative Classifiers, (2016), arXiv:1506.02169 [stat.AP]
60. I. Kotyzev, S.J. Prince, M.A. Brubaker, Normalizing Flows: An Introduction and Review of Current Methods. IEEE PAMI **43**, 3964 (2021). https://doi.org/10.1109/TPAMI.2020.2992934. arXiv:1908.09257 [stat.ML]
61. M. Algren, T. Golling, M. Guth, C. Pollard, J. A. Raine, Flow Away your Differences: Conditional Normalizing Flows as an Improvement to Reweighting, (2023), arXiv:2304.14963 [hep-ph]
62. B. Efron, R. Tibshirani, An Introduction to the Bootstrap, Chapman & Hall/CRC Monographs on Statistics & Applied Probability, Taylor & Francis, 1994, ISBN: 9780412042317, URL: https://doi.org/10.1201/9780429246593
63. ATLAS Collaboration, Luminosity determination in pp collisions at $\sqrt{s} = 13$ TeV using the ATLAS detector at the LHC, Eur. Phys. J. C 83 (2023) 982, https://doi.org/10.1140/epjc/s10052-023-11747-w arXiv:2212.09379 [hep-ex]
64. ATLAS Collaboration, ATLAS data quality operations and performance for 2015–2018 data-taking, JINST 15 (2020) P04003, https://doi.org/10.1088/1748-0221/15/04/P04003 arXiv:1911.04632 [physics.ins-det]
65. ATLAS Collaboration, Performance of electron and photon triggers in ATLAS during LHC Run 2, Eur. Phys. J. C 80 (2020) 47, https://doi.org/10.1140/epjc/s10052-019-7500-2 arXiv:1909.00761 [hep-ex]
66. ATLAS Collaboration, Performance of the ATLAS muon triggers in Run 2, JINST 15 (2020) P09015, https://doi.org/10.1088/1748-0221/15/09/p09015 arXiv:2004.13447 [physics.ins-det]
67. S. Frixione, G. Ridolfi, P. Nason, A positive-weight next-to-leading-order Monte Carlo for heavy flavour hadroproduction. JHEP **09**, 126 (2007). https://doi.org/10.1088/1126-6708/2007/09/126. arXiv:0707.3088 [hep-ph]
68. P. Nason, A new method for combining NLO QCD with shower Monte Carlo algorithms. JHEP **11**, 040 (2004). https://doi.org/10.1088/1126-6708/2004/11/040. arXiv:hep-ph/0409146
69. S. Frixione, P. Nason, C. Oleari, Matching NLO QCD computations with parton shower simulations: the POWHEG method. JHEP **11**, 070 (2007). https://doi.org/10.1088/1126-6708/2007/11/070. arXiv:0709.2092 [hep-ph]
70. S. Alioli, P. Nason, C. Oleari, E. Re, A general framework for implementing NLO calculations in shower Monte Carlo programs: the POWHEG BOX. JHEP **06**, 043 (2010). https://doi.org/10.1007/JHEP06(2010)043. arXiv:1002.2581 [hep-ph]
71. NNPDF Collaboration, R. D. Ball et al., Parton distributions for the LHC run II, JHEP 04 (2015) 040, https://doi.org/10.1007/JHEP04(2015)040 arXiv:1410.8849 [hep-ph]
72. ATLAS Collaboration, Studies on top-quark Monte Carlo modelling for Top2016, ATL-PHYS-PUB-2016-020, 2016, URL: https://cds.cern.ch/record/2216168
73. T. Sjostrand et al., An introduction to PYTHIA 8.2, Comput. Phys. Commun. 191 (2015) 159, https://doi.org/10.1016/j.cpc.2015.01.024 arXiv:1410.3012 [hep-ph]
74. NNPDF Collaboration, R. D. Ball et al., Parton distributions with LHC data, Nucl. Phys. B 867 (2013) 244, https://doi.org/10.1016/j.nuclphysb.2012.10.003 arXiv:1207.1303 [hep-ph]
75. M. Bahr et al., Herwig++ physics and manual. Eur. Phys. J. C **58**, 639 (2008). https://doi.org/10.1140/epjc/s10052-008-0798-9. arXiv:0803.0883 [hep-ph]
76. L.A. Harland-Lang, A.D. Martin, P. Motylinski, R.S. Thorne, Parton distributions in the LHC era: MMHT 2014 PDFs. Eur. Phys. J. C **75**, 204 (2015). https://doi.org/10.1140/epjc/s10052-015-3397-6. arXiv:1412.3989 [hep-ph]
77. S. Frixione, E. Laenen, P. Motylinski, C. White, B.R. Webber, Single-top hadroproduction in association with a W boson. JHEP **07**, 029 (2008). https://doi.org/10.1088/1126-6708/2008/07/029. arXiv:0805.3067 [hep-ex]
78. E. Bothmann et al., Event generation with Sherpa 2.2, SciPost Phys. 7 (2019) 034, https://doi.org/10.21468/SciPostPhys.7.3.034 arXiv:1905.09127 [hep-ph]
79. T. Gleisberg, S. Hoche, Comix, a new matrix element generator. JHEP **12**, 039 (2008). https://doi.org/10.1088/1126-6708/2008/12/039. arXiv:0808.3674 [hep-ph]
80. F. Buccioni et al., OpenLoops 2. Eur. Phys. J. C **79**, 866 (2019). https://doi.org/10.1140/epjc/s10052-019-7306-2. arXiv:1907.13071 [hep-ph]
81. F. Cascioli, P. Maierhöfer, S. Pozzorini, Scattering Amplitudes with Open Loops. Phys. Rev. Lett. **108**, 111601 (2012). https://doi.org/10.1103/PhysRevLett.108.111601. arXiv:1111.5206 [hep-ph]
82. A. Denner, S. Dittmaier, L. Hofer, Collier: A fortran-based complex one-loop library in extended regularizations. Comput. Phys.

Commun. **212**, 220 (2017). https://doi.org/10.1016/j.cpc.2016.10.013. arXiv:1604.06792 [hep-ph]

83. S. Schumann, F. Krauss, A parton shower algorithm based on Catani-Seymour dipole factorisation. JHEP **03**, 038 (2008). https://doi.org/10.1088/1126-6708/2008/03/038. arXiv:0709.1027 [hep-ph]
84. S. Hoche, F. Krauss, M. Schonherr, F. Siegert, A critical appraisal of NLO+PS matching methods. JHEP **09**, 049 (2012). https://doi.org/10.1007/JHEP09(2012)049. arXiv:1111.1220 [hep-ph]
85. S. Hoche, F. Krauss, M. Schonherr, F. Siegert, QCD matrix elements + parton showers: The NLO case. JHEP **04**, 027 (2013). https://doi.org/10.1007/JHEP04(2013)027. arXiv:1207.5030 [hep-ph]
86. S. Catani, F. Krauss, B.R. Webber, R. Kuhn, QCD Matrix Elements + Parton Showers. JHEP **11**, 063 (2001). https://doi.org/10.1088/1126-6708/2001/11/063. arXiv:hep-ph/0109231
87. S. Hoche, F. Krauss, S. Schumann, F. Siegert, QCD matrix elements and truncated showers. JHEP **05**, 053 (2009). https://doi.org/10.1088/1126-6708/2009/05/053. arXiv:0903.1219 [hep-ph]
88. C. Anastasiou, L. Dixon, K. Melnikov, F. Petriello, High-precision QCD at hadron colliders: Electroweak gauge boson rapidity distributions at next-to-next-to leading order. Phys. Rev. D **69**, 094008 (2004). https://doi.org/10.1103/PhysRevD.69.094008. arXiv:hep-ph/0312266
89. P. Nason, G. Zanderighi, W^+W^-, WZ and ZZ production in the POWHEG-BOX-V2. Eur. Phys. J. C **74**, 2702 (2014). https://doi.org/10.1140/epjc/s10052-013-2702-5. arXiv:1311.1365 [hep-ph]
90. ATLAS Collaboration, Measurement of the Z/γ^* boson transverse momentum distribution in pp collisions at $\sqrt{s} = 7$ TeV with the ATLAS detector, JHEP 09 (2014) 145, https://doi.org/10.1007/JHEP09(2014)145 arXiv:1406.3660 [hep-ex]
91. H.-L. Lai et al., New parton distributions for collider physics. Phys. Rev. D **82**, 074024 (2010). https://doi.org/10.1103/PhysRevD.82.074024. arXiv:1007.2241 [hep-ph]
92. J. Pumplin et al., New Generation of Parton Distributions with Uncertainties from Global QCD Analysis. JHEP **07**, 012 (2002). https://doi.org/10.1088/1126-6708/2002/07/012. arXiv:hep-ph/0201195
93. ATLAS Collaboration, The Pythia 8.A3 tune description of ATLAS minimum bias and inelastic measurements incorporating the Donnachie-Landshoff diffractive model, ATL-PHYS-PUB-2016-017, 2016, URL: https://cds.cern.ch/record/2206965
94. ATLAS Collaboration, Reconstruction of primary vertices at the ATLAS experiment in Run 1 proton-proton collisions at the LHC, Eur. Phys. J. C 77 (2017) 332, https://doi.org/10.1140/epjc/s10052-017-4887-5 arXiv:1611.10235 [physics.ins-det]
95. ATLAS Collaboration, Alignment of the ATLAS Inner Detector in Run 2, Eur. Phys. J. C 80 (2020) 1194, https://doi.org/10.1140/epjc/s10052-020-08700-6 arXiv:2007.07624 [hep-ex]
96. ATLAS Collaboration, Performance of the ATLAS track reconstruction algorithms in dense environments in LHC Run 2, Eur. Phys. J. C 77 (2017) 673, https://doi.org/10.1140/epjc/s10052-017-5225-7 arXiv:1704.07983 [hep-ex]
97. ATLAS Collaboration, Electron and photon efficiencies in LHC Run 2 with the ATLAS experiment, JHEP 05 (2024) 162, https://doi.org/10.1007/JHEP05(2024)162 arXiv:2308.13362 [hep-ex]
98. ATLAS Collaboration, Muon reconstruction and identification efficiency in ATLAS using the full Run 2 pp collision data set at $\sqrt{s} = 13$ TeV, Eur. Phys. J. C 81 (2021) 578, https://doi.org/10.1140/epjc/s10052-021-09233-2 arXiv:2012.00578 [hep-ex]
99. ATLAS Collaboration, Jet reconstruction and performance using particle flow with the ATLAS Detector, Eur. Phys. J. C 77 (2017) 466, https://doi.org/10.1140/epjc/s10052-017-5031-2 arXiv:1703.10485 [hep-ex]
100. M. Cacciari, G.P. Salam, G. Soyez, The anti-k_t jet clustering algorithm. JHEP **04**, 063 (2008). https://doi.org/10.1088/1126-6708/2008/04/063. arXiv:0802.1189 [hep-ph]
101. M. Cacciari, G.P. Salam, G. Soyez, FastJet user manual. Eur. Phys. J. C **72**, 1896 (2012). https://doi.org/10.1140/epjc/s10052-012-1896-2. arXiv:1111.6097 [hep-ph]
102. ATLAS Collaboration, Tagging and suppression of pileup jets with the ATLAS detector, ATLAS-CONF-2014-018, 2014, URL: https://cds.cern.ch/record/1700870
103. A. Paszke et al., 'PyTorch: An Imperative Style, High-Performance Deep Learning Library', Advances in Neural Information Processing Systems 32, Curran Associates, Inc., 2019 8024, arXiv:1912.01703 [cs.LG]
104. C.R. Harris et al., Array programming with NumPy. Nature **585**, 357 (2020). https://doi.org/10.1038/s41586-020-2649-2
105. P. Virtanen et al., SciPy 1.0: Fundamental Algorithms for Scientific Computing in Python, Nature Methods 17 (2020) 261, https://doi.org/10.1038/s41592-019-0686-2 arXiv:1907.10121 [cs.MS]
106. J.D. Hunter, Matplotlib: A 2D graphics environment. Computing in Science & Engineering **9**, 90 (2007). https://doi.org/10.1109/MCSE.2007.55
107. Pandas Development Team, Pandas, 2020, URL: https://doi.org/10.5281/zenodo.3509134
108. M. L. Waskom, Seaborn: Statistical Data Visualization, Journal of Open Source Software 6 (2021) 3021, https://doi.org/10.21105/joss.03021
109. E. Rodrigues et al., The Scikit HEP Project – overview and prospects, EPJ Web Conf. 245 (2020) 06028, ed. by C. Doglioni et al., https://doi.org/10.1051/epjconf/202024506028 arXiv:2007.03577 [physics.comp-ph]
110. I. Loshchilov, F. Hutter, Fixing Weight Decay Regularization in Adam, ICLR (2018), arXiv:1711.05101
111. I. Loshchilov, F. Hutter, SGDR: Stochastic Gradient Descent with Restarts, ICLR (2017), arXiv:1608.03983
112. C. Durkan, A. Bekasov, I. Murray, G. Papamakarios, Neural Spline Flows, 2019, arXiv:1906.04032 [stat.ML]
113. C. Huang, R. T. Q. Chen, C. Tsirigotis, A. C. Courville, Convex Potential Flows: Universal Probability Distributions with Optimal Transport and Convex Optimization, ICLR (2021), arXiv:2012.05942
114. M. Algren, J. A. Raine, T. Golling, Decorrelation using optimal transport, Eur. Phys. J. C 84 (2024), https://doi.org/10.1140/epjc/s10052-024-12868-6 arXiv:2307.05187 [hep-ph]
115. J. T. Barron, Continuously Differentiable Exponential Linear Units, CoRR (2017), arXiv:1704.07483
116. ATLAS Collaboration, Calibration of light-flavour b-jet mistagging rates using ATLAS proton-proton collision data at $\sqrt{s} = 13$ TeV, ATLAS-CONF-2018-006, 2018, URL: https://cds.cern.ch/record/2314418
117. A. Wehenkel et al., Addressing Misspecification in Simulation-based Inference through Data-driven Calibration, 2024, arXiv:2405.08719 [stat.ML]
118. ATLAS Collaboration, ATLAS Computing Acknowledgements, ATL-SOFT-PUB-2025-001, 2025, URL: https://cds.cern.ch/record/2922210

ATLAS Collaboration*

G. Aad[105], E. Aakvaag[17], B. Abbott[124], S. Abdelhameed[120a], K. Abeling[57], N. J. Abicht[51], S. H. Abidi[30], M. Aboelela[46], A. Aboulhorma[36e], H. Abramowicz[156], H. Abreu[155], Y. Abulaiti[121], B. S. Acharya[71a,71b,l], A. Ackermann[65a], C. Adam Bourdarios[4], L. Adamczyk[88a], S. V. Addepalli[148], M. J. Addison[104], J. Adelman[119], A. Adiguzel[22c], T. Adye[138], A. A. Affolder[140], Y. Afik[41], M. N. Agaras[13], A. Aggarwal[103], C. Agheorghiesei[28c], F. Ahmadov[40,aa], S. Ahuja[98], X. Ai[64e], G. Aielli[78a,78b], A. Aikot[168], M. Ait Tamlihat[36e], B. Aitbenchikh[36a], M. Akbiyik[103], T. P. A. Åkesson[101], A. V. Akimov[150], D. Akiyama[173], N. N. Akolkar[25], S. Aktas[22a], K. Al Khoury[43], G. L. Alberghi[24b], J. Albert[170], P. Albicocco[55], G. L. Albouy[62], S. Alderweireldt[54], Z. L. Alegria[125], M. Aleksa[37], I. N. Aleksandrov[40], C. Alexa[28b], T. Alexopoulos[10], F. Alfonsi[24b], M. Algren[58], M. Alhroob[172], B. Ali[136], H. M. J. Ali[94,t], S. Ali[32], S. W. Alibocus[95], M. Aliev[34c], G. Alimonti[73a], W. Alkakhi[57], C. Allaire[68], B. M. M. Allbrooke[151], J. S. Allen[104], J. F. Allen[54], C. A. Allendes Flores[141f], P. P. Allport[21], A. Aloisio[74a,74b], F. Alonso[93], C. Alpigiani[143], Z. M. K. Alsolami[94], M. Alvarez Estevez[102], A. Alvarez Fernandez[103], M. Alves Cardoso[58], M. G. Alviggi[74a,74b], M. Aly[104], Y. Amaral Coutinho[85b], A. Ambler[107], C. Amelung[37], M. Amerl[104], C. G. Ames[112], D. Amidei[109], B. Amini[56], K. Amirie[159], S. P. Amor Dos Santos[134a], K. R. Amos[168], D. Amperiadou[157], S. An[86], V. Ananiev[129], C. Anastopoulos[144], T. Andeen[11], J. K. Anders[37], A. C. Anderson[61], S. Y. Andrean[49a,49b], A. Andreazza[73a,73b], S. Angelidakis[9], A. Angerami[43], A. V. Anisenkov[39], A. Annovi[76a], C. Antel[58], E. Antipov[150], M. Antonelli[55], F. Anulli[77a], M. Aoki[86], T. Aoki[158], M. A. Aparo[151], L. Aperio Bella[50], C. Appelt[156], A. Apyan[27], S. J. Arbiol Val[89], C. Arcangeletti[55], A. T. H. Arce[53], J.-F. Arguin[111], S. Argyropoulos[157], J.-H. Arling[50], O. Arnaez[4], H. Arnold[150], G. Artoni[77a,77b], H. Asada[114], K. Asai[122], S. Asai[158], N. A. Asbah[37], R. A. Ashby Pickering[172], K. Assamagan[30], R. Astalos[29a], K. S. V. Astrand[101], S. Atashi[163], R. J. Atkin[34a], H. Atmani[36f], P. A. Atmasiddha[132], K. Augsten[136], A. D. Auriol[21], V. A. Austrup[104], G. Avolio[37], K. Axiotis[58], G. Azuelos[111,af], D. Babal[29b], H. Bachacou[139], K. Bachas[157,p], A. Bachiu[35], E. Bachmann[52], A. Badea[41], T. M. Baer[109], P. Bagnaia[77a,77b], M. Bahmani[19], D. Bahner[56], K. Bai[127], J. T. Baines[138], L. Baines[97], O. K. Baker[177], E. Bakos[16], D. Bakshi Gupta[8], L. E. Balabram Filho[85b], V. Balakrishnan[124], R. Balasubramanian[4], E. M. Baldin[39], P. Balek[88a], E. Ballabene[24a,24b], F. Balli[139], L. M. Baltes[65a], W. K. Balunas[33], J. Balz[103], I. Bamwidhi[120b], E. Banas[89], M. Bandieramonte[133], A. Bandyopadhyay[25], S. Bansal[25], L. Barak[156], M. Barakat[50], E. L. Barberio[108], D. Barberis[59a,59b], M. Barbero[105], M. Z. Barel[118], T. Barillari[113], M.-S. Barisits[37], T. Barklow[148], P. Baron[126], D. A. Baron Moreno[104], A. Baroncelli[64a], A. J. Barr[130], J. D. Barr[99], F. Barreiro[102], J. Barreiro Guimarães da Costa[14], M. G. Barros Teixeira[134a], S. Barsov[39], F. Bartels[65a], R. Bartoldus[148], A. E. Barton[94], P. Bartos[29a], A. Basan[103], M. Baselga[51], A. Bassalat[68,b], M. J. Basso[160a], S. Bataju[46], R. Bate[169], R. L. Bates[61], S. Batlamous[102], B. Batool[146], M. Battaglia[140], D. Battulga[19], M. Bauce[77a,77b], M. Bauer[81], P. Bauer[25], L. T. Bazzano Hurrell[31], J. B. Beacham[53], T. Beau[131], J. Y. Beaucamp[93], P. H. Beauchemin[162], P. Bechtle[25], H. P. Beck[20,o], K. Becker[172], A. J. Beddall[84], V. A. Bednyakov[40], C. P. Bee[150], L. J. Beemster[16], T. A. Beermann[37], M. Begalli[85d], M. Begel[30], A. Behera[150], J. K. Behr[50], J. F. Beirer[37], F. Beisiegel[25], M. Belfkir[120b], G. Bella[156], L. Bellagamba[24b], A. Bellerive[35], P. Bellos[21], K. Beloborodov[39], D. Benchekroun[36a], F. Bendebba[36a], Y. Benhammou[156], K. C. Benkendorfer[63], L. Beresford[50], M. Beretta[55], E. Bergeaas Kuutmann[166], N. Berger[4], B. Bergmann[136], J. Beringer[18a], G. Bernardi[5], C. Bernius[148], F. U. Bernlochner[25], F. Bernon[37], A. Berrocal Guardia[13], T. Berry[98], P. Berta[137], A. Berthold[52], S. Bethke[113], A. Betti[77a,77b], A. J. Bevan[97], N. K. Bhalla[56], S. Bhatta[150], D. S. Bhattacharya[171], P. Bhattarai[148], Z. M. Bhatti[121], K. D. Bhide[56], V. S. Bhopatkar[125], R. M. Bianchi[133], G. Bianco[24a,24b], O. Biebel[112], M. Biglietti[79a], C. S. Billingsley[46], Y. Bimgdi[36f], M. Bindi[57], A. Bingham[176], A. Bingul[22b], C. Bini[77a,77b], G. A. Bird[33], M. Birman[174], M. Biros[137], S. Biryukov[151], T. Bisanz[51], E. Bisceglie[45a,45b], J. P. Biswal[138], D. Biswas[146], I. Bloch[50], A. Blue[61], U. Blumenschein[97], J. Blumenthal[103], V. S. Bobrovnikov[39], M. Boehler[56], B. Boehm[171], D. Bogavac[37], A. G. Bogdanchikov[39], L. S. Boggia[131], C. Bohm[49a], V. Boisvert[98], P. Bokan[37], T. Bold[88a], M. Bomben[5], M. Bona[97], M. Boonekamp[139], A. G. Borbély[61], I. S. Bordulev[39], G. Borissov[94], D. Bortoletto[130], D. Boscherini[24b], M. Bosman[13], K. Bouaouda[36a], N. Bouchhar[168], L. Boudet[4], J. Boudreau[133], E. V. Bouhova-Thacker[94], D. Boumediene[42], R. Bouquet[59a,59b], A. Boveia[123], J. Boyd[37], D. Boye[30], I. R. Boyko[40], L. Bozianu[58], J. Bracinik[21], N. Brahimi[4], G. Brandt[176], O. Brandt[33], B. Brau[106], J. E. Brau[127], R. Brener[174],

L. Brenner[118], R. Brenner[166], S. Bressler[174], G. Brianti[80a,80b], D. Britton[61], D. Britzger[113], I. Brock[25], R. Brock[110], G. Brooijmans[43], A. J. Brooks[70], E. M. Brooks[160b], E. Brost[30], L. M. Brown[160a,170], L. E. Bruce[63], T. L. Bruckler[130], P. A. Bruckman de Renstrom[89], B. Brüers[50], A. Bruni[24b], G. Bruni[24b], D. Brunner[49a,49b], M. Bruschi[24b], N. Bruscino[77a,77b], T. Buanes[17], Q. Buat[143], D. Buchin[113], A. G. Buckley[61], O. Bulekov[39], B. A. Bullard[148], S. Burdin[95], C. D. Burgard[51], A. M. Burger[37], B. Burghgrave[8], O. Burlayenko[56], J. Burleson[167], J. T. P. Burr[33], J. C. Burzynski[147], E. L. Busch[43], V. Büscher[103], P. J. Bussey[61], J. M. Butler[26], C. M. Buttar[61], J. M. Butterworth[99], W. Buttinger[138], C. J. Buxo Vazquez[110], A. R. Buzykaev[39], S. Cabrera Urbán[168], L. Cadamuro[68], D. Caforio[60], H. Cai[133], Y. Cai[14,115c], Y. Cai[115a], V. M. M. Cairo[37], O. Cakir[3a], N. Calace[37], P. Calafiura[18a], G. Calderini[131], P. Calfayan[35], G. Callea[61], L. P. Caloba[85b], D. Calvet[42], S. Calvet[42], R. Camacho Toro[131], S. Camarda[37], D. Camarero Munoz[27], P. Camarri[78a,78b], M. T. Camerlingo[74a,74b], D. Cameron[37], C. Camincher[170], M. Campanelli[99], A. Camplani[44], V. Canale[74a,74b], A. C. Canbay[3a], E. Canonero[98], J. Cantero[168], Y. Cao[167], F. Capocasa[27], M. Capua[45a,45b], A. Carbone[73a,73b], R. Cardarelli[78a], J. C. J. Cardenas[8], M. P. Cardiff[27], G. Carducci[45a,45b], T. Carli[37], G. Carlino[74a], J. I. Carlotto[13], B. T. Carlson[133,q], E. M. Carlson[160a,170], J. Carmignani[95], L. Carminati[73a,73b], A. Carnelli[139], M. Carnesale[37], S. Caron[117], E. Carquin[141f], I. B. Carr[108], S. Carrá[73a], G. Carratta[24a,24b], A. M. Carroll[127], M. P. Casado[13,i], M. Caspar[50], F. L. Castillo[4], L. Castillo Garcia[13], V. Castillo Gimenez[168], N. F. Castro[134a,134e], A. Catinaccio[37], J. R. Catmore[129], T. Cavaliere[4], V. Cavaliere[30], L. J. Caviedes Betancourt[23b], Y. C. Cekmecelioglu[50], E. Celebi[84], S. Cella[37], V. Cepaitis[58], K. Cerny[126], A. S. Cerqueira[85a], A. Cerri[151], L. Cerrito[78a,78b], F. Cerutti[18a], B. Cervato[146], A. Cervelli[24b], G. Cesarini[55], S. A. Cetin[84], P. M. Chabrillat[131], D. Chakraborty[119], J. Chan[18a], W. Y. Chan[158], J. D. Chapman[33], E. Chapon[139], B. Chargeishvili[154b], D. G. Charlton[21], M. Chatterjee[20], C. Chauhan[137], Y. Che[115a], S. Chekanov[6], S. V. Chekulaev[160a], G. A. Chelkov[40,a], A. Chen[109], B. Chen[156], B. Chen[170], H. Chen[115a], H. Chen[30], J. Chen[64c], J. Chen[147], M. Chen[130], S. Chen[90], S. J. Chen[115a], X. Chen[64c], X. Chen[15,ae], Y. Chen[64a], C. L. Cheng[175], H. C. Cheng[66a], S. Cheong[148], A. Cheplakov[40], E. Cheremushkina[50], E. Cherepanova[118], R. Cherkaoui El Moursli[36e], E. Cheu[7], K. Cheung[67], L. Chevalier[139], V. Chiarella[55], G. Chiarelli[76a], N. Chiedde[105], G. Chiodini[72a], A. S. Chisholm[21], A. Chitan[28b], M. Chitishvili[168], M. V. Chizhov[40,r], K. Choi[11], Y. Chou[143], E. Y. S. Chow[117], K. L. Chu[174], M. C. Chu[66a], X. Chu[14,115c], Z. Chubinidze[55], J. Chudoba[135], J. J. Chwastowski[89], D. Cieri[113], K. M. Ciesla[88a], V. Cindro[96], A. Ciocio[18a], F. Cirotto[74a,74b], Z. H. Citron[174], M. Citterio[73a], D. A. Ciubotaru[28b], A. Clark[58], P. J. Clark[54], N. Clarke Hall[99], C. Clarry[159], J. M. Clavijo Columbie[50], S. E. Clawson[50], C. Clement[49a,49b], Y. Coadou[105], M. Cobal[71a,71c], A. Coccaro[59b], R. F. Coelho Barrue[134a], R. Coelho Lopes De Sa[106], S. Coelli[73a], L. S. Colangeli[159], B. Cole[43], J. Collot[62], P. Conde Muiño[134a,134g], M. P. Connell[34c], S. H. Connell[34c], E. I. Conroy[130], F. Conventi[74a,ag], H. G. Cooke[21], A. M. Cooper-Sarkar[130], F. A. Corchia[24a24b], A. Cordeiro Oudot Choi[131], L. D. Corpe[42], M. Corradi[77a,77b], F. Corriveau[107,y], A. Cortes-Gonzalez[19], M. J. Costa[168], F. Costanza[4], D. Costanzo[144], B. M. Cote[123], J. Couthures[4], G. Cowan[98], K. Cranmer[175], L. Cremer[51], D. Cremonini[24a,24b], S. Crépé-Renaudin[62], F. Crescioli[131], M. Cristinziani[146], M. Cristoforetti[80a,80b], V. Croft[118], J. E. Crosby[125], G. Crosetti[45a,45b], A. Cueto[102], H. Cui[99], Z. Cui[7], W. R. Cunningham[61], F. Curcio[168], J. R. Curran[54], P. Czodrowski[37], M. J. Da Cunha Sargedas De Sousa[59a,59b], J. V. Da Fonseca Pinto[85b], C. Da Via[104], W. Dabrowski[88a], T. Dado[37], S. Dahbi[153], T. Dai[109], D. Dal Santo[20], C. Dallapiccola[106], M. Dam[44], G. D'amen[30], V. D'Amico[112], J. Damp[103], J. R. Dandoy[35], D. Dannheim[37], M. Danninger[147], V. Dao[150], G. Darbo[59b], S. J. Das[30], F. Dattola[50], S. D'Auria[73a,73b], A. D'Avanzo[74a,74b], C. David[34a], T. Davidek[137], I. Dawson[97], H. A. Day-hall[136], K. De[8], C. De Almeida Rossi[159], R. De Asmundis[74a], N. De Biase[50], S. De Castro[24a,24b], N. De Groot[117], P. de Jong[118], H. De la Torre[119], A. De Maria[115a], A. De Salvo[77a], U. De Sanctis[78a,78b], F. De Santis[72a,72b], A. De Santo[151], J. B. De Vivie De Regie[62], J. Debevc[96], D. V. Dedovich[40], J. Degens[95], A. M. Deiana[46], F. Del Corso[24a,24b], J. Del Peso[102], L. Delagrange[131], F. Deliot[139], C. M. Delitzsch[51], M. Della Pietra[74a,74b], D. Della Volpe[58], A. Dell'Acqua[37], L. Dell'Asta[73a,73b], M. Delmastro[4], C. C. Delogu[103], P. A. Delsart[62], S. Demers[177], M. Demichev[40], S. P. Denisov[39], L. D'Eramo[42], D. Derendarz[89], F. Derue[131], P. Dervan[95], K. Desch[25], C. Deutsch[25], F. A. Di Bello[59a,59b], A. Di Ciaccio[78a,78b], L. Di Ciaccio[4], A. Di Domenico[77a,77b], C. Di Donato[74a,74b], A. Di Girolamo[37], G. Di Gregorio[37], A. Di Luca[80a,80b], B. Di Micco[79a,79b], R. Di Nardo[79a,79b], K. F. Di Petrillo[41], M. Diamantopoulou[35], F. A. Dias[118], T. Dias Do Vale[147], M. A. Diaz[141a,141b], A. R. Didenko[40], M. Didenko[168], E. B. Diehl[109], S. Díez Cornell[50], C. Diez Pardos[146], C. Dimitriadi[166],

A. Dimitrievska[21], J. Dingfelder[25], T. Dingley[130], I.-M. Dinu[28b], S. J. Dittmeier[65b], F. Dittus[37], M. Divisek[137], B. Dixit[95], F. Djama[105], T. Djobava[154b], C. Doglioni[101,104], A. Dohnalova[29a], Z. Dolezal[137], K. Domijan[88a], K. M. Dona[41], M. Donadelli[85d], B. Dong[110], J. Donini[42], A. D'Onofrio[74a,74b], M. D'Onofrio[95], J. Dopke[138], A. Doria[74a], N. Dos Santos Fernandes[134a], P. Dougan[104], M. T. Dova[93], A. T. Doyle[61], M. A. Draguet[130], M. P. Drescher[57], E. Dreyer[174], I. Drivas-koulouris[10], M. Drnevich[121], M. Drozdova[58], D. Du[64a], T. A. du Pree[118], F. Dubinin[39], M. Dubovsky[29a], E. Duchovni[174], G. Duckeck[112], O. A. Ducu[28b], D. Duda[54], A. Dudarev[37], E. R. Duden[27], M. D'uffizi[104], L. Duflot[68], M. Dührssen[37], I. Duminica[28g], A. E. Dumitriu[28b], M. Dunford[65a], S. Dungs[51], K. Dunne[49a,49b], A. Duperrin[105], H. Duran Yildiz[3a], M. Düren[60], A. Durglishvili[154b], D. Duvnjak[35], B. L. Dwyer[119], G. I. Dyckes[18a], M. Dyndal[88a], B. S. Dziedzic[37], Z. O. Earnshaw[151], G. H. Eberwein[130], B. Eckerova[29a], S. Eggebrecht[57], E. Egidio Purcino De Souza[85e], L. F. Ehrke[58], G. Eigen[17], K. Einsweiler[18a], T. Ekelof[166], P. A. Ekman[101], S. El Farkh[36b], Y. El Ghazali[64a], H. El Jarrari[37], A. El Moussaouy[36a], V. Ellajosyula[166], M. Ellert[166], F. Ellinghaus[176], N. Ellis[37], J. Elmsheuser[30], M. Elsawy[120a], M. Elsing[37], D. Emeliyanov[138], Y. Enari[86], I. Ene[18a], S. Epari[13], P. A. Erland[89], D. Ernani Martins Neto[89], M. Errenst[176], M. Escalier[68], C. Escobar[168], E. Etzion[156], G. Evans[134a,134b], H. Evans[70], L. S. Evans[98], A. Ezhilov[39], S. Ezzarqtouni[36a], F. Fabbri[24a,24b], L. Fabbri[24a,24b], G. Facini[99], V. Fadeyev[140], R. M. Fakhrutdinov[39], D. Fakoudis[103], S. Falciano[77a], L. F. Falda Ulhoa Coelho[134a], F. Fallavollita[113], G. Falsetti[45a,45b], J. Faltova[137], C. Fan[167], K. Y. Fan[66b], Y. Fan[14], Y. Fang[14,115c], M. Fanti[73a,73b], M. Faraj[71a,71b], Z. Farazpay[100], A. Farbin[8], A. Farilla[79a], T. Farooque[110], J. N. Farr[177], S. M. Farrington[54,138], F. Fassi[36e], D. Fassouliotis[9], M. Faucci Giannelli[78a,78b], W. J. Fawcett[33], L. Fayard[68], P. Federic[137], P. Federicova[135], O. L. Fedin[39,a], M. Feickert[175], L. Feligioni[105], D. E. Fellers[127], C. Feng[64b], Z. Feng[118], M. J. Fenton[163], L. Ferencz[50], R. A. M. Ferguson[94], P. Fernandez Martinez[69], M. J. V. Fernoux[105], J. Ferrando[94], A. Ferrari[166], P. Ferrari[117,118], R. Ferrari[75a], D. Ferrere[58], C. Ferretti[109], M. P. Fewell[1], D. Fiacco[77a,77b], F. Fiedler[103], P. Fiedler[136], S. Filimonov[39], A. Filipčič[96], E. K. Filmer[160a], F. Filthaut[117], M. C. N. Fiolhais[134a,134c,c], L. Fiorini[168], W. C. Fisher[110], T. Fitschen[104], P. M. Fitzhugh[139], I. Fleck[146], P. Fleischmann[109], T. Flick[176], M. Flores[34d,ac], L. R. Flores Castillo[66a], L. Flores Sanz De Acedo[37], F. M. Follega[80a,80b], N. Fomin[33], J. H. Foo[159], A. Formica[139], A. C. Forti[104], E. Fortin[37], A. W. Fortman[18a], M. G. Foti[18a], L. Fountas[9,j], D. Fournier[68], H. Fox[94], P. Francavilla[76a,76b], S. Francescato[63], S. Franchellucci[58], M. Franchini[24a,24b], S. Franchino[65a], D. Francis[37], L. Franco[117], V. Franco Lima[37], L. Franconi[50], M. Franklin[63], G. Frattari[27], Y. Y. Frid[156], J. Friend[61], N. Fritzsche[37], A. Froch[58], D. Froidevaux[37], J. A. Frost[130], Y. Fu[64a], S. Fuenzalida Garrido[141f], M. Fujimoto[105], K. Y. Fung[66a], E. Furtado De Simas Filho[85e], M. Furukawa[158], J. Fuster[168], A. Gaa[57], A. Gabrielli[24a,24b], A. Gabrielli[159], P. Gadow[37], G. Gagliardi[59a,59b], L. G. Gagnon[18a], S. Gaid[165], S. Galantzan[156], J. Gallagher[1], E. J. Gallas[130], A. L. Gallen[166], B. J. Gallop[138], K. K. Gan[123], S. Ganguly[158], Y. Gao[54], F. M. Garay Walls[141a,141b], B. Garcia[30], C. García[168], A. Garcia Alonso[118], A. G. Garcia Caffaro[177], J. E. García Navarro[168], M. Garcia-Sciveres[18a], G. L. Gardner[132], R. W. Gardner[41], N. Garelli[162], R. B. Garg[148], J. M. Gargan[54], C. A. Garner[159], C. M. Garvey[34a], V. K. Gassmann[162], G. Gaudio[75a], V. Gautam[13], P. Gauzzi[77a,77b], J. Gavranovic[96], I. L. Gavrilenko[39], A. Gavrilyuk[39], C. Gay[169], G. Gaycken[127], E. N. Gazis[10], A. A. Geanta[28b], A. Gekow[123], C. Gemme[59b], M. H. Genest[62], A. D. Gentry[116], S. George[98], W. F. George[21], T. Geralis[48], A. A. Gerwin[124], P. Gessinger-Befurt[37], M. E. Geyik[176], M. Ghani[172], K. Ghorbanian[97], A. Ghosal[146], A. Ghosh[163], A. Ghosh[7], B. Giacobbe[24b], S. Giagu[77a,77b], T. Giani[118], A. Giannini[64a], S. M. Gibson[98], M. Gignac[140], D. T. Gil[88b], A. K. Gilbert[88a], B. J. Gilbert[43], D. Gillberg[35], G. Gilles[118], L. Ginabat[131], D. M. Gingrich[2,af], M. P. Giordani[71a,71c], P. F. Giraud[139], G. Giugliarelli[71a,71c], D. Giugni[73a], F. Giuli[78a,78b], I. Gkialas[9,j], L. K. Gladilin[39], C. Glasman[102], G. R. Gledhill[127], G. Glemža[50], M. Glisic[127], I. Gnesi[45b], Y. Go[30], M. Goblirsch-Kolb[37], B. Gocke[51], D. Godin[111], B. Gokturk[22a], S. Goldfarb[108], T. Golling[58], M. G. D. Gololo[34g], D. Golubkov[39], J. P. Gombas[110], A. Gomes[134a,134b], G. Gomes Da Silva[146], A. J. Gomez Delegido[168], R. Gonçalo[134a], L. Gonella[21], A. Gongadze[154c], F. Gonnella[21], J. L. Gonski[148], R. Y. González Andana[54], S. González de la Hoz[168], R. Gonzalez Lopez[95], C. Gonzalez Renteria[18a], M. V. Gonzalez Rodrigues[50], R. Gonzalez Suarez[166], S. Gonzalez-Sevilla[58], L. Goossens[37], B. Gorini[37], E. Gorini[72a,72b], A. Gorišek[96], T. C. Gosart[132], A. T. Goshaw[53], M. I. Gostkin[40], S. Goswami[125], C. A. Gottardo[37], S. A. Gotz[112], M. Gouighri[36b], V. Goumarre[50], A. G. Goussiou[143], N. Govender[34c], R. P. Grabarczyk[130], I. Grabowska-Bold[88a], K. Graham[35], E. Gramstad[129], S. Grancagnolo[72a,72b], C. M. Grant[1,139], P. M. Gravila[28f], F. G. Gravili[72a,72b], H. M. Gray[18a], M. Greco[72a,72b], M. J. Green[1], C. Grefe[25], A. S. Grefsrud[17], I. M. Gregor[50],

K. T. Greif[163], P. Grenier[148], S. G. Grewe[113], A. A. Grillo[140], K. Grimm[32], S. Grinstein[13,u], J.-F. Grivaz[68], E. Gross[174], J. Grosse-Knetter[57], L. Guan[109], J. G. R. Guerrero Rojas[168], G. Guerrieri[37], R. Gugel[103], J. A. M. Guhit[109], A. Guida[19], E. Guilloton[172], S. Guindon[37], F. Guo[14,115c], J. Guo[64c], L. Guo[50], L. Guo[14], Y. Guo[109], A. Gupta[51], R. Gupta[133], S. Gurbuz[25], S. S. Gurdasani[56], G. Gustavino[77a,77b], P. Gutierrez[124], L. F. Gutierrez Zagazeta[132], M. Gutsche[52], C. Gutschow[99], C. Gwenlan[130], C. B. Gwilliam[95], E. S. Haaland[129], A. Haas[121], M. Habedank[61], C. Haber[18a], H. K. Hadavand[8], A. Hadef[52], A. I. Hagan[94], J. J. Hahn[146], E. H. Haines[99], M. Haleem[171], J. Haley[125], G. D. Hallewell[105], L. Halser[20], K. Hamano[170], M. Hamer[25], E. J. Hampshire[98], J. Han[64b], L. Han[115a], L. Han[64a], S. Han[18a], Y. F. Han[159], K. Hanagaki[86], M. Hance[140], D. A. Hangal[43], H. Hanif[147], M. D. Hank[132], J. B. Hansen[44], P. H. Hansen[44], D. Harada[58], T. Harenberg[176], S. Harkusha[178], M. L. Harris[106], Y. T. Harris[25], J. Harrison[13], N. M. Harrison[123], P. F. Harrison[172], N. M. Hartman[113], N. M. Hartmann[112], R. Z. Hasan[98,138], Y. Hasegawa[145], F. Haslbeck[130], S. Hassan[17], R. Hauser[110], C. M. Hawkes[21], R. J. Hawkings[37], Y. Hayashi[158], D. Hayden[110], C. Hayes[109], R. L. Hayes[118], C. P. Hays[130], J. M. Hays[97], H. S. Hayward[95], F. He[64a], M. He[14,115c], Y. He[50], Y. He[99], N. B. Heatley[97], V. Hedberg[101], A. L. Heggelund[129], N. D. Hehir[97,*], C. Heidegger[56], K. K. Heidegger[56], J. Heilman[35], S. Heim[50], T. Heim[18a], J. G. Heinlein[132], J. J. Heinrich[127], L. Heinrich[113,ad], J. Hejbal[135], A. Held[175], S. Hellesund[17], C. M. Helling[169], S. Hellman[49a,49b], R. C. W. Henderson[94], L. Henkelmann[33], A. M. Henriques Correia[37], H. Herde[101], Y. Hernández Jiménez[150], L. M. Herrmann[25], T. Herrmann[52], G. Herten[56], R. Hertenberger[112], L. Hervas[37], M. E. Hesping[103], N. P. Hessey[160a], J. Hessler[113], M. Hidaoui[36b], N. Hidic[137], E. Hill[159], S. J. Hillier[21], J. R. Hinds[110], F. Hinterkeuser[25], M. Hirose[128], S. Hirose[161], D. Hirschbuehl[176], T. G. Hitchings[104], B. Hiti[96], J. Hobbs[150], R. Hobincu[28e], N. Hod[174], M. C. Hodgkinson[144], B. H. Hodkinson[130], A. Hoecker[37], D. D. Hofer[109], J. Hofer[168], T. Holm[25], M. Holzbock[37], L. B. A. H. Hommels[33], B. P. Honan[104], J. J. Hong[70], J. Hong[64c], T. M. Hong[133], B. H. Hooberman[167], W. H. Hopkins[6], M. C. Hoppesch[167], Y. Horii[114], M. E. Horstmann[113], S. Hou[153], M. R. Housenga[167], A. S. Howard[96], J. Howarth[61], J. Hoya[6], M. Hrabovsky[126], A. Hrynevich[50], T. Hryn'ova[4], P. J. Hsu[67], S.-C. Hsu[143], T. Hsu[68], M. Hu[18a], Q. Hu[64a], S. Huang[33], X. Huang[14,115c], Y. Huang[144], Y. Huang[103], Y. Huang[14], Z. Huang[104], Z. Hubacek[136], M. Huebner[25], F. Huegging[25], T. B. Huffman[130], M. Hufnagel Maranha De Faria[85a], C. A. Hugli[50], M. Huhtinen[37], S. K. Huiberts[17], R. Hulsken[107], N. Huseynov[12,g], J. Huston[110], J. Huth[63], R. Hyneman[148], G. Iacobucci[58], G. Iakovidis[30], L. Iconomidou-Fayard[68], J. P. Iddon[37], P. Iengo[74a,74b], R. Iguchi[158], Y. Iiyama[158], T. Iizawa[130], Y. Ikegami[86], D. Iliadis[157], N. Ilic[159], H. Imam[85c], G. Inacio Goncalves[85d], T. Ingebretsen Carlson[49a,49b], J. M. Inglis[97], G. Introzzi[75a,75b], M. Iodice[79a], V. Ippolito[77a,77b], R. K. Irwin[95], M. Ishino[158], W. Islam[175], C. Issever[19], S. Istin[22a,aj], H. Ito[173], R. Iuppa[80a,80b], A. Ivina[174], J. M. Izen[47], V. Izzo[74a], P. Jacka[135], P. Jackson[1], C. S. Jagfeld[112], G. Jain[160a], P. Jain[50], K. Jakobs[56], T. Jakoubek[174], J. Jamieson[61], W. Jang[158], M. Javurkova[106], P. Jawahar[104], L. Jeanty[127], J. Jejelava[154a,ab], P. Jenni[56,f], C. E. Jessiman[35], C. Jia[64b], H. Jia[169], J. Jia[150], X. Jia[14,115c], Z. Jia[115a], C. Jiang[54], S. Jiggins[50], J. Jimenez Pena[13], S. Jin[115a], A. Jinaru[28b], O. Jinnouchi[142], P. Johansson[144], K. A. Johns[7], J. W. Johnson[140], F. A. Jolly[50], D. M. Jones[151], E. Jones[50], K. S. Jones[8], P. Jones[33], R. W. L. Jones[94], T. J. Jones[95], H. L. Joos[37,57], R. Joshi[123], J. Jovicevic[16], X. Ju[18a], J. J. Junggeburth[37], T. Junkermann[65a], A. Juste Rozas[13,u], M. K. Juzek[89], S. Kabana[141e], A. Kaczmarska[89], M. Kado[113], H. Kagan[123], M. Kagan[148], A. Kahn[132], C. Kahra[103], T. Kaji[158], E. Kajomovitz[155], N. Kakati[174], I. Kalaitzidou[56], C. W. Kalderon[30], N. J. Kang[140], D. Kar[34g], K. Karava[130], M. J. Kareem[160b], E. Karentzos[25], O. Karkout[118], S. N. Karpov[40], Z. M. Karpova[40], V. Kartvelishvili[94], A. N. Karyukhin[39], E. Kasimi[157], J. Katzy[50], S. Kaur[35], K. Kawade[145], M. P. Kawale[124], C. Kawamoto[90], T. Kawamoto[64a], E. F. Kay[37], F. I. Kaya[162], S. Kazakos[110], V. F. Kazanin[39], Y. Ke[150], J. M. Keaveney[34a], R. Keeler[170], G. V. Kehris[63], J. S. Keller[35], J. J. Kempster[151], O. Kepka[135], B. P. Kerridge[138], S. Kersten[176], B. P. Kerševan[96], L. Keszeghova[29a], S. Ketabchi Haghighat[159], R. A. Khan[133], A. Khanov[125], A. G. Kharlamov[39], T. Kharlamova[39], E. E. Khoda[143], M. Kholodenko[134a], T. J. Khoo[19], G. Khoriauli[171], J. Khubua[154b], Y. A. R. Khwaira[131], B. Kibirige[34g], D. Kim[6], D. W. Kim[49a,49b], Y. K. Kim[41], N. Kimura[99], M. K. Kingston[57], A. Kirchhoff[57], C. Kirfel[25], F. Kirfel[25], J. Kirk[138], A. E. Kiryunin[113], S. Kita[161], C. Kitsaki[10], O. Kivernyk[25], M. Klassen[162], C. Klein[35], L. Klein[171], M. H. Klein[46], S. B. Klein[58], U. Klein[95], A. Klimentov[30], T. Klioutchnikova[37], P. Kluit[118], S. Kluth[113], E. Kneringer[81], T. M. Knight[159], A. Knue[51], M. Kobel[52], D. Kobylianskii[174], S. F. Koch[130], M. Kocian[148], P. Kodyš[137], D. M. Koeck[127], P. T. Koenig[25], T. Koffas[35], O. Kolay[52], I. Koletsou[4], T. Komarek[89], K. Köneke[57], A. X. Y. Kong[1], T. Kono[122], N. Konstantinidis[99], P. Kontakakis[58], B. Konya[101],

R. Kopeliansky[43], S. Koperny[88a], K. Korcyl[89], K. Kordas[157,e], A. Korn[99], S. Korn[57], I. Korolkov[13], N. Korotkova[39], B. Kortman[118], O. Kortner[113], S. Kortner[113], W. H. Kostecka[119], V. V. Kostyukhin[146], A. Kotsokechagia[37], A. Kotwal[53], A. Koulouris[37], A. Kourkoumeli-Charalampidi[75a,75b], C. Kourkoumelis[9], E. Kourlitis[113], O. Kovanda[127], R. Kowalewski[170], W. Kozanecki[127], A. S. Kozhin[39], V. A. Kramarenko[39], G. Kramberger[96], P. Kramer[25], M. W. Krasny[131], A. Krasznahorkay[37], A. C. Kraus[119], J. W. Kraus[176], J. A. Kremer[50], T. Kresse[52], L. Kretschmann[176], J. Kretzschmar[95], K. Kreul[19], P. Krieger[159], K. Krizka[21], K. Kroeninger[51], H. Kroha[113], J. Kroll[135], J. Kroll[132], K. S. Krowpman[110], U. Kruchonak[40], H. Krüger[25], N. Krumnack[83], M. C. Kruse[53], O. Kuchinskaia[39], S. Kuday[3a], S. Kuehn[37], R. Kuesters[56], T. Kuhl[50], V. Kukhtin[40], Y. Kulchitsky[40], S. Kuleshov[141b,141d], M. Kumar[34g], N. Kumari[50], P. Kumari[160b], A. Kupco[135], T. Kupfer[51], A. Kupich[39], O. Kuprash[56], H. Kurashige[87], L. L. Kurchaninov[160a], O. Kurdysh[68], Y. A. Kurochkin[38], A. Kurova[39], M. Kuze[142], A. K. Kvam[106], J. Kvita[126], T. Kwan[107], N. G. Kyriacou[109], L. A. O. Laatu[105], C. Lacasta[168], F. Lacava[77a,77b], H. Lacker[19], D. Lacour[131], N. N. Lad[99], E. Ladygin[40], A. Lafarge[42], B. Laforge[131], T. Lagouri[177], F. Z. Lahbabi[36a], S. Lai[57], J. E. Lambert[170], S. Lammers[70], W. Lampl[7], C. Lampoudis[157,e], G. Lamprinoudis[103], A. N. Lancaster[119], E. Lançon[30], U. Landgraf[56], M. P. J. Landon[97], V. S. Lang[56], O. K. B. Langrekken[129], A. J. Lankford[163], F. Lanni[37], K. Lantzsch[25], A. Lanza[75a], M. Lanzac Berrocal[168], J. F. Laporte[139], T. Lari[73a], F. Lasagni Manghi[24b], M. Lassnig[37], V. Latonova[135], S. D. Lawlor[144], Z. Lawrence[104], R. Lazaridou[172], M. Lazzaroni[73a,73b], B. Le[104], H. D. M. Le[110], E. M. Le Boulicaut[177], L. T. Le Pottier[18a], B. Leban[24a,24b], A. Lebedev[83], M. LeBlanc[104], F. Ledroit-Guillon[62], S. C. Lee[153], S. Lee[49a,49b], T. F. Lee[95], L. L. Leeuw[34c], M. Lefebvre[170], C. Leggett[18a], G. Lehmann Miotto[37], M. Leigh[58], W. A. Leight[106], W. Leinonen[117], A. Leisos[157,s], M. A. L. Leite[85c], C. E. Leitgeb[19], R. Leitner[137], K. J. C. Leney[46], T. Lenz[25], S. Leone[76a], C. Leonidopoulos[54], A. Leopold[149], R. Les[110], C. G. Lester[33], M. Levchenko[39], J. Levêque[4], L. J. Levinson[174], G. Levrini[24a,24b], M. P. Lewicki[89], C. Lewis[143], D. J. Lewis[4], L. Lewitt[144], A. Li[30], B. Li[64b], C. Li[64a], C.-Q. Li[113], H. Li[64a], H. Li[64b], H. Li[115a], H. Li[15], H. Li[64b], J. Li[64c], K. Li[14], L. Li[64c], M. Li[14,115c], S. Li[14,115c], S. Li[64c,64d,d], T. Li[5], X. Li[107], Z. Li[158], Z. Li[14,115c], Z. Li[64a], S. Liang[14,115c], Z. Liang[14], M. Liberatore[139], B. Liberti[78a], K. Lie[66c], J. Lieber Marin[85e], H. Lien[70], H. Lin[109], K. Lin[110], L. Linden[112], R. E. Lindley[7], J. H. Lindon[2], J. Ling[63], E. Lipeles[132], A. Lipniacka[17], A. Lister[169], J. D. Little[70], B. Liu[14], B. X. Liu[115b], D. Liu[64c,64d], E. H. L. Liu[21], J. B. Liu[64a], J. K. K. Liu[33], K. Liu[64d], K. Liu[64c,64d], M. Liu[64a], M. Y. Liu[64a], P. Liu[14], Q. Liu[64c,64d,143], X. Liu[64a], X. Liu[64b], Y. Liu[115b,115c], Y. L. Liu[64b], Y. W. Liu[64a], S. L. Lloyd[97], E. M. Lobodzinska[50], P. Loch[7], E. Lodhi[159], T. Lohse[19], K. Lohwasser[144], E. Loiacono[50], J. D. Lomas[21], J. D. Long[43], I. Longarini[163], R. Longo[167], I. Lopez Paz[69], A. Lopez Solis[50], N. A. Lopez-canelas[7], N. Lorenzo Martinez[4], A. M. Lory[112], M. Losada[120a], G. Löschcke Centeno[151], O. Loseva[39], X. Lou[49a,49b], X. Lou[14,115c], A. Lounis[68], P. A. Love[94], G. Lu[14,115c], M. Lu[68], S. Lu[132], Y. J. Lu[153], H. J. Lubatti[143], C. Luci[77a,77b], F. L. Lucio Alves[115a], F. Luehring[70], O. Lukianchuk[68], B. S. Lunday[132], O. Lundberg[149], B. Lund-Jensen[149,*], N. A. Luongo[6], M. S. Lutz[37], A. B. Lux[26], D. Lynn[30], R. Lysak[135], E. Lytken[101], V. Lyubushkin[40], T. Lyubushkina[40], M. M. Lyukova[150], M.Firdaus M. Soberi[54], H. Ma[30], K. Ma[64a], L. L. Ma[64b], W. Ma[64a], Y. Ma[125], J. C. MacDonald[103], P. C. Machado De Abreu Farias[85e], R. Madar[42], T. Madula[99], J. Maeda[87], T. Maeno[30], P. T. Mafa[34c], H. Maguire[144], V. Maiboroda[139], A. Maio[134a,134b,134d], K. Maj[88a], O. Majersky[50], S. Majewski[127], N. Makovec[68], V. Maksimovic[16], B. Malaescu[131], Pa. Malecki[89], V. P. Maleev[39], F. Malek[62,n], M. Mali[96], D. Malito[98], U. Mallik[82,*], S. Maltezos[10], S. Malyukov[40], J. Mamuzic[13], G. Mancini[55], M. N. Mancini[27], G. Manco[75a,75b], J. P. Mandalia[97], S. S. Mandarry[151], I. Mandić[96], L. Manhaes de Andrade Filho[85a], I. M. Maniatis[174], J. Manjarres Ramos[92], D. C. Mankad[174], A. Mann[112], S. Manzoni[37], L. Mao[64c], X. Mapekula[34c], A. Marantis[157,s], G. Marchiori[5], M. Marcisovsky[135], C. Marcon[73a], M. Marinescu[21], S. Marium[50], M. Marjanovic[124], A. Markhoos[56], M. Markovitch[68], M. K. Maroun[106], E. J. Marshall[94], Z. Marshall[18a], S. Marti-Garcia[168], J. Martin[99], T. A. Martin[138], V. J. Martin[54], B. Martin dit Latour[17], L. Martinelli[77a,77b], M. Martinez[13,u], P. Martinez Agullo[168], V. I. Martinez Outschoorn[106], P. Martinez Suarez[13], S. Martin-Haugh[138], G. Martinovicova[137], V. S. Martoiu[28b], A. C. Martyniuk[99], A. Marzin[37], D. Mascione[80a,80b], L. Masetti[103], J. Masik[104], A. L. Maslennikov[39], S. L. Mason[43], P. Massarotti[74a,74b], P. Mastrandrea[76a,76b], A. Mastroberardino[45a,45b], T. Masubuchi[128], T. T. Mathew[127], T. Mathisen[166], J. Matousek[137], D. M. Mattern[51], J. Maurer[28b], T. Maurin[61], A. J. Maury[68], B. Maček[96], D. A. Maximov[39], A. E. May[104], R. Mazini[34g], I. Maznas[119], M. Mazza[110], S. M. Mazza[140], E. Mazzeo[73a,73b], J. P. Mc Gowan[170], S. P. Mc Kee[109], C. A. Mc Lean[6], C. C. McCracken[169], E. F. McDonald[108],

A. E. McDougall[118], L. F. Mcelhinney[94], J. A. Mcfayden[151], R. P. McGovern[132], R. P. Mckenzie[34g], T. C. Mclachlan[50], D. J. Mclaughlin[99], S. J. McMahon[138], C. M. Mcpartland[95], R. A. McPherson[170,y], S. Mehlhase[112], A. Mehta[95], D. Melini[168], B. R. Mellado Garcia[34g], A. H. Melo[57], F. Meloni[50], A. M. Mendes Jacques Da Costa[104], H. Y. Meng[159], L. Meng[94], S. Menke[113], M. Mentink[37], E. Meoni[45a,45b], G. Mercado[119], S. Merianos[157], C. Merlassino[71a,71c], L. Merola[74a,74b], C. Meroni[73a,73b], J. Metcalfe[6], A. S. Mete[6], E. Meuser[103], C. Meyer[70], J.-P. Meyer[139], R. P. Middleton[138], L. Mijović[54], G. Mikenberg[174], M. Mikestikova[135], M. Mikuž[96], H. Mildner[103], A. Milic[37], D. W. Miller[41], E. H. Miller[148], L. S. Miller[35], A. Milov[174], D. A. Milstead[49a,49b], T. Min[115a], A. A. Minaenko[39], I. A. Minashvili[154b], A. I. Mincer[121], B. Mindur[88a], M. Mineev[40], Y. Mino[90], L. M. Mir[13], M. Miralles Lopez[61], M. Mironova[18a], M. Missio[117], A. Mitra[172], V. A. Mitsou[168], Y. Mitsumori[114], O. Miu[159], P. S. Miyagawa[97], T. Mkrtchyan[65a], M. Mlinarevic[99], T. Mlinarevic[99], M. Mlynarikova[37], S. Mobius[20], P. Mogg[112], M. H. Mohamed Farook[116], A. F. Mohammed[14,115c], S. Mohapatra[43], G. Mokgatitswane[34g], L. Moleri[174], B. Mondal[146], S. Mondal[136], K. Mönig[50], E. Monnier[105], L. Monsonis Romero[168], J. Montejo Berlingen[13], A. Montella[49a,49b], M. Montella[123], F. Montereali[79a,79b], F. Monticelli[93], S. Monzani[71a,71c], A. Morancho Tarda[44], N. Morange[68], A. L. Moreira De Carvalho[50], M. Moreno Llácer[168], C. Moreno Martinez[58], J. M. Moreno Perez[23b], P. Morettini[59b], S. Morgenstern[37], M. Morii[63], M. Morinaga[158], M. Moritsu[91], F. Morodei[77a,77b], P. Moschovakos[37], B. Moser[130], M. Mosidze[154b], T. Moskalets[46], P. Moskvitina[117], J. Moss[32,k], P. Moszkowicz[88a], A. Moussa[36d], Y. Moyal[174], E. J. W. Moyse[106], O. Mtintsilana[34g], S. Muanza[105], J. Mueller[133], D. Muenstermann[94], R. Müller[37], G. A. Mullier[166], A. J. Mullin[33], J. J. Mullin[132], A. E. Mulski[63], D. P. Mungo[159], D. Munoz Perez[168], F. J. Munoz Sanchez[104], M. Murin[104], W. J. Murray[138,172], M. Muškinja[96], C. Mwewa[30], A. G. Myagkov[39,a], A. J. Myers[8], G. Myers[109], M. Myska[136], B. P. Nachman[18a], K. Nagai[130], K. Nagano[86], R. Nagasaka[158], J. L. Nagle[30,ah], E. Nagy[105], A. M. Nairz[37], Y. Nakahama[86], K. Nakamura[86], K. Nakkalil[5], H. Nanjo[128], E. A. Narayanan[46], Y. Narukawa[158], I. Naryshkin[39], L. Nasella[73a,73b], S. Nasri[120b], C. Nass[25], G. Navarro[23a], J. Navarro-Gonzalez[168], R. Nayak[156], A. Nayaz[19], P. Y. Nechaeva[39], S. Nechaeva[24a,24b], F. Nechansky[135], L. Nedic[130], T. J. Neep[21], A. Negri[75a,75b], M. Negrini[24b], C. Nellist[118], C. Nelson[107], K. Nelson[109], S. Nemecek[135], M. Nessi[37,h], M. S. Neubauer[167], F. Neuhaus[103], J. Neundorf[50], J. Newell[95], P. R. Newman[21], C. W. Ng[133], Y. W. Y. Ng[50], B. Ngair[120a], H. D. N. Nguyen[111], R. B. Nickerson[130], R. Nicolaidou[139], J. Nielsen[140], M. Niemeyer[57], J. Niermann[37], N. Nikiforou[37], V. Nikolaenko[39,a], I. Nikolic-Audit[131], K. Nikolopoulos[21], P. Nilsson[30], I. Ninca[50], G. Ninio[156], A. Nisati[77a], N. Nishu[2], R. Nisius[113], N. Nitika[71a,71c], J.-E. Nitschke[52], E. K. Nkadimeng[34g], T. Nobe[158], T. Nommensen[152], M. B. Norfolk[144], B. J. Norman[35], M. Noury[36a], J. Novak[96], T. Novak[96], L. Novotny[136], R. Novotny[116], L. Nozka[126], K. Ntekas[163], N. M. J. Nunes De Moura Junior[85b], J. Ocariz[131], A. Ochi[87], I. Ochoa[134a], S. Oerdek[50,v], J. T. Offermann[41], A. Ogrodnik[137], A. Oh[104], C. C. Ohm[149], H. Oide[86], R. Oishi[158], M. L. Ojeda[37], Y. Okumura[158], L. F. Oleiro Seabra[134a], I. Oleksiyuk[58], S. A. Olivares Pino[141d], G. Oliveira Correa[13], D. Oliveira Damazio[30], J. L. Oliver[163], Ö. O. Öncel[56], A. P. O'Neill[20], A. Onofre[134a,134e], P. U. E. Onyisi[11], M. J. Oreglia[41], D. Orestano[79a,79b], N. Orlando[13], R. S. Orr[159], L. M. Osojnak[132], R. Ospanov[64a], Y. Osumi[114], G. Otero y Garzon[31], H. Otono[91], P. S. Ott[65a], G. J. Ottino[18a], M. Ouchrif[36d], F. Ould-Saada[129], T. Ovsiannikova[143], M. Owen[61], R. E. Owen[138], V. E. Ozcan[22a], F. Ozturk[89], N. Ozturk[8], S. Ozturk[84], H. A. Pacey[130], A. Pacheco Pages[13], C. Padilla Aranda[13], G. Padovano[77a,77b], S. Pagan Griso[18a], G. Palacino[70], A. Palazzo[72a,72b], J. Pampel[25], J. Pan[177], T. Pan[66a], D. K. Panchal[11], C. E. Pandini[118], J. G. Panduro Vazquez[138], H. D. Pandya[1], H. Pang[15], P. Pani[50], G. Panizzo[71a,71c], L. Panwar[131], L. Paolozzi[58], S. Parajuli[167], A. Paramonov[6], C. Paraskevopoulos[55], D. Paredes Hernandez[66b], A. Pareti[75a,75b], K. R. Park[43], T. H. Park[159], M. A. Parker[33], F. Parodi[59a,59b], V. A. Parrish[54], J. A. Parsons[43], U. Parzefall[56], B. Pascual Dias[111], L. Pascual Dominguez[102], E. Pasqualucci[77a], S. Passaggio[59b], F. Pastore[98], P. Patel[89], U. M. Patel[53], J. R. Pater[104], T. Pauly[37], F. Pauwels[137], C. I. Pazos[162], M. Pedersen[129], R. Pedro[134a], S. V. Peleganchuk[39], O. Penc[37], E. A. Pender[54], S. Peng[15], G. D. Penn[177], K. E. Penski[112], M. Penzin[39], B. S. Peralva[85d], A. P. Pereira Peixoto[143], L. Pereira Sanchez[148], D. V. Perepelitsa[30,ah], G. Perera[106], E. Perez Codina[160a], M. Perganti[10], H. Pernegger[37], S. Perrella[77a,77b], O. Perrin[42], K. Peters[50], R. F. Y. Peters[104], B. A. Petersen[37], T. C. Petersen[44], E. Petit[105], V. Petousis[136], C. Petridou[157,e], T. Petru[137], A. Petrukhin[146], M. Pettee[18a], A. Petukhov[84], K. Petukhova[37], R. Pezoa[141f], L. Pezzotti[37], G. Pezzullo[177], A. J. Pfleger[37], T. M. Pham[175], T. Pham[108], P. W. Phillips[138], G. Piacquadio[150], E. Pianori[18a], F. Piazza[127], R. Piegaia[31], D. Pietreanu[28b], A. D. Pilkington[104], M. Pinamonti[71a,71c],

J. L. Pinfold[2], B. C. Pinheiro Pereira[134a], J. Pinol Bel[13], A. E. Pinto Pinoargote[139], L. Pintucci[71a,71c], K. M. Piper[151], A. Pirttikoski[58], D. A. Pizzi[35], L. Pizzimento[66b], A. Pizzini[118], M.-A. Pleier[30], V. Pleskot[137], E. Plotnikova[40], G. Poddar[97], R. Poettgen[101], L. Poggioli[131], S. Polacek[137], G. Polesello[75a], A. Poley[147,160a], A. Polini[24b], C. S. Pollard[172], Z. B. Pollock[123], E. Pompa Pacchi[124], N. I. Pond[99], D. Ponomarenko[70], L. Pontecorvo[37], S. Popa[28a], G. A. Popeneciu[28d], A. Poreba[37], D. M. Portillo Quintero[160a], S. Pospisil[136], M. A. Postill[144], P. Postolache[28c], K. Potamianos[172], P. A. Potepa[88a], I. N. Potrap[40], C. J. Potter[33], H. Potti[152], J. Poveda[168], M. E. Pozo Astigarraga[37], A. Prades Ibanez[78a,78b], J. Pretel[170], D. Price[104], M. Primavera[72a], L. Primomo[71a,71c], M. A. Principe Martin[102], R. Privara[126], T. Procter[61], M. L. Proffitt[143], N. Proklova[132], K. Prokofiev[66c], G. Proto[113], J. Proudfoot[6], M. Przybycien[88a], W. W. Przygoda[88b], A. Psallidas[48], J. E. Puddefoot[144], D. Pudzha[56], D. Pyatiizbyantseva[39], J. Qian[109], R. Qian[110], D. Qichen[104], Y. Qin[13], T. Qiu[54], A. Quadt[57], M. Queitsch-Maitland[104], G. Quetant[58], R. P. Quinn[169], G. Rabanal Bolanos[63], D. Rafanoharana[56], F. Raffaeli[78a,78b], F. Ragusa[73a,73b], J. L. Rainbolt[41], J. A. Raine[58], S. Rajagopalan[30], E. Ramakoti[39], L. Rambelli[59a,59b], I. A. Ramirez-Berend[35], K. Ran[50,115c], D. S. Rankin[132], N. P. Rapheeha[34g], H. Rasheed[28b], V. Raskina[131], D. F. Rassloff[65a], A. Rastogi[18a], S. Rave[103], S. Ravera[59a,59b], B. Ravina[57], I. Ravinovich[174], M. Raymond[37], A. L. Read[129], N. P. Readioff[144], D. M. Rebuzzi[75a,75b], G. Redlinger[30], A. S. Reed[113], K. Reeves[27], J. A. Reidelsturz[176], D. Reikher[127], A. Rej[51], C. Rembser[37], M. Renda[28b], F. Renner[50], A. G. Rennie[163], A. L. Rescia[50], S. Resconi[73a], M. Ressegotti[59a,59b], S. Rettie[37], J. G. Reyes Rivera[110], E. Reynolds[18a], O. L. Rezanova[39], P. Reznicek[137], H. Riani[36d], N. Ribaric[53], E. Ricci[80a,80b], R. Richter[113], S. Richter[49a,49b], E. Richter-Was[88b], M. Ridel[131], S. Ridouani[36d], P. Rieck[121], P. Riedler[37], E. M. Riefel[49a,49b], J. O. Rieger[118], M. Rijssenbeek[150], M. Rimoldi[37], L. Rinaldi[24a,24b], P. Rincke[57], T. T. Rinn[30], M. P. Rinnagel[112], G. Ripellino[166], I. Riu[13], J. C. Rivera Vergara[170], F. Rizatdinova[125], E. Rizvi[97], B. R. Roberts[18a], S. S. Roberts[140], S. H. Robertson[107,y], D. Robinson[33], M. Robles Manzano[103], A. Robson[61], A. Rocchi[78a,78b], C. Roda[76a,76b], S. Rodriguez Bosca[37], Y. Rodriguez Garcia[23a], A. M. Rodríguez Vera[119], S. Roe[37], J. T. Roemer[37], A. R. Roepe-Gier[140], O. Røhne[129], R. A. Rojas[37], C. P. A. Roland[131], J. Roloff[30], A. Romaniouk[81], E. Romano[75a,75b], M. Romano[24b], A. C. Romero Hernandez[167], N. Rompotis[95], L. Roos[131], S. Rosati[77a], B. J. Rosser[41], E. Rossi[130], E. Rossi[74a,74b], L. P. Rossi[63], L. Rossini[56], R. Rosten[123], M. Rotaru[28b], B. Rottler[56], C. Rougier[92], D. Rousseau[68], D. Rousso[50], A. Roy[167], S. Roy-Garand[159], A. Rozanov[105], Z. M. A. Rozario[61], Y. Rozen[155], A. Rubio Jimenez[168], V. H. Ruelas Rivera[19], T. A. Ruggeri[1], A. Ruggiero[130], A. Ruiz-Martinez[168], A. Rummler[37], Z. Rurikova[56], N. A. Rusakovich[40], H. L. Russell[170], G. Russo[77a,77b], J. P. Rutherfoord[7], S. Rutherford Colmenares[33], M. Rybar[137], E. B. Rye[129], A. Ryzhov[46], J. A. Sabater Iglesias[58], H.F-W. Sadrozinski[140], F. Safai Tehrani[77a], B. Safarzadeh Samani[138], S. Saha[1], M. Sahinsoy[84], A. Saibel[168], M. Saimpert[139], M. Saito[158], T. Saito[158], A. Sala[73a,73b], D. Salamani[37], A. Salnikov[148], J. Salt[168], A. Salvador Salas[156], D. Salvatore[45a,45b], F. Salvatore[151], A. Salzburger[37], D. Sammel[56], E. Sampson[94], D. Sampsonidis[157,e], D. Sampsonidou[127], J. Sánchez[168], V. Sanchez Sebastian[168], H. Sandaker[129], C. O. Sander[50], J. A. Sandesara[106], M. Sandhoff[176], C. Sandoval[23b], L. Sanfilippo[65a], D. P. C. Sankey[138], T. Sano[90], A. Sansoni[55], L. Santi[37,77b], C. Santoni[42], H. Santos[134a,134b], A. Santra[174], E. Sanzani[24a,24b], K. A. Saoucha[165], J. G. Saraiva[134a,134d], J. Sardain[7], O. Sasaki[86], K. Sato[161], C. Sauer[37], E. Sauvan[4], P. Savard[159,af], R. Sawada[158], C. Sawyer[138], L. Sawyer[100], C. Sbarra[24b], A. Sbrizzi[24a,24b], T. Scanlon[99], J. Schaarschmidt[143], U. Schäfer[103], A. C. Schaffer[46,68], D. Schaile[112], R. D. Schamberger[150], C. Scharf[19], M. M. Schefer[20], V. A. Schegelsky[39], D. Scheirich[137], M. Schernau[141e], C. Scheulen[58], C. Schiavi[59a,59b], M. Schioppa[45a,45b], B. Schlag[148], S. Schlenker[37], J. Schmeing[176], M. A. Schmidt[176], K. Schmieden[103], C. Schmitt[103], N. Schmitt[103], S. Schmitt[50], L. Schoeffel[139], A. Schoening[65b], P. G. Scholer[35], E. Schopf[130], M. Schott[25], J. Schovancova[37], S. Schramm[58], T. Schroer[58], H.-C. Schultz-Coulon[65a], M. Schumacher[56], B. A. Schumm[140], Ph. Schune[139], A. J. Schuy[143], H. R. Schwartz[140], A. Schwartzman[148], T. A. Schwarz[109], Ph. Schwemling[139], R. Schwienhorst[110], F. G. Sciacca[20], A. Sciandra[30], G. Sciolla[27], F. Scuri[76a], C. D. Sebastiani[95], K. Sedlaczek[119], S. C. Seidel[116], A. Seiden[140], B. D. Seidlitz[43], C. Seitz[50], J. M. Seixas[85b], G. Sekhniaidze[74a], L. Selem[62], N. Semprini-Cesari[24a,24b], A. Semushin[39,178], D. Sengupta[58], V. Senthilkumar[168], L. Serin[68], M. Sessa[78a,78b], H. Severini[124], F. Sforza[59a,59b], A. Sfyrla[58], Q. Sha[14], E. Shabalina[57], A. H. Shah[33], R. Shaheen[149], J. D. Shahinian[132], D. Shaked Renous[174], L. Y. Shan[14], M. Shapiro[18a], A. Sharma[37], A. S. Sharma[169], P. Sharma[30], P. B. Shatalov[39], K. Shaw[151], S. M. Shaw[104], Q. Shen[64c], D. J. Sheppard[147], P. Sherwood[99], L. Shi[99], X. Shi[14], S. Shimizu[86], C. O. Shimmin[177], I. P. J. Shipsey[130,*], S. Shirabe[91], M. Shiyakova[40,w],

M. J. Shochet[41], D. R. Shope[129], B. Shrestha[124], S. Shrestha[123,ai], I. Shreyber[39], M. J. Shroff[170], P. Sicho[135], A. M. Sickles[167], E. Sideras Haddad[34g,164], A. C. Sidley[118], A. Sidoti[24b], F. Siegert[52], Dj. Sijacki[16], F. Sili[93], J. M. Silva[54], I. Silva Ferreira[85b], M. V. Silva Oliveira[30], S. B. Silverstein[49a], S. Simion[68], R. Simoniello[37], E. L. Simpson[104], H. Simpson[151], L. R. Simpson[109], S. Simsek[84], S. Sindhu[57], P. Sinervo[159], S. Singh[30], S. Sinha[50], S. Sinha[104], M. Sioli[24a,24b], I. Siral[37], E. Sitnikova[50], J. Sjölin[49a,49b], A. Skaf[57], E. Skorda[21], P. Skubic[124], M. Slawinska[89], I. Slazyk[17], V. Smakhtin[174], B. H. Smart[138], S.Yu. Smirnov[39], Y. Smirnov[39], L. N. Smirnova[39,a], O. Smirnova[101], A. C. Smith[43], D. R. Smith[163], E. A. Smith[41], J. L. Smith[104], R. Smith[148], H. Smitmanns[103], M. Smizanska[94], K. Smolek[136], A. A. Snesarev[39], H. L. Snoek[118], S. Snyder[30], R. Sobie[170,y], A. Soffer[156], C. A. Solans Sanchez[37], E.Yu. Soldatov[39], U. Soldevila[168], A. A. Solodkov[39], S. Solomon[27], A. Soloshenko[40], K. Solovieva[56], O. V. Solovyanov[42], P. Sommer[52], A. Sonay[13], W. Y. Song[160b], A. Sopczak[136], A. L. Sopio[54], F. Sopkova[29b], J. D. Sorenson[116], I. R. Sotarriva Alvarez[142], V. Sothilingam[65a], O. J. Soto Sandoval[141b,141c], S. Sottocornola[70], R. Soualah[165], Z. Soumaimi[36e], D. South[50], N. Soybelman[174], S. Spagnolo[72a,72b], M. Spalla[113], D. Sperlich[56], G. Spigo[37], B. Spisso[74a,74b], D. P. Spiteri[61], M. Spousta[137], E. J. Staats[35], R. Stamen[65a], A. Stampekis[21], E. Stanecka[89], W. Stanek-Maslouska[50], M. V. Stange[52], B. Stanislaus[18a], M. M. Stanitzki[50], B. Stapf[50], E. A. Starchenko[39], G. H. Stark[140], J. Stark[92], P. Staroba[135], P. Starovoitov[65a], S. Stärz[107], R. Staszewski[89], G. Stavropoulos[48], A. Stefl[37], P. Steinberg[30], B. Stelzer[147,160a], H. J. Stelzer[133], O. Stelzer[160a], H. Stenzel[60], T. J. Stevenson[151], G. A. Stewart[37], J. R. Stewart[125], M. C. Stockton[37], G. Stoicea[28b], M. Stolarski[134a], S. Stonjek[113], A. Straessner[52], J. Strandberg[149], S. Strandberg[49a,49b], M. Stratmann[176], M. Strauss[124], T. Strebler[105], P. Strizenec[29b], R. Ströhmer[171], D. M. Strom[127], R. Stroynowski[46], A. Strubig[49a,49b], S. A. Stucci[30], B. Stugu[17], J. Stupak[124], N. A. Styles[50], D. Su[148], S. Su[64a], W. Su[64d], X. Su[64a], D. Suchy[29a], K. Sugizaki[158], V. V. Sulin[39], M. J. Sullivan[95], D. M. S. Sultan[130], L. Sultanaliyeva[39], S. Sultansoy[3b], T. Sumida[90], S. Sun[175], W. Sun[14], O. Sunneborn Gudnadottir[166], N. Sur[105], M. R. Sutton[151], H. Suzuki[161], M. Svatos[135], M. Swiatlowski[160a], T. Swirski[171], I. Sykora[29a], M. Sykora[137], T. Sykora[137], D. Ta[103], K. Tackmann[50,v], A. Taffard[163], R. Tafirout[160a], J. S. Tafoya Vargas[68], Y. Takubo[86], M. Talby[105], A. A. Talyshev[39], K. C. Tam[66b], N. M. Tamir[156], A. Tanaka[158], J. Tanaka[158], R. Tanaka[68], M. Tanasini[150], Z. Tao[169], S. Tapia Araya[141f], S. Tapprogge[103], A. Tarek Abouelfadl Mohamed[110], S. Tarem[155], K. Tariq[14], G. Tarna[28b], G. F. Tartarelli[73a], M. J. Tartarin[92], P. Tas[137], M. Tasevsky[135], E. Tassi[45a,45b], A. C. Tate[167], G. Tateno[158], Y. Tayalati[36e,x], G. N. Taylor[108], W. Taylor[160b], P. Teixeira-Dias[98], J. J. Teoh[159], K. Terashi[158], J. Terron[102], S. Terzo[13], M. Testa[55], R. J. Teuscher[159,y], A. Thaler[81], O. Theiner[58], T. Theveneaux-Pelzer[105], O. Thielmann[176], D. W. Thomas[98], J. P. Thomas[21], E. A. Thompson[18a], P. D. Thompson[21], E. Thomson[132], R. E. Thornberry[46], C. Tian[64a], Y. Tian[58], V. Tikhomirov[39,a], Yu.A. Tikhonov[39], S. Timoshenko[39], D. Timoshyn[137], E. X. L. Ting[1], P. Tipton[177], A. Tishelman-Charny[30], S. H. Tlou[34g], K. Todome[142], S. Todorova-Nova[137], S. Todt[52], L. Toffolin[71a,71c], M. Togawa[86], J. Tojo[91], S. Tokár[29a], K. Tokushuku[86], O. Toldaiev[70], G. Tolkachev[105], M. Tomoto[86,114], L. Tompkins[148,m], E. Torrence[127], H. Torres[92], E. Torró Pastor[168], M. Toscani[31], C. Tosciri[41], M. Tost[11], D. R. Tovey[144], I. S. Trandafir[28b], T. Trefzger[171], A. Tricoli[30], I. M. Trigger[160a], S. Trincaz-Duvoid[131], D. A. Trischuk[27], B. Trocmé[62], A. Tropina[40], L. Truong[34c], M. Trzebinski[89], A. Trzupek[89], F. Tsai[150], M. Tsai[109], A. Tsiamis[157], P. V. Tsiareshka[40], S. Tsigaridas[160a], A. Tsirigotis[157,s], V. Tsiskaridze[159], E. G. Tskhadadze[154a], M. Tsopoulou[157], Y. Tsujikawa[90], I. I. Tsukerman[39], V. Tsulaia[18a], S. Tsuno[86], K. Tsuri[122], D. Tsybychev[150], Y. Tu[66b], A. Tudorache[28b], V. Tudorache[28b], A. N. Tuna[63], S. Turchikhin[59a,59b], I. Turk Cakir[3a], R. Turra[73a], T. Turtuvshin[40,z], P. M. Tuts[43], S. Tzamarias[157,e], E. Tzovara[103], F. Ukegawa[161], P. A. Ulloa Poblete[141b,141c], E. N. Umaka[30], G. Unal[37], A. Undrus[30], G. Unel[163], J. Urban[29b], P. Urrejola[141a], G. Usai[8], R. Ushioda[142], M. Usman[111], F. Ustuner[54], Z. Uysal[84], V. Vacek[136], B. Vachon[107], T. Vafeiadis[37], A. Vaitkus[99], C. Valderanis[112], E. Valdes Santurio[49a,49b], M. Valente[160a], S. Valentinetti[24a,24b], A. Valero[168], E. Valiente Moreno[168], A. Vallier[92], J. A. Valls Ferrer[168], D. R. Van Arneman[118], T. R. Van Daalen[143], A. Van Der Graaf[51], P. Van Gemmeren[6], M. Van Rijnbach[37], S. Van Stroud[99], I. Van Vulpen[118], P. Vana[137], M. Vanadia[78a,78b], U. M. Vande Voorde[149], W. Vandelli[37], E. R. Vandewall[125], D. Vannicola[156], L. Vannoli[55], R. Vari[77a], E. W. Varnes[7], C. Varni[18b], D. Varouchas[68], L. Varriale[168], K. E. Varvell[152], M. E. Vasile[28b], L. Vaslin[86], A. Vasyukov[40], L. M. Vaughan[125], R. Vavricka[103], T. Vazquez Schroeder[37], J. Veatch[32], V. Vecchio[104], M. J. Veen[106], I. Veliscek[30], L. M. Veloce[159], F. Veloso[134a,134c], S. Veneziano[77a], A. Ventura[72a,72b], S. Ventura Gonzalez[139], A. Verbytskyi[113], M. Verducci[76a,76b], C. Vergis[97], M. Verissimo De Araujo[85b], W. Verkerke[118], J. C. Vermeulen[118], C. Vernieri[148], M. Vessella[163],

M. C. Vetterli[147,af], A. Vgenopoulos[103], N. Viaux Maira[141f], T. Vickey[144], O. E. Vickey Boeriu[144], G. H. A. Viehhauser[130], L. Vigani[65b], M. Vigl[113], M. Villa[24a,24b], M. Villaplana Perez[168], E. M. Villhauer[54], E. Vilucchi[55], M. G. Vincter[35], A. Visibile[118], C. Vittori[37], I. Vivarelli[24a,24b], E. Voevodina[113], F. Vogel[112], J. C. Voigt[52], P. Vokac[136], Yu. Volkotrub[88b], E. Von Toerne[25], B. Vormwald[37], V. Vorobel[137], K. Vorobev[39], M. Vos[168], K. Voss[146], M. Vozak[118], L. Vozdecky[124], N. Vranjes[16], M. Vranjes Milosavljevic[16], M. Vreeswijk[118], N. K. Vu[64c,64d], R. Vuillermet[37], O. Vujinovic[103], I. Vukotic[41], I. K. Vyas[35], S. Wada[161], C. Wagner[148], J. M. Wagner[18a], W. Wagner[176], S. Wahdan[176], H. Wahlberg[93], C. H. Waits[124], J. Walder[138], R. Walker[112], W. Walkowiak[146], A. Wall[132], E. J. Wallin[101], T. Wamorkar[6], A. Z. Wang[140], C. Wang[103], C. Wang[11], H. Wang[18a], J. Wang[66c], P. Wang[104], P. Wang[99], R. Wang[63], R. Wang[6], S. M. Wang[153], S. Wang[14], T. Wang[64a], W. T. Wang[82], W. Wang[14], X. Wang[167], X. Wang[64c], Y. Wang[64d], Y. Wang[115a], Y. Wang[64a], Z. Wang[109], Z. Wang[53,64c,64d], Z. Wang[109], A. Warburton[107], R. J. Ward[21], N. Warrack[61], S. Waterhouse[98], A. T. Watson[21], H. Watson[54], M. F. Watson[21], E. Watton[61,138], G. Watts[143], B. M. Waugh[99], J. M. Webb[56], C. Weber[30], H. A. Weber[19], M. S. Weber[20], S. M. Weber[65a], C. Wei[64a], Y. Wei[56], A. R. Weidberg[130], E. J. Weik[121], J. Weingarten[51], C. Weiser[56], C. J. Wells[50], T. Wenaus[30], B. Wendland[51], T. Wengler[37], N. S. Wenke[113], N. Wermes[25], M. Wessels[65a], A. M. Wharton[94], A. S. White[63], A. White[8], M. J. White[1], D. Whiteson[163], L. Wickremasinghe[128], W. Wiedenmann[175], M. Wielers[138], C. Wiglesworth[44], D. J. Wilbern[124], H. G. Wilkens[37], J. J. H. Wilkinson[33], D. M. Williams[43], H. H. Williams[132], S. Williams[33], S. Willocq[106], B. J. Wilson[104], D. J. Wilson[104], P. J. Windischhofer[41], F. I. Winkel[31], F. Winklmeier[127], B. T. Winter[56], J. K. Winter[104], M. Wittgen[148], M. Wobisch[100], T. Wojtkowski[62], Z. Wolffs[118], J. Wollrath[37], M. W. Wolter[89], H. Wolters[134a,134c], M. C. Wong[140], E. L. Woodward[43], S. D. Worm[50], B. K. Wosiek[89], K. W. Woźniak[89], S. Wozniewski[57], K. Wraight[61], C. Wu[21], M. Wu[115b], M. Wu[117], S. L. Wu[175], X. Wu[58], X. Wu[64a], Y. Wu[64a], Z. Wu[4], J. Wuerzinger[113,ad], T. R. Wyatt[104], B. M. Wynne[54], S. Xella[44], L. Xia[115a], M. Xia[15], M. Xie[64a], A. Xiong[127], J. Xiong[18a], D. Xu[14], H. Xu[64a], L. Xu[64a], R. Xu[132], T. Xu[109], Y. Xu[143], Z. Xu[54], Z. Xu[115a], B. Yabsley[152], S. Yacoob[34a], Y. Yamaguchi[86], E. Yamashita[158], H. Yamauchi[161], T. Yamazaki[18a], Y. Yamazaki[87], S. Yan[61], Z. Yan[106], H. J. Yang[64c,64d], H. T. Yang[64a], S. Yang[64a], T. Yang[66c], X. Yang[37], X. Yang[14], Y. Yang[46], Y. Yang[64a], W.-M. Yao[18a], H. Ye[57], J. Ye[14], S. Ye[30], X. Ye[64a], Y. Yeh[99], I. Yeletskikh[40], B. Yeo[18b], M. R. Yexley[99], T. P. Yildirim[130], P. Yin[43], K. Yorita[173], S. Younas[28b], C. J. S. Young[37], C. Young[148], C. Yu[14,115c], Y. Yu[64a], J. Yuan[14,115c], M. Yuan[109], R. Yuan[64c,64d], L. Yue[99], M. Zaazoua[64a], B. Zabinski[89], I. Zahir[36a], E. Zaid[54], Z. K. Zak[89], T. Zakareishvili[168], S. Zambito[58], J. A. Zamora Saa[141b,141d], J. Zang[158], D. Zanzi[56], R. Zanzottera[73a,73b], O. Zaplatilek[136], C. Zeitnitz[176], H. Zeng[14], J. C. Zeng[167], D. T. Zenger Jr[27], O. Zenin[39], T. Ženiš[29a], S. Zenz[97], S. Zerradi[36a], D. Zerwas[68], M. Zhai[14,115c], D. F. Zhang[144], J. Zhang[64b], J. Zhang[6], K. Zhang[14,115c], L. Zhang[64a], L. Zhang[115a], P. Zhang[14,115c], R. Zhang[175], S. Zhang[109], S. Zhang[92], T. Zhang[158], X. Zhang[64c], Y. Zhang[143], Y. Zhang[99], Y. Zhang[115a], Z. Zhang[18a], Z. Zhang[64b], Z. Zhang[68], H. Zhao[143], T. Zhao[64b], Y. Zhao[140], Z. Zhao[64a], Z. Zhao[64a], A. Zhemchugov[40], J. Zheng[115a], K. Zheng[167], X. Zheng[64a], Z. Zheng[148], D. Zhong[167], B. Zhou[109], H. Zhou[7], N. Zhou[64c], Y. Zhou[15], Y. Zhou[115a], Y. Zhou[7], C. G. Zhu[64b], J. Zhu[109], X. Zhu[64d], Y. Zhu[64c], Y. Zhu[64a], X. Zhuang[14], K. Zhukov[70], N. I. Zimine[40], J. Zinsser[65b], M. Ziolkowski[146], L. Živković[16], A. Zoccoli[24a,24b], K. Zoch[63], T. G. Zorbas[144], O. Zormpa[48], W. Zou[43], L. Zwalinski[37]

[1] Department of Physics, University of Adelaide, Adelaide, Australia
[2] Department of Physics, University of Alberta, Edmonton, AB, Canada
[3] [(a)]Department of Physics, Ankara University, Ankara, Türkiye; [(b)]Division of Physics, TOBB University of Economics and Technology, Ankara, Türkiye
[4] LAPP, CNRS/IN2P3, Université Savoie Mont Blanc, Annecy, France
[5] APC, CNRS/IN2P3, Université Paris Cité, Paris, France
[6] High Energy Physics Division, Argonne National Laboratory, Argonne, IL, USA
[7] Department of Physics, University of Arizona, Tucson, AZ, USA
[8] Department of Physics, University of Texas at Arlington, Arlington, TX, USA
[9] Physics Department, National and Kapodistrian University of Athens, Athens, Greece
[10] Physics Department, National Technical University of Athens, Zografou, Greece
[11] Department of Physics, University of Texas at Austin, Austin, TX, USA
[12] Institute of Physics, Azerbaijan Academy of Sciences, Baku, Azerbaijan

[13] Institut de Física d'Altes Energies (IFAE), Barcelona Institute of Science and Technology, Barcelona, Spain
[14] Institute of High Energy Physics, Chinese Academy of Sciences, Beijing, China
[15] Physics Department, Tsinghua University, Beijing, China
[16] Institute of Physics, University of Belgrade, Belgrade, Serbia
[17] Department for Physics and Technology, University of Bergen, Bergen, Norway
[18] [(a)]Physics Division, Lawrence Berkeley National Laboratory, Berkeley, CA, USA; [(b)]University of California, Berkeley, CA, USA
[19] Institut für Physik, Humboldt Universität zu Berlin, Berlin, Germany
[20] Albert Einstein Center for Fundamental Physics and Laboratory for High Energy Physics, University of Bern, Bern, Switzerland
[21] School of Physics and Astronomy, University of Birmingham, Birmingham, UK
[22] [(a)]Department of Physics, Bogazici University, Istanbul, Türkiye; [(b)]Department of Physics Engineering, Gaziantep University, Gaziantep, Türkiye; [(c)]Department of Physics, Istanbul University, Istanbul, Türkiye
[23] [(a)]Facultad de Ciencias y Centro de Investigaciónes, Universidad Antonio Nariño, Bogotá, Colombia; [(b)]Departamento de Física, Universidad Nacional de Colombia, Bogotá, Colombia
[24] [(a)]Dipartimento di Fisica e Astronomia A. Righi, Università di Bologna, Bologna, Italy; [(b)]INFN Sezione di Bologna, Bologna, Italy
[25] Physikalisches Institut, Universität Bonn, Bonn, Germany
[26] Department of Physics, Boston University, Boston, MA, USA
[27] Department of Physics, Brandeis University, Waltham, MA, USA
[28] [(a)]Transilvania University of Brasov, Brasov, Romania; [(b)]Horia Hulubei National Institute of Physics and Nuclear Engineering, Bucharest, Romania; [(c)]Department of Physics, Alexandru Ioan Cuza University of Iasi, Iasi, Romania ; [(d)]National Institute for Research and Development of Isotopic and Molecular Technologies, Physics Department, Cluj-Napoca, Romania; [(e)]National University of Science and Technology Politechnica, Bucharest, Romania; [(f)]West University in Timisoara, Timisoara, Romania; [(g)]Faculty of Physics, University of Bucharest, Bucharest, Romania
[29] [(a)]Faculty of Mathematics, Physics and Informatics, Comenius University, Bratislava, Slovakia; [(b)]Department of Subnuclear Physics, Institute of Experimental Physics of the Slovak Academy of Sciences, Kosice, Slovak Republic
[30] Physics Department, Brookhaven National Laboratory, Upton, NY, USA
[31] Universidad de Buenos Aires, Facultad de Ciencias Exactas y Naturales, Departamento de Física, y CONICET, Instituto de Física de Buenos Aires (IFIBA), Buenos Aires, Argentina
[32] California State University, Long Beach, CA, USA
[33] Cavendish Laboratory, University of Cambridge, Cambridge, UK
[34] [(a)]Department of Physics, University of Cape Town, Cape Town, South Africa; [(b)]iThemba Labs, Western Cape, South Africa; [(c)]Department of Mechanical Engineering Science, University of Johannesburg, Johannesburg, South Africa; [(d)]National Institute of Physics, University of the Philippines Diliman (Philippines), Quezon City, Philippines; [(e)]University of South Africa, Department of Physics, Pretoria, South Africa; [(f)]University of Zululand, KwaDlangezwa, South Africa; [(g)]School of Physics, University of the Witwatersrand, Johannesburg, South Africa
[35] Department of Physics, Carleton University, Ottawa, ON, Canada
[36] [(a)]Faculté des Sciences Ain Chock, Université Hassan II de Casablanca, Casablanca, Morocco; [(b)]Faculté des Sciences, Université Ibn-Tofail, Kénitra, Morocco; [(c)]Faculté des Sciences Semlalia, LPHEA-Marrakech, Université Cadi Ayyad, Marrakech, Morocco; [(d)]LPMR, Faculté des Sciences, Université Mohamed Premier, Oujda, Morocco; [(e)]Faculté des sciences, Université Mohammed V, Rabat, Morocco; [(f)]Institute of Applied Physics, Mohammed VI Polytechnic University, Ben Guerir, Morocco
[37] CERN, Geneva, Switzerland
[38] Affiliated with an Institute Formerly Covered by a Cooperation Agreement with CERN, Geneva, Switzerland
[39] Affiliated with an Institute Covered by a Cooperation Agreement with CERN, Geneva, Switzerland
[40] Affiliated with an International Laboratory Covered by a Cooperation Agreement with CERN, Geneva, Switzerland
[41] Enrico Fermi Institute, University of Chicago, Chicago, IL, USA
[42] LPC, CNRS/IN2P3, Université Clermont Auvergne, Clermont-Ferrand, France
[43] Nevis Laboratory, Columbia University, Irvington, NY, USA
[44] Niels Bohr Institute, University of Copenhagen, Copenhagen, Denmark
[45] [(a)]Dipartimento di Fisica, Università della Calabria, Rende, Italy; [(b)]Laboratori Nazionali di Frascati, INFN Gruppo Collegato di Cosenza, Cosenza, Italy

[46] Physics Department, Southern Methodist University, Dallas, TX, USA
[47] Physics Department, University of Texas at Dallas, Richardson, TX, USA
[48] National Centre for Scientific Research “Demokritos”, Agia Paraskevi, Greece
[49] [(a)]Department of Physics, Stockholm University, Stockholm, Sweden; [(b)]Oskar Klein Centre, Stockholm, Sweden
[50] Deutsches Elektronen-Synchrotron DESY, Hamburg and Zeuthen, Germany
[51] Fakultät Physik , Technische Universität Dortmund, Dortmund, Germany
[52] Institut für Kern- und Teilchenphysik, Technische Universität Dresden, Dresden, Germany
[53] Department of Physics, Duke University, Durham, NC, USA
[54] SUPA-School of Physics and Astronomy, University of Edinburgh, Edinburgh, UK
[55] INFN e Laboratori Nazionali di Frascati, Frascati, Italy
[56] Physikalisches Institut, Albert-Ludwigs-Universität Freiburg, Freiburg, Germany
[57] II. Physikalisches Institut, Georg-August-Universität Göttingen, Göttingen, Germany
[58] Département de Physique Nucléaire et Corpusculaire, Université de Genève, Geneva, Switzerland
[59] [(a)]Dipartimento di Fisica, Università di Genova, Genoa, Italy; [(b)]INFN Sezione di Genova, Genoa, Italy
[60] II. Physikalisches Institut, Justus-Liebig-Universität Giessen, Giessen, Germany
[61] SUPA-School of Physics and Astronomy, University of Glasgow, Glasgow, UK
[62] LPSC, CNRS/IN2P3, Grenoble INP, Université Grenoble Alpes, Grenoble, France
[63] Laboratory for Particle Physics and Cosmology, Harvard University, Cambridge, MA, USA
[64] [(a)]Department of Modern Physics and State Key Laboratory of Particle Detection and Electronics, University of Science and Technology of China, Hefei, China; [(b)]Institute of Frontier and Interdisciplinary Science and Key Laboratory of Particle Physics and Particle Irradiation (MOE), Shandong University, Qingdao, China; [(c)]State Key Laboratory of Dark Matter Physics, School of Physics and Astronomy, Key Laboratory for Particle Astrophysics and Cosmology (MOE), Shanghai Jiao Tong University, SKLPPC, Shanghai, China; [(d)]State Key Laboratory of Dark Matter Physics, Tsung-Dao Lee Institute, Shanghai Jiao Tong University, Shanghai, China; [(e)]School of Physics, Zhengzhou University, Zhengzhou, China
[65] [(a)]Kirchhoff-Institut für Physik, Ruprecht-Karls-Universität Heidelberg, Heidelberg, Germany; [(b)]Physikalisches Institut, Ruprecht-Karls-Universität Heidelberg, Heidelberg, Germany
[66] [(a)]Department of Physics, Chinese University of Hong Kong, Shatin, N.T., Hong Kong, China; [(b)]Department of Physics, University of Hong Kong, Pok Fu La, Hong Kong, China; [(c)]Department of Physics and Institute for Advanced Study, Hong Kong University of Science and Technology, Clear Water Bay, Kowloon, Hong Kong, China
[67] Department of Physics, National Tsing Hua University, Hsinchu, Taiwan
[68] IJCLab, CNRS/IN2P3, Université Paris-Saclay, 91405 Orsay, France
[69] Centro Nacional de Microelectrónica (IMB-CNM-CSIC), Barcelona, Spain
[70] Department of Physics, Indiana University, Bloomington, IN, USA
[71] [(a)]INFN Gruppo Collegato di Udine, Sezione di Trieste, Udine, Italy; [(b)]ICTP, Trieste, Italy; [(c)]Dipartimento Politecnico di Ingegneria e Architettura, Università di Udine, Udine, Italy
[72] [(a)]INFN Sezione di Lecce, Lecce, Italy; [(b)]Dipartimento di Matematica e Fisica, Università del Salento, Lecce, Italy
[73] [(a)]INFN Sezione di Milano, Milan, Italy; [(b)]Dipartimento di Fisica, Università di Milano, Milan, Italy
[74] [(a)]INFN Sezione di Napoli, Naples, Italy; [(b)]Dipartimento di Fisica, Università di Napoli, Naples, Italy
[75] [(a)]INFN Sezione di Pavia, Pavia, Italy; [(b)]Dipartimento di Fisica, Università di Pavia, Pavia, Italy
[76] [(a)]INFN Sezione di Pisa, Pisa, Italy; [(b)]Dipartimento di Fisica E. Fermi, Università di Pisa, Pisa, Italy
[77] [(a)]INFN Sezione di Roma, Rome, Italy; [(b)]Dipartimento di Fisica, Sapienza Università di Roma, Rome, Italy
[78] [(a)]INFN Sezione di Roma Tor Vergata, Rome, Italy; [(b)]Dipartimento di Fisica, Università di Roma Tor Vergata, Rome, Italy
[79] [(a)]INFN Sezione di Roma Tre, Rome, Italy; [(b)]Dipartimento di Matematica e Fisica, Università Roma Tre, Rome, Italy
[80] [(a)]INFN-TIFPA, Povo, Italy; [(b)]Università degli Studi di Trento, Trento, Italy
[81] Department of Astro and Particle Physics, Universität Innsbruck, Innsbruck, Austria
[82] University of Iowa, Iowa City, IA, USA
[83] Department of Physics and Astronomy, Iowa State University, Ames, IA, USA
[84] Istinye University, Sariyer, Istanbul, Türkiye
[85] [(a)]Departamento de Engenharia Elétrica, Universidade Federal de Juiz de Fora (UFJF), Juiz de Fora,

Brazil; [(b)]Universidade Federal do Rio De Janeiro COPPE/EE/IF, Rio de Janeiro, Brazil; [(c)]Instituto de Física, Universidade de São Paulo, São Paulo, Brazil; [(d)]Rio de Janeiro State University, Rio de Janeiro, Brazil; [(e)]Federal University of Bahia, Bahia, Brazil
[86] KEK, High Energy Accelerator Research Organization, Tsukuba, Japan
[87] Graduate School of Science, Kobe University, Kobe, Japan
[88] [(a)]AGH University of Krakow, Faculty of Physics and Applied Computer Science, Kraków, Poland; [(b)]Marian Smoluchowski Institute of Physics, Jagiellonian University, Kraków, Poland
[89] Institute of Nuclear Physics Polish Academy of Sciences, Kraków, Poland
[90] Faculty of Science, Kyoto University, Kyoto, Japan
[91] Research Center for Advanced Particle Physics and Department of Physics, Kyushu University, Fukuoka , Japan
[92] L2IT, CNRS/IN2P3, UPS, Université de Toulouse, Toulouse, France
[93] Instituto de Física La Plata, Universidad Nacional de La Plata and CONICET, La Plata, Argentina
[94] Physics Department, Lancaster University, Lancaster, UK
[95] Oliver Lodge Laboratory, University of Liverpool, Liverpool, UK
[96] Department of Experimental Particle Physics, Jožef Stefan Institute and Department of Physics, University of Ljubljana, Ljubljana, Slovenia
[97] Department of Physics and Astronomy, Queen Mary University of London, London, UK
[98] Department of Physics, Royal Holloway University of London, Egham, UK
[99] Department of Physics and Astronomy, University College London, London, UK
[100] Louisiana Tech University, Ruston, LA, USA
[101] Fysiska institutionen, Lunds universitet, Lund, Sweden
[102] Departamento de Física Teorica C-15 and CIAFF, Universidad Autónoma de Madrid, Madrid, Spain
[103] Institut für Physik, Universität Mainz, Mainz, Germany
[104] School of Physics and Astronomy, University of Manchester, Manchester, UK
[105] CPPM, CNRS/IN2P3, Aix-Marseille Université, Marseille, France
[106] Department of Physics, University of Massachusetts, Amherst, MA, USA
[107] Department of Physics, McGill University, Montreal, QC, Canada
[108] School of Physics, University of Melbourne, Victoria, Australia
[109] Department of Physics, University of Michigan, Ann Arbor, MI, USA
[110] Department of Physics and Astronomy, Michigan State University, East Lansing, MI, USA
[111] Group of Particle Physics, University of Montreal, Montreal, QC, Canada
[112] Fakultät für Physik, Ludwig-Maximilians-Universität München, Munich, Germany
[113] Max-Planck-Institut für Physik (Werner-Heisenberg-Institut), Munich, Germany
[114] Graduate School of Science and Kobayashi-Maskawa Institute, Nagoya University, Nagoya, Japan
[115] [(a)]Department of Physics, Nanjing University, Nanjing, China; [(b)]School of Science, Shenzhen Campus of Sun Yat-sen University, Guangzhou, China; [(c)]University of Chinese Academy of Science (UCAS), Beijing, China
[116] Department of Physics and Astronomy, University of New Mexico, Albuquerque, NM, USA
[117] Institute for Mathematics, Astrophysics and Particle Physics, Radboud University/Nikhef, Nijmegen, Netherlands
[118] Nikhef National Institute for Subatomic Physics and University of Amsterdam, Amsterdam, Netherlands
[119] Department of Physics, Northern Illinois University, DeKalb, IL, USA
[120] [(a)]New York University Abu Dhabi, Abu Dhabi, United Arab Emirates; [(b)]United Arab Emirates University, Al Ain, United Arab Emirates
[121] Department of Physics, New York University, New York, NY, USA
[122] Ochanomizu University, Otsuka, Bunkyo-ku, Tokyo, Japan
[123] Ohio State University, Columbus, OH, USA
[124] Homer L. Dodge Department of Physics and Astronomy, University of Oklahoma, Norman, OK, USA
[125] Department of Physics, Oklahoma State University, Stillwater, OK, USA
[126] Joint Laboratory of Optics, Palacký University, Olomouc, Czech Republic
[127] Institute for Fundamental Science, University of Oregon, Eugene, OR, USA
[128] Graduate School of Science, University of Osaka, Osaka, Japan
[129] Department of Physics, University of Oslo, Oslo, Norway
[130] Department of Physics, Oxford University, Oxford, UK
[131] LPNHE, CNRS/IN2P3, Sorbonne Université, Université Paris Cité, Paris, France

[132] Department of Physics, University of Pennsylvania, Philadelphia, PA, USA
[133] Department of Physics and Astronomy, University of Pittsburgh, Pittsburgh, PA, USA
[134] [(a)]Laboratório de Instrumentação e Física Experimental de Partículas-LIP, Lisbon, Portugal; [(b)]Departamento de Física, Faculdade de Ciências, Universidade de Lisboa, Lisbon, Portugal; [(c)]Departamento de Física, Universidade de Coimbra, Coimbra, Portugal; [(d)]Centro de Física Nuclear da Universidade de Lisboa, Lisbon, Portugal; [(e)]Departamento de Física, Escola de Ciências, Universidade do Minho, Braga, Portugal; [(f)]Departamento de Física Teórica y del Cosmos, Universidad de Granada, Granada, Spain; [(g)]Departamento de Física, Instituto Superior Técnico, Universidade de Lisboa, Lisbon, Portugal
[135] Institute of Physics of the Czech Academy of Sciences, Prague, Czech Republic
[136] Czech Technical University in Prague, Prague, Czech Republic
[137] Faculty of Mathematics and Physics, Charles University, Prague, Czech Republic
[138] Particle Physics Department, Rutherford Appleton Laboratory, Didcot, UK
[139] IRFU, CEA, Université Paris-Saclay, Gif-sur-Yvette, France
[140] Santa Cruz Institute for Particle Physics, University of California Santa Cruz, Santa Cruz, CA, USA
[141] [(a)]Departamento de Física, Pontificia Universidad Católica de Chile, Santiago, Chile; [(b)]Millennium Institute for Subatomic Physics at High Energy Frontier (SAPHIR), Santiago, Chile; [(c)]Instituto de Investigación Multidisciplinario en Ciencia y Tecnología, y Departamento de Física, Universidad de La Serena, La Serena, Chile; [(d)]Department of Physics, Universidad Andres Bello, Santiago, Chile; [(e)]Instituto de Alta Investigación, Universidad de Tarapacá, Arica, Chile; [(f)]Departamento de Física, Universidad Técnica Federico Santa María, Valparaiso, Chile
[142] Department of Physics, Institute of Science, Tokyo, Japan
[143] Department of Physics, University of Washington, Seattle, WA, USA
[144] Department of Physics and Astronomy, University of Sheffield, Sheffield, UK
[145] Department of Physics, Shinshu University, Nagano, Japan
[146] Department Physik, Universität Siegen, Siegen, Germany
[147] Department of Physics, Simon Fraser University, Burnaby, BC, Canada
[148] SLAC National Accelerator Laboratory, Stanford, CA, USA
[149] Department of Physics, Royal Institute of Technology, Stockholm, Sweden
[150] Departments of Physics and Astronomy, Stony Brook University, Stony Brook, NY, USA
[151] Department of Physics and Astronomy, University of Sussex, Brighton, UK
[152] School of Physics, University of Sydney, Sydney, Australia
[153] Institute of Physics, Academia Sinica, Taipei, Taiwan
[154] [(a)]E. Andronikashvili Institute of Physics, Iv. Javakhishvili Tbilisi State University, Tbilisi, Georgia; [(b)]High Energy Physics Institute, Tbilisi State University, Tbilisi, Georgia; [(c)]University of Georgia, Tbilisi, Georgia
[155] Department of Physics, Technion, Israel Institute of Technology, Haifa, Israel
[156] Raymond and Beverly Sackler School of Physics and Astronomy, Tel Aviv University, Tel Aviv, Israel
[157] Department of Physics, Aristotle University of Thessaloniki, Thessaloníki, Greece
[158] International Center for Elementary Particle Physics and Department of Physics, University of Tokyo, Tokyo, Japan
[159] Department of Physics, University of Toronto, Toronto, ON, Canada
[160] [(a)]TRIUMF, Vancouver, BC, Canada; [(b)]Department of Physics and Astronomy, York University, Toronto, ON, Canada
[161] Division of Physics and Tomonaga Center for the History of the Universe, Faculty of Pure and Applied Sciences, University of Tsukuba, Tsukuba, Japan
[162] Department of Physics and Astronomy, Tufts University, Medford, MA, USA
[163] Department of Physics and Astronomy, University of California Irvine, Irvine, CA, USA
[164] University of West Attica, Athens, Greece
[165] University of Sharjah, Sharjah, United Arab Emirates
[166] Department of Physics and Astronomy, University of Uppsala, Uppsala, Sweden
[167] Department of Physics, University of Illinois, Urbana, IL, USA
[168] Instituto de Física Corpuscular (IFIC), Centro Mixto Universidad de Valencia - CSIC, Valencia, Spain
[169] Department of Physics, University of British Columbia, Vancouver, BC, Canada
[170] Department of Physics and Astronomy, University of Victoria, Victoria, BC, Canada
[171] Fakultät für Physik und Astronomie, Julius-Maximilians-Universität Würzburg, Würzburg, Germany
[172] Department of Physics, University of Warwick, Coventry, UK
[173] Waseda University, Tokyo, Japan

[174] Department of Particle Physics and Astrophysics, Weizmann Institute of Science, Rehovot, Israel
[175] Department of Physics, University of Wisconsin, Madison, WI, USA
[176] Fakultät für Mathematik und Naturwissenschaften, Fachgruppe Physik, Bergische Universität Wuppertal, Wuppertal, Germany
[177] Department of Physics, Yale University, New Haven, CT, USA
[178] Yerevan Physics Institute, Yerevan, Armenia

[a] Also at Affiliated with an Institute Covered by a Cooperation Agreement with CERN, Geneva, Switzerland
[b] Also at An-Najah National University, Nablus, Palestine
[c] Also at Borough of Manhattan Community College, City University of New York, New York, NY, USA
[d] Also at Center for High Energy Physics, Peking University, Beijing, China
[e] Also at Center for Interdisciplinary Research and Innovation (CIRI-AUTH), Thessaloníki, Greece
[f] Also at CERN, Geneva, Switzerland
[g] Also at CMD-AC UNEC Research Center, Azerbaijan State University of Economics (UNEC), Baku, Azerbaijan
[h] Also at Département de Physique Nucléaire et Corpusculaire, Université de Genève, Geneva, Switzerland
[i] Also at Departament de Fisica de la Universitat Autonoma de Barcelona, Barcelona, Spain
[j] Also at Department of Financial and Management Engineering, University of the Aegean, Chios, Greece
[k] Also at Department of Physics, California State University, Sacramento, USA
[l] Also at Department of Physics, King's College London, London, UK
[m] Also at Department of Physics, Stanford University, Stanford, CA, USA
[n] Also at Department of Physics, Stellenbosch University, Stellenbosch, South Africa
[o] Also at Department of Physics, University of Fribourg, Fribourg, Switzerland
[p] Also at Department of Physics, University of Thessaly, Volos, Greece
[q] Also at Department of Physics, Westmont College, Santa Barbara, USA
[r] Also at Faculty of Physics, Sofia University 'St. Kliment Ohridski', Sofia, Bulgaria
[s] Also at Hellenic Open University, Patras, Greece
[t] Also at Imam Mohammad Ibn Saud Islamic University, Riyadh, Saudi Arabia
[u] Also at Institucio Catalana de Recerca i Estudis Avancats, ICREA, Barcelona, Spain
[v] Also at Institut für Experimentalphysik, Universität Hamburg, Hamburg, Germany
[w] Also at Institute for Nuclear Research and Nuclear Energy (INRNE) of the Bulgarian Academy of Sciences, Sofia, Bulgaria
[x] Also at Institute of Applied Physics, Mohammed VI Polytechnic University, Ben Guerir, Morocco
[y] Also at Institute of Particle Physics (IPP), Toronto, Canada
[z] Also at Institute of Physics and Technology, Mongolian Academy of Sciences, Ulaanbaatar, Mongolia
[aa] Also at Institute of Physics, Azerbaijan Academy of Sciences, Baku, Azerbaijan
[ab] Also at Institute of Theoretical Physics, Ilia State University, Tbilisi, Georgia
[ac] Also at National Institute of Physics, University of the Philippines Diliman (Philippines), Quezon City, Philippines
[ad] Also at Technical University of Munich, Munich, Germany
[ae] Also at The Collaborative Innovation Center of Quantum Matter (CICQM), Beijing, China
[af] Also at TRIUMF, Vancouver, BC, Canada
[ag] Also at Università di Napoli Parthenope, Naples, Italy
[ah] Also at University of Colorado Boulder, Department of Physics, Colorado, USA
[ai] Also at Washington College, Chestertown, MD, USA
[aj] Also at Physics Department, Yeditepe University, Istanbul, Türkiye
* Deceased